The eventful life of ETGs in low density environments

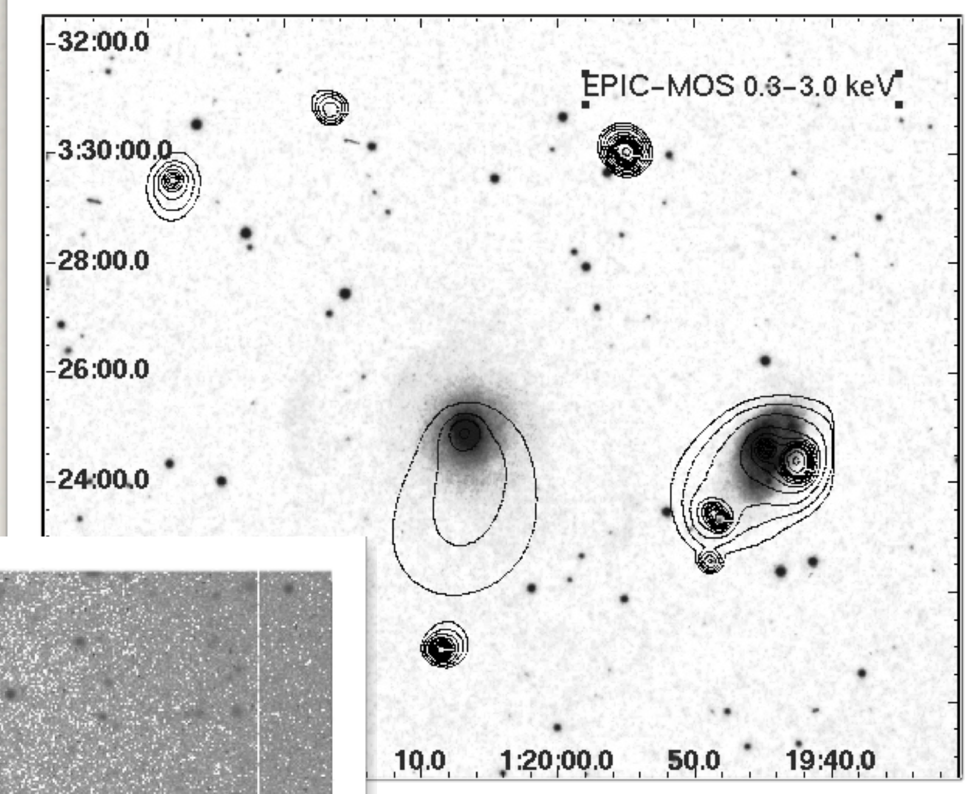

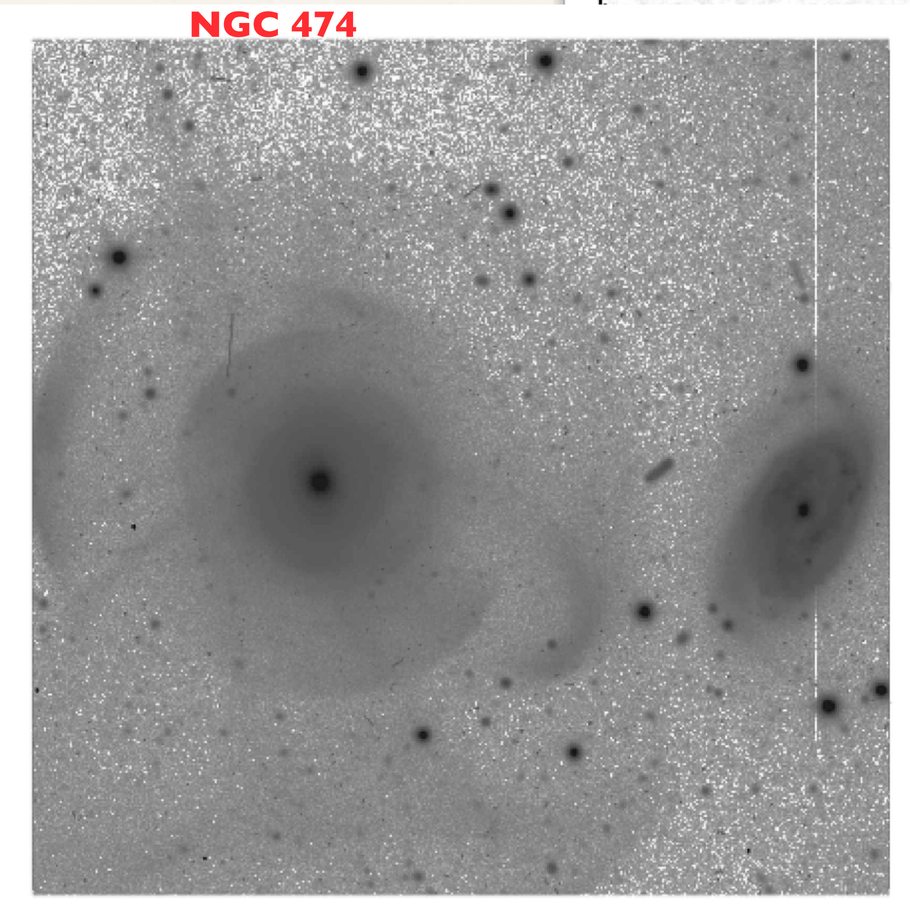

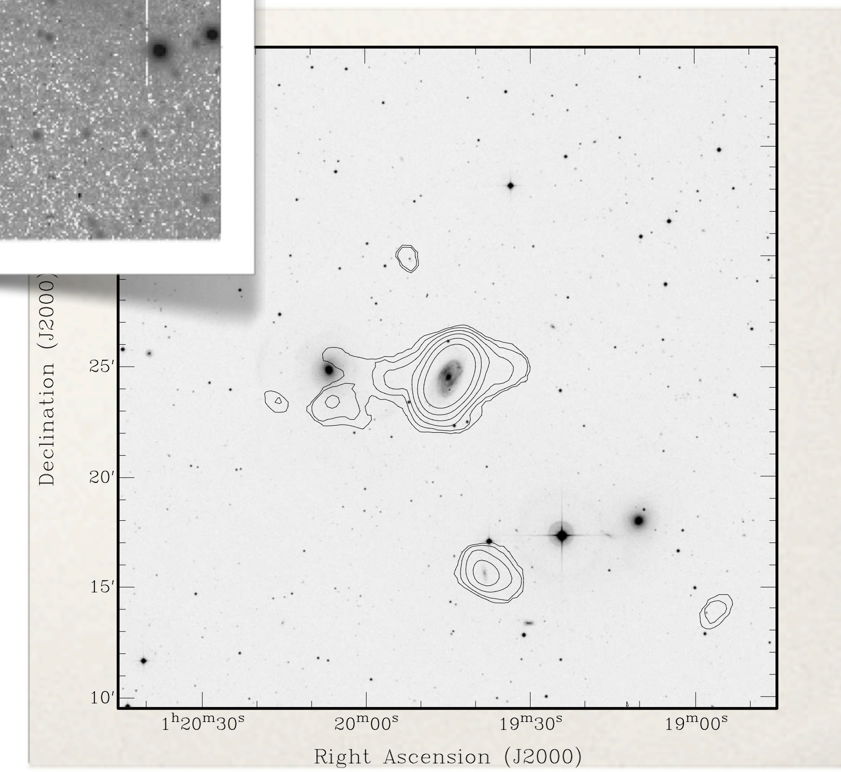

A multi-wavelength approach

Roberto Rampazzo
INAF Osservatorio Astronomico di Padova

Francesca Annibali — OA Pd
Alessandro Bressan, Lucio Buson,
Marcel Clemens
Luciana Bianchi — JHU
Antonietta Marino
Ruth Grützbauch — Univ. Nottingham
Pasquale Panuzzo — CEA (Saclay)
Ginevra Trinchieri — OA Brera
Anna Wolter
Werner Zeilinger — IfA Wien

introduction

Nearby ETGs' life in LDE seems definitely *less inactive* than taught 15-20 years ago:

a) Gas reservoirs ETGs have a multiphase Inter Stellar Medium: the hot (T ~ 10^6-10^7 K) (see e.g. Forman & Jones 1985; Fabbiano et al. 1992; O'Sullivan et al. 2001), X-ray emitting gas dominates with respect to the warm (10^4 K) (see e.g. Phillips et al. 1986; Bertola et al. 1992; Goudfrooji et al. 1994; Macchetto et al. 1996) and cold gas (10 K) (e.g. Sadler et al. 1992; Morganti et al. 2006) components. The warm gas (10^3-10^6 $M_{\odot}$) is often associated to dust structures (Goudfrooji et al. 1994).

b) Interaction/merging signatures A significant fraction of ETGs show morphological and kinematical signatures of recent interaction events (shells, ripples, tails as well as counter-rotation etc.) (see e.g. Malin & Carter 1983; Corsini & Bertola 1998; Reduzzi et al. 1996; Colbert et al. 2001; Emsellem et al. (2004); Tal et al. 2009). E.g. the fraction of galaxies showing shell/ripples is near to 20% (Malin & Carter 1983).

c) The presence of younger stellar components (a "rejuvenation") in ETGs is often and often diagnosed by stellar population models applied to optical data-sets (Longhetti et al 1998, 1999, 2000; Trager et al. 2000; Kuntschner et al. 2002; Thomas et al. 2005; Clemens et al. 2006, 09; Annibali et al. 2007). Mid InfraRed (Spitzer (Temi et al. 2004; Kaneda et al. 2008)) and Far UV (GALEX (e.g. Rampazzo et al. 07; Marino et al. 2009)) studies seem to support this view.

Galaxies' mass regulates the *timescale* (*'downsizing'*) and the environment the *timing*...

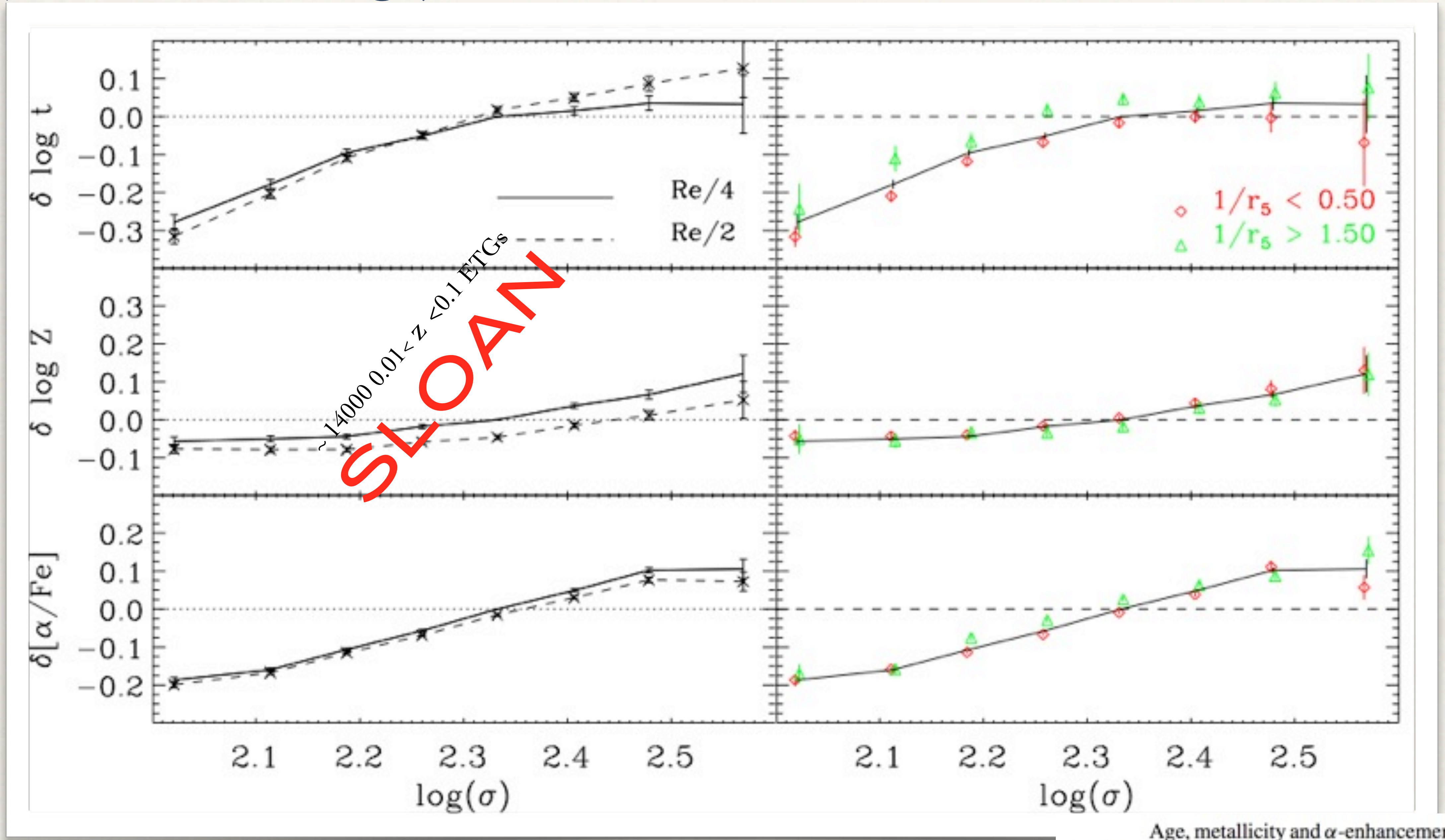

Age, metallicity and α-enhancement variations as a function of σ. A linear regression analysis has been carried out simultaneously on the Hβ, Hδ, Mg1, Mg2, Mgb, Fe4383, Fe4531, Fe5270, Fe5335 and C4668 indices. Left-hand panel: radial variation. The two lines in each plot refer to index values corrected to $r_e/4$ (solid line) and $r_e/2$ (dashed line). Right-hand panel: effect of environment. The solid line represents the entire sample, diamonds only those objects in low-density environments ($1/r_5 < 0.5$) and triangles only those in high-density environments ($1/r_5 > 1.5$). Values are differences with respect to those of the entire sample at $\sigma = 200\,\mathrm{km\,s^{-1}}$. The central σ bins typically contain $>10^3$ galaxies, whereas the highest bin contains only 16.

Clemens M., Bressan A., Nikolic B. & Rampazzo R. , 2009, MNRAS, 392, L35

the challenge is to build up ...

A) a coherent and exhaustive local picture (more than half of the stellar mass in the Local Universe is found in massive spheroidal galaxies) i.e. to understand in detail the connection between the ETGs star formation history (i.e gas duty cycle, AGN feedback etc.) and to the secular and/or external mechanisms driving their evolution

and

B) to link the local to the "Great picture" i.e. comparison with the integral properties (Color-magnitude relation (e.g. Bower et al. 92; Schweizer & Seitzer 1992, Tanaka et al. 05) Fundamental plane (e.g. Bender, Burstein & Faber 1992; Di Serego Alighieri et al. 2005; Treu et al 2005)) derived from large samples and more distant samples of galaxies (e.g. Dunlop 2001; Ivison et al. 2002; Chapman et al. 2003; Cimatti et al. 2004; Glazebrook et al. 2004).

talk overview

✦ Anatomy of 65 nearby ETGs:

from nuclear to environmental properties

- The sample properties

			Type of information
Optical spectroscopy:	the underlying stellar population the origin and the powering mechanisms of the ionized gas		Nuclear up to $r_e/2$
On going works insights from:	MIR	Spitzer IRS-spectroscopy	Nuclear
	Far UV	GALEX imaging	Nuclear & galactic scale
	X-ray	The hot gas and the environment	Nuclear, galactic & group scale
	ETGs in LDE	a) Group dynamical analysis b) Group Luminosity Function	Environment
Future investigations:	1) modeling of the extended SED of the ETGs		Nuclear
	2) nuclear, galactic group scale ionized gas distribution and kinematics dynamical evolution of groups		Environment

The sample properties

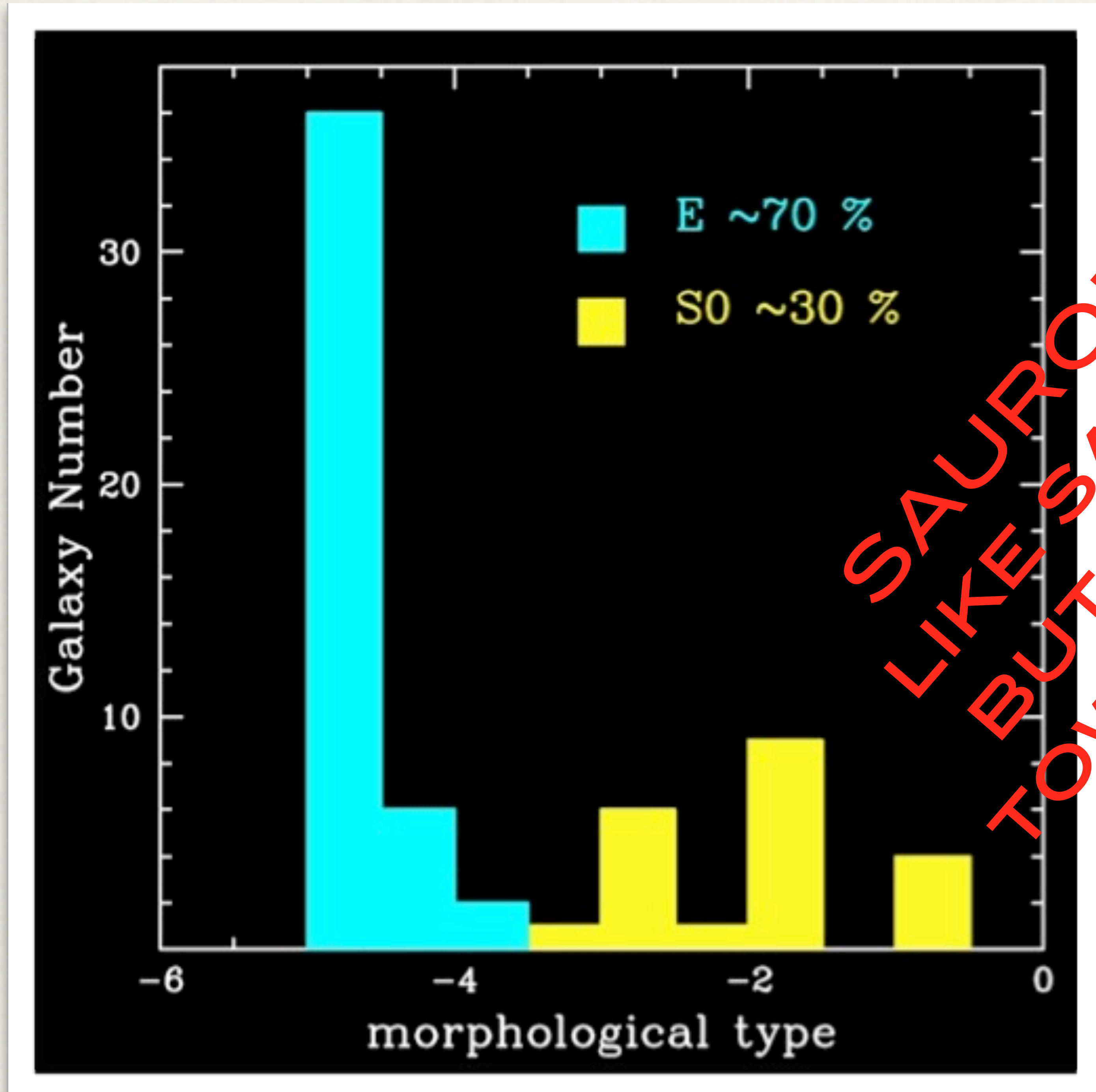

SAURON - LIKE SAMPLE BUT BIASED TOWARDS LDE

ident	RSA	RC3	V_{hel} km s^{-1}	ρ_{xyz} Gal. Mpc^{-3}
NGC 128	S02(8) pec	S0 pec sp	4227	
NGC 777	E1	E1	5040	
NGC 1052	E3/S0	E4	1475	0.49
NGC 1209	E6	E6:	2619	0.13
NGC 1297	S02/3(0)	SAB0 pec:	1550	0.71
NGC 1366	E7/S01(7)	S0 sp	1310	0.16
NGC 1380	S03(7)/Sa	SA0	1844	1.54
NGC 1389	S01(5)/SB01	SAB(s)0-:	986	1.50
NGC 1407	E0/S01(0)	E0	1766	0.42
NGC 1426	E4	E4	1443	0.66
NGC 1453	E0	E2	3906	
NGC 1521	E3	E3	4165	
NGC 1533	SB02(2)/SBa	SB0-	773	0.89
NGC 1553	S01/2(5)pec	SA(r)0	1280	0.97
NGC 1947	S03(0) pec	S0- pec	1100	0.24
NGC 2749	E3	E3	4180	
NGC 2911	S0p or S03(2)	SA(s)0: pec	3131	
NGC 2962	RSB02/Sa	RSAB(rs)0+	2117	0.15
NGC 2974	E4	E4	1890	0.26
NGC 313[illegible]	[illegible]	E:	1731	0.11
NGC 325[illegible]	E1	E1	2778	0.72
NGC 326[illegible]	E2	E2	2818	0.69
NGC [illegible]89	S03/Sa	SAB(rs)+	693	0.39
NGC [illegible]557	E3	E3	3038	0.28
NGC 3607	S03(3)	SA(s)0:	934	0.34
NGC 3818	E5	E5	1701	0.20
NGC 3962	E1	E1	1822	0.32
NGC 4374	E1	E1	1060	3.99
NGC 4552	S01(0)	E	322	2.97
NGC 4636	E0/S01(6)	E0-1	937	1.33
NGC 4696	(E3)	E+1 pec	2958	0.00
NGC 4697	E6	E6	1241	0.60
NGC 5011	E2	E1-2	3104	0.27
NGC 5044	E0	E0	2704	0.38
NGC 5077	S01/2(4)	E3+	2764	0.23
NGC 5090	E2	E2	3421	
NGC 5193	S01(0)	E pec	3711	
NGC 5266	S03(5) pec	SA0-:	3074	0.35
NGC 5328	E4	E1:	4671	
NGC 5363	[S03(5)]	I0:	1138	0.28
NGC 5638	E1	E1	1676	0.79
NGC 5812	E0	E0	1930	0.19
NGC 5813	E1	E1-2	1972	0.88
NGC 5831	E4	E3	1656	0.83
NGC 5846	S01(0)	E0+	1709	0.84
NGC 5898	S02/3(0)	E0	2267	0.23
NGC 6721	E1	E+:	4416	
NGC 6758	E2 (merger)	E+:	3404	
NGC 6776	E1 pec	E+pec	5480	
NGC 6868	E3/S02/3(3)	E2	2854	0.47
NGC 6875	S0/a(merger)	SAB(s)0- pec:	3121	
NGC 6876	E3	E3	3836	
NGC 6958	R?S01(3)	E+	2652	0.12
NGC 7007	S02/3/a	SA0-:	2954	0.14
NGC 7079	SBa	SB(s)0	2670	0.19
NGC 7097	E4	E5	2404	0.26
NGC 7135	S01 pec	SA0- pec	2718	0.32
NGC 7192	S02(0)	E+:	2904	0.28
NGC 7332	S02/3(8)	S0 pec sp	1207	0.12
NGC 7377	S02/3/Sa pec	SA(s)0+	3291	
IC 1459	E4	E	1659	0.28
IC 2006	E1	E	1350	0.12
IC 3370	E2 pec	E2+	2934	0.20
IC 4296	E0	E	3762	
IC 5063	S03(3)pec/Sa	SA(s)0+:	3402	

Rampazzo R., Annibali F., Bressan A., Longhetti M., Padoan F., Zeilinger W.W. 2005, A&A, 433, 497

Annibali F., Bressan A., Rampazzo R., Zeilinger W.W. 2006, A&A 445, 79

Fast & Slow rotators

Fast	(68%)	SAURON	(75%)
Slow	(32%)		(25%)

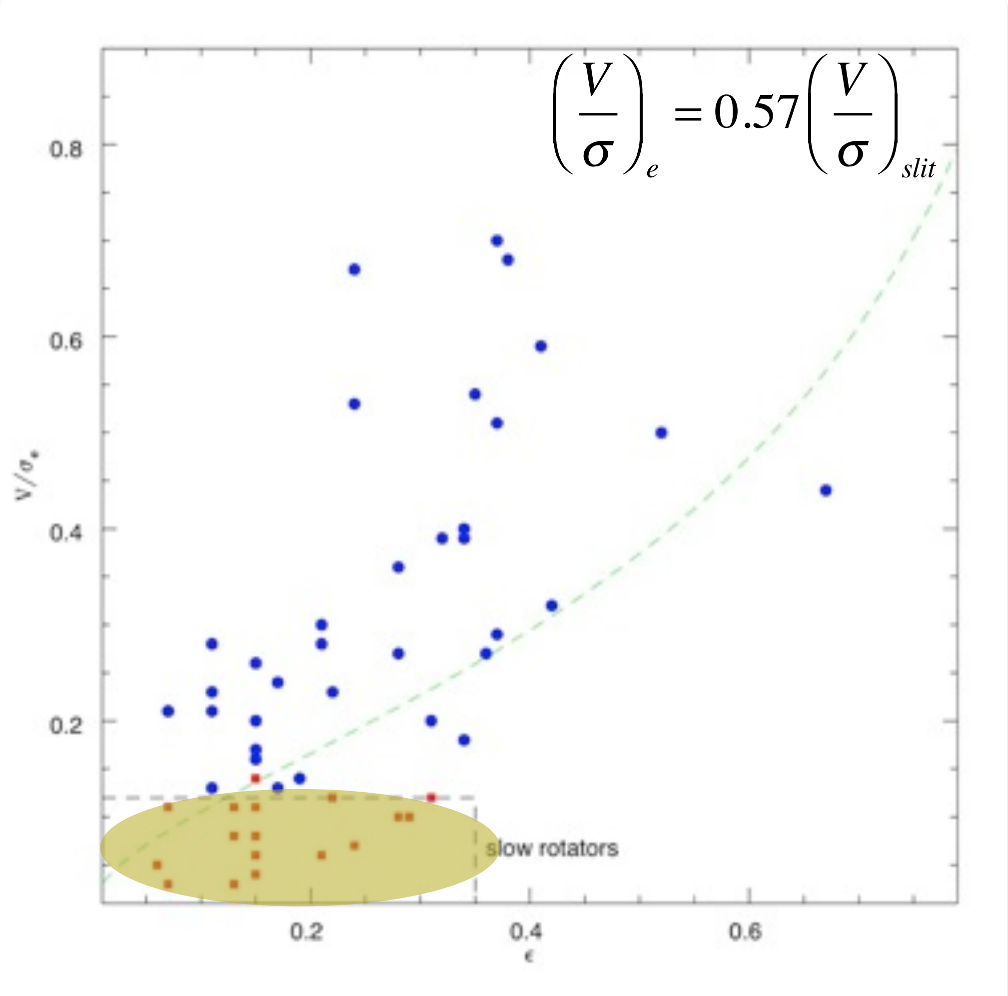

$(V/\sigma,\varepsilon)$ diagram for 52(/65) ETGs in our sample. The red and blue symbols refer to slow and fast rotators respectively. The green dashed line approximately traces the lower envelope described by the location of the observed fast rotating galaxies in this diagram, as well as the yellow ellipse indicate the region where the slow rotators are generally observed.

Fast rotators consist of galaxies with a significant disk component: no distinction between E fast-rotators with disky isophotes and S0 fast rotators. The difference between Fast & Slow rotators is not their degree of anisotropy, but their intrinsic shape (Cappellari et al. 2008)

Table A1. kinematic and morphological overview

ident	RSA	ϵ	$(V/\sigma)_{scaled}$	Rot. class	Gas vs. stars kinematic peculiarities	Gas vs. stars morphological peculiarities
NGC 128	S02(8) pec	0.67	0.44	F	CR g-s (1)	g-d and g-maj t≈23° (5)
NGC 777	E1	0.21	0.06	S		
NGC 1052	E3/S0	0.28	0.27	F	CR g-g (1,5)	
NGC 1209	E6	0.52	0.50	F		X-like struct.; NW linear feature (2)
NGC 1297	S02/3(0)	0.13				
NGC 1366	E7/S01(7)	0.56				
NGC 1380	S03(7)/Sa	0.41	0.59	F		
NGC 1389	S01(5)/SB01	0.37				
NGC 1407	E0/S01(0)	0.07	0.11	S	rotat. min. axis (5)	
NGC 1426	E4	0.34	0.40	F		
NGC 1453	E0	0.17				g-d and g-maj t (5)
NGC 1521	E3	0.35	0.54	F		
NGC 1533	SB02(2)/SBa	0.19				
NGC 1553	S01/2(5)pec	0.38	0.68	F		shells (3)
NGC 1947	S03(0) pec	0.11	0.23	F	rotat. min. axis (5)	dust-lane min. axis (5)
NGC 2749	E3	0.07	0.21	F	rotat. min. axis (5)	
NGC 2911	S0p or S03(2)	0.32				
NGC 2962	RSB02/Sa	0.37	0.51	F		
NGC 2974	E4	0.37	0.70	F		shells (2); g-d and g-maj t≈20° (5)
NGC 3136	E4	0.24	0.67	F	CR s-s (5)	
NGC 3258	E1	0.13	0.08	S	CR g-s (1)	
NGC 3268	E2	0.24	0.53	F		
NGC 3489	S03/Sa	0.37	0.29	F	gas rot. min. axis (5)	
NGC 3557	E3	0.21	0.30	F		SW fan; asym. outer isophotes (2)
NGC 3607	S03(3)	0.11	0.28	F		
NGC 3818	E5	0.36	0.27	F		
NGC 3962	E1	0.22	0.23	F		gas disk+outer arc-like struct. (5)
NGC 4374	E1	0.13	0.03	S		
NGC 4552	S01(0)	0.06	0.05	S		shells (3)
NGC 4636	E0/S01(6)	0.24	0.07	S	gas irr. motion (5)	
NGC 4696	(E3)	0.34	0.18	F		Faint outer shells (2)
NGC 4697	E6	0.32	0.39	F		Non spherical inner isophotes (2)
NGC 5011	E2	0.15	0.11	S		
NGC 5044	E0	0.11	0.13	F	CR s-s; gas irr.motion (5)	gas fil. shape (5)
NGC 5077	S01/2(4)	0.15	0.06	S	CR s-s (5); g-d and g-maj t≈90° (5)	
NGC 5090	E2	0.15	0.17	F		
NGC 5193	S01(0)	0.07				
NGC 5266	S03(5) pec	0.31	0.12	S	stellar rot. min. axis (5)	dust-lane and gas along min. axis (5)
NGC 5328	E4	0.31				
NGC 5363	[S03(5)]	0.34	0.39	F		dust -lane along min. axis (5)
NGC 5638	E1	0.11	0.21	F		
NGC 5812	E0	0.13	0.11	S		Tidal tail (2)
NGC 5813	E1	0.15	0.14	S	CR s-s; gas irr. motion (5)	gas fil. shape (5)
NGC 5831	E4	0.15	0.08	S	CR s-s (6,7)	
NGC 5846	S01(0)	0.07	0.03	S	gas irr. motion (5)	Faint outer shells (2)
NGC 5898	S02/3(0)	0.07	0.21	F	CR g-s (1)	Three spiral arm-like tidal tails (2)
NGC 6721	E1	0.15	0.26	F		
NGC 6758	E2 (merger)	0.22	0.12	S	CR g-s (5)	
NGC 6776	E1 pec	0.17	0.24	F		shell or loops NE (3,4); gas fil. shape (5)
NGC 6868	E3/S02/3(3)	0.19	0.14	F	CR g-s (5)	
NGC 6875	S0/a(merger)	0.41				
NGC 6876	E3	0.13				
NGC 6958	R?S01(3)	0.15	0.20	F		Shells (2,3)
NGC 7007	S02/3/a	0.42			CR g-s (1)	g-d and g-maj t≈30° (5)
NGC 7079	SBa	0.32	0.96	F	CR g-s + s-s (1)	
NGC 7097	E4	0.29	0.10	S	CR s-s (1)	
NGC 7135	S01 pec	0.31	0.20	F		jet-like debris and shells (3)
NGC 7192	S02(0)	0.15	0.04	S	CR s-s (5)	Shell (2)
NGC 7332	S02/3(8)	0.42	0.32	F	CR g-g (1)	
NGC 7377	S02/3/Sa pec	0.19				
IC 1459	E4	0.28	0.10	S	CR g-g (1)	shells (2)
IC 2006	E1	0.15	0.16	F	CR g-s (1)	
IC 3370	E2 pec	0.21	0.28	F		X-like struct.; broad N fan (2); polar ring ? (5)
IC 4296	E0	0.17	0.13	F	CR s-s (5)	
IC 5063	S03(3)pec/Sa	0.28	0.26	F		

In columns 4 and 5 we tabulate $(V/\sigma)_{scaled}=0.57(V/\sigma)_{slit}$ and the rotation class, respectively (see Cappellari et al. (2007)). Column 5 Rotator class (F=fast rotators; S=slow rotators). Legenda: **CR g-s**: counter rotation gas vs. stars; **CR s-s**: counter rotation stars vs. stars; **CR g-g**: counter rotation gas vs. gas; **stars rotat. min. axis**: stars rotate along the galaxy minor axis; **g-d and g-maj t**: gas disk and galaxy major axis are tilted by the reported angle, if provided in the literature. References: (1) Corsini & Bertola (1998); (2) Tal et al. (2009); (3) Malin & Carter (1983); (4) Pierfederici & Rampazzo (2004); (5) the description of the kinematic and morphological peculiarities of the galaxies and full references are reported in the on-line notes of Paper I and Paper II; (6) Davies et al. (1983); (7) Emsellem et al. (2004).

Optical: the underlying stellar population

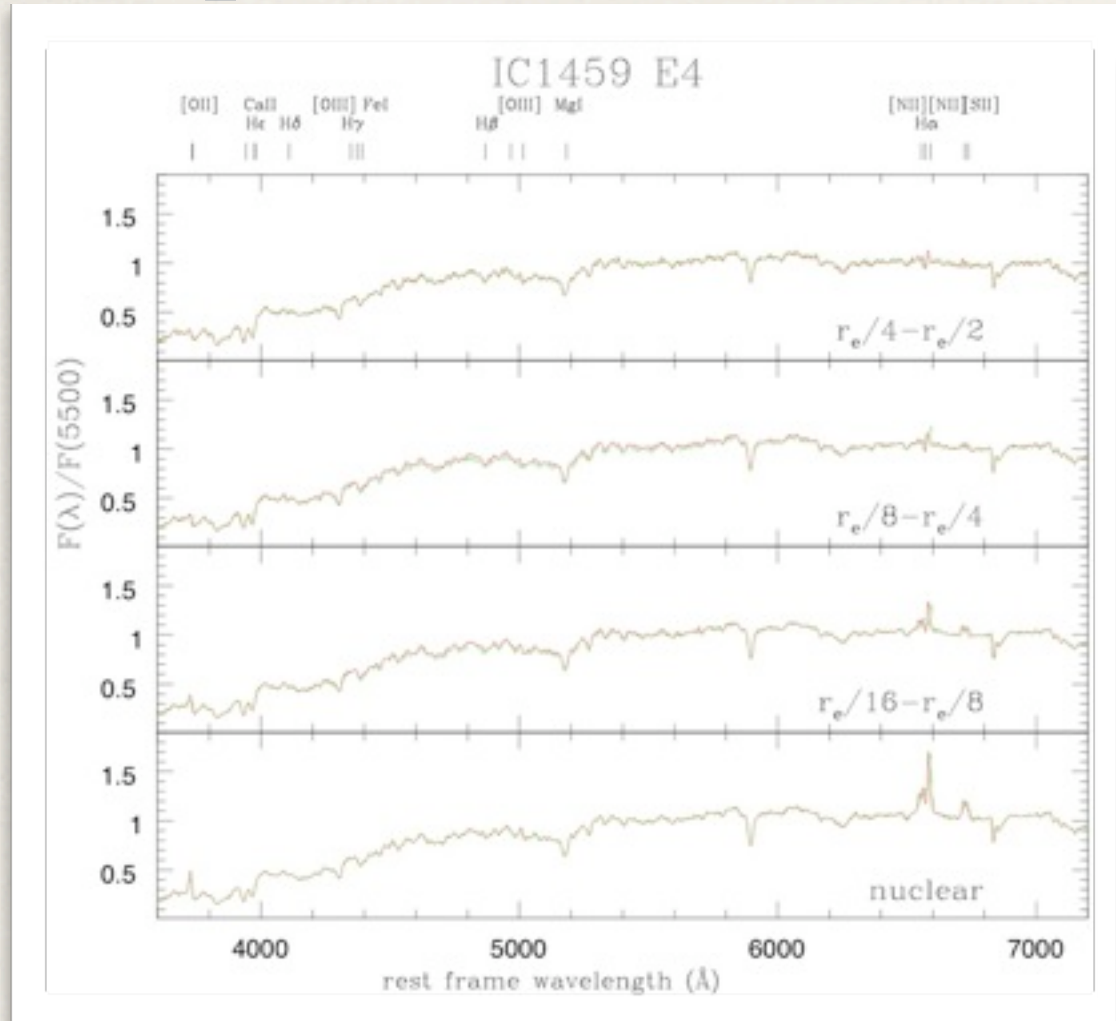

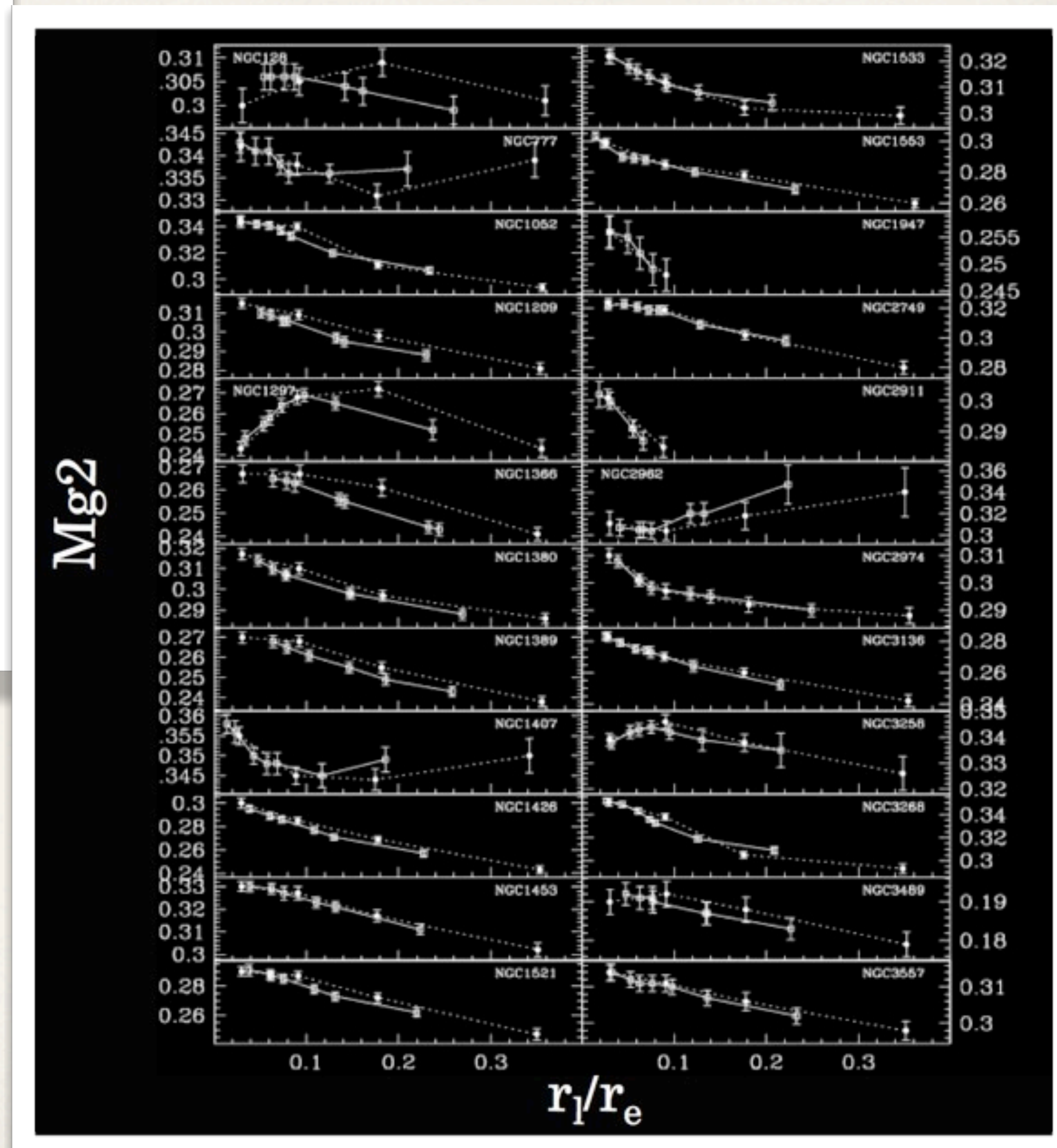

Examples of Mg2 radial gradient. We compute radial gradients for each of the 25 line-strength indices including Hβ, Mg2, Fe5270, Fe5335.

For each ETG we extracted 25 line-strength indices in:

7 luminosity weighted apertures
$$\left.\begin{array}{c} 1.5'' \\ 2.5'' \\ 10'' \\ r_e/10 \\ r_e/8 \\ r_e/4 \\ r_e/2 \end{array}\right\}$$

4 gradients
$$\left.\begin{array}{c} 0 \le r_e \le r_e/16 \\ r_e/16 \le r_e \le r_e/8 \\ r_e/8 \le r_e \le r_e/4 \\ r_e/4 \le r_e \le r_e/2 \end{array}\right\}$$

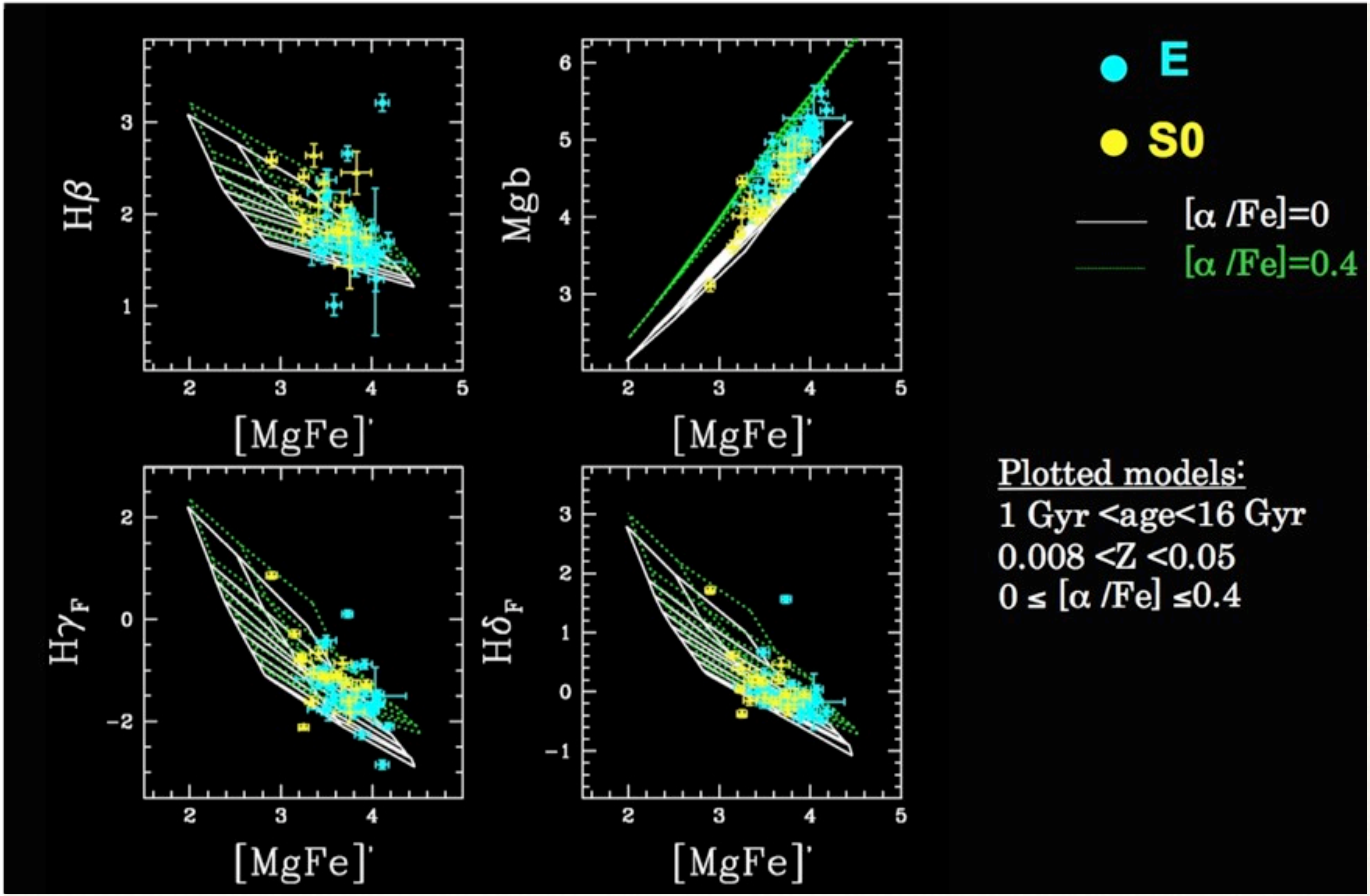

Lick line-strength indices (r_e/8 aperture) of our sample compared with SSP models.

Annibali F., Bressan A., Rampazzo R., Zeilinger W.W., Danese L. , 2007, A&A, 463, 455

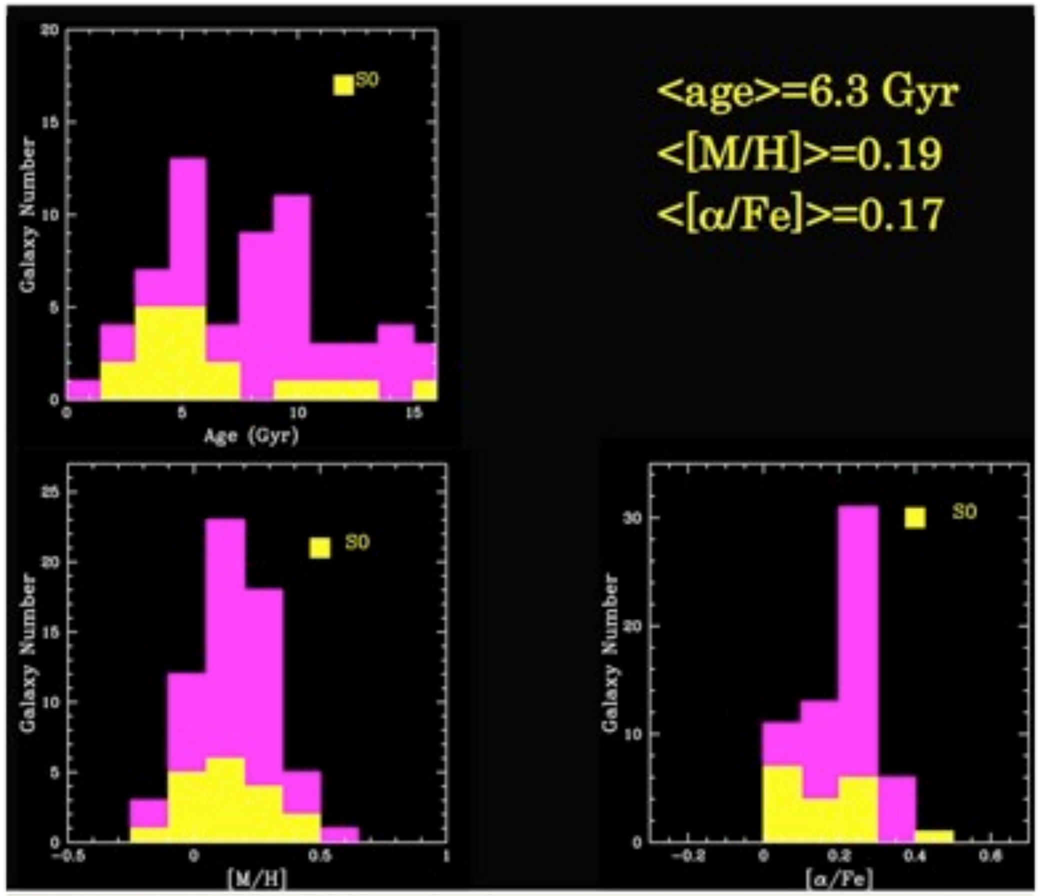

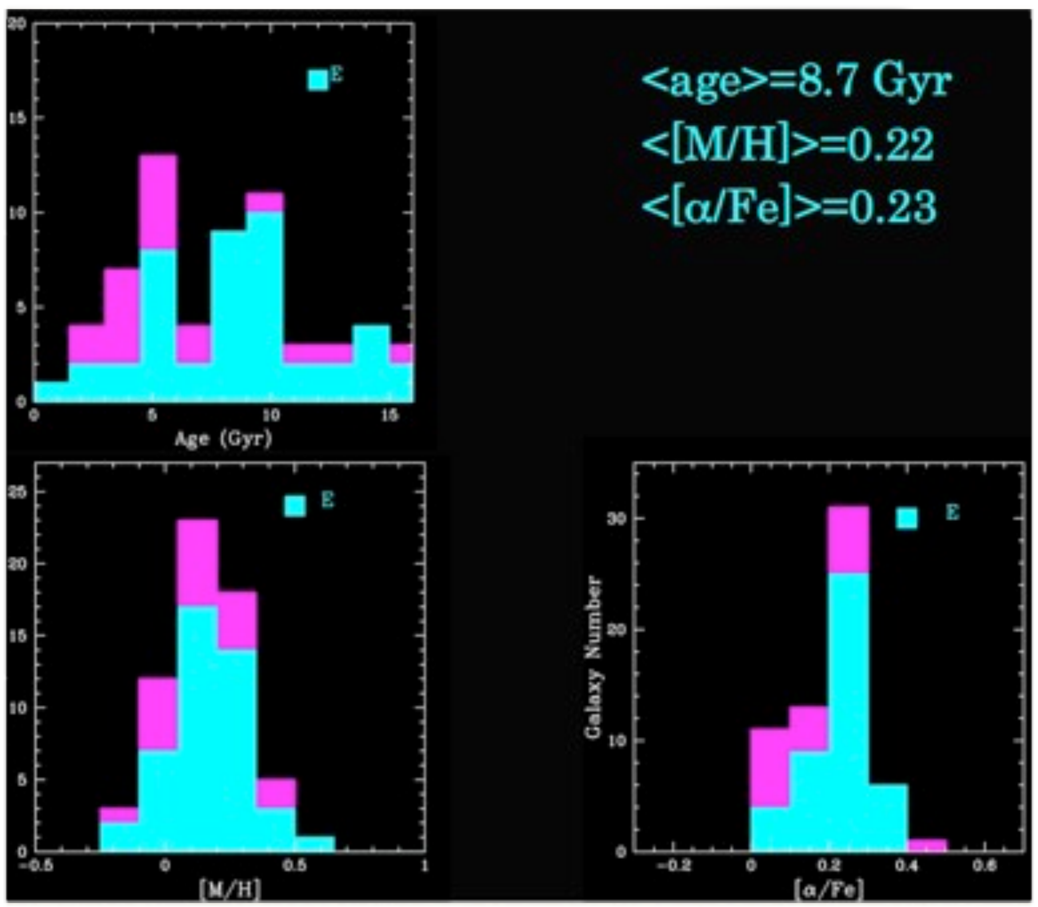

Average Age, metallicity [M/H] and α-enhancement [α/Fe] of lenticular galaxies (data in yellow) and Ellipticals (data in cyan).

Table 7. Average ages, metallicities and α/Fe ratios ($r_e/8$ aperture)

Ident.	σ_c km s^{-1}	age Gyr	Z	[α/Fe]
NGC 128	183	9.7 ± 1.7	0.024 ± 0.004	0.16 ± 0.03
NGC 777	317	5.4 ± 2.1	0.045 ± 0.020	0.28 ± 0.10
NGC 1052	215	14.5 ± 4.2	0.032 ± 0.007	0.34 ± 0.05
NGC 1209	240	4.8 ± 0.9	0.051 ± 0.012	0.14 ± 0.02
NGC 1297	115	15.5 ± 1.2	0.012 ± 0.001	0.29 ± 0.04
NGC 1366	120	5.9 ± 1.	0.024 ± 0.004	0.08 ± 0.03
NGC 1380	240	4.4 ± 0.7	0.038 ± 0.006	0.24 ± 0.02
NGC 1389	139	4.5 ± 0.6	0.032 ± 0.005	0.08 ± 0.02
NGC 1407	286	8.8 ± 1.5	0.033 ± 0.005	0.32 ± 0.03
NGC 1426	162	9.0 ± 2.5	0.024 ± 0.005	0.07 ± 0.05
NGC 1453	289	9.4 ± 2.1	0.033 ± 0.007	0.22 ± 0.03
NGC 1521	235	3.2 ± 0.4	0.037 ± 0.006	0.09 ± 0.02
NGC 1533	174	11.9 ± 6.9	0.023 ± 0.020	0.21 ± 0.10
NGC 1553	180	4.8 ± 0.7	0.031 ± 0.004	0.10 ± 0.02
NGC 1947	142	5.9 ± 0.8	0.023 ± 0.003	0.05 ± 0.02
NGC 2749	248	10.8 ± 2.3	0.027 ± 0.006	0.25 ± 0.04
NGC 2911	235	5.7 ± 2.0	0.034 ± 0.019	0.25 ± 0.10
NGC 2974	220	13.9 ± 3.6	0.021 ± 0.005	0.23 ± 0.06
NGC 3136	230	1.5 ± 0.1	0.089 ± 0.004	0.36 ± 0.02
NGC 3258	271	4.5 ± 0.8	0.047 ± 0.013	0.21 ± 0.03
NGC 3268	227	9.8 ± 1.7	0.023 ± 0.004	0.34 ± 0.04
NGC 3489	129	1.7 ± 0.1	0.034 ± 0.004	0.05 ± 0.02
NGC 3557	265	5.8 ± 0.8	0.034 ± 0.004	0.17 ± 0.02
NGC 3607	220	3.1 ± 0.5	0.047 ± 0.012	0.24 ± 0.03
NGC 3818	191	8.8 ± 1.2	0.024 ± 0.003	0.25 ± 0.03
NGC 3962	225	10.0 ± 1.2	0.024 ± 0.003	0.22 ± 0.03
NGC 4374	282	9.8 ± 3.4	0.025 ± 0.010	0.24 ± 0.08
NGC 4552	264	6.0 ± 1.4	0.043 ± 0.012	0.21 ± 0.03
NGC 4636	209	13.5 ± 3.6	0.023 ± 0.006	0.29 ± 0.06
NGC 4696	254	16.0 ± 4.5	0.014 ± 0.004	0.30 ± 0.10
NGC 4697	174	10.0 ± 1.4	0.016 ± 0.002	0.14 ± 0.04
NGC 5011	249	7.2 ± 1.9	0.025 ± 0.008	0.25 ± 0.06
NGC 5044	239	14.2 ± 10.	0.015 ± 0.022	0.34 ± 0.17
NGC 5077	260	15.0 ± 4.6	0.024 ± 0.007	0.18 ± 0.06
NGC 5090	269	10.0 ± 1.7	0.028 ± 0.005	0.26 ± 0.04
NGC 5193	209	6.8 ± 1.1	0.018 ± 0.002	0.26 ± 0.04
NGC 5266	199	7.4 ± 1.4	0.019 ± 0.003	0.15 ± 0.05
NGC 5328	303	12.4 ± 3.7	0.027 ± 0.006	0.15 ± 0.05
NGC 5363	199	12.1 ± 2.3	0.020 ± 0.004	0.16 ± 0.05
NGC 5638	168	9.1 ± 2.3	0.024 ± 0.008	0.24 ± 0.05
NGC 5812	200	8.5 ± 2.1	0.027 ± 0.008	0.22 ± 0.05
NGC 5813	239	11.7 ± 1.6	0.018 ± 0.002	0.26 ± 0.04
NGC 5831	164	8.8 ± 3.5	0.016 ± 0.011	0.21 ± 0.09
NGC 5846	250	8.4 ± 1.3	0.033 ± 0.005	0.25 ± 0.03
NGC 5898	220	7.7 ± 1.3	0.030 ± 0.004	0.10 ± 0.03
NGC 6721	262	5.0 ± 0.8	0.040 ± 0.007	0.24 ± 0.02
NGC 6758	242	16.0 ± 2.5	0.016 ± 0.002	0.32 ± 0.05
NGC 6776	242	2.7 ± 0.5	0.033 ± 0.010	0.21 ± 0.05
NGC 6868	277	9.2 ± 1.8	0.033 ± 0.006	0.19 ± 0.03
NGC 6876	230	9.8 ± 1.6	0.023 ± 0.003	0.26 ± 0.03
NGC 6958	223	3.0 ± 0.3	0.038 ± 0.006	0.20 ± 0.03
NGC 7007	125	3.4 ± 0.6	0.031 ± 0.010	0.15 ± 0.05
NGC 7079	155	6.7 ± 1.1	0.016 ± 0.003	0.21 ± 0.05
NGC 7097	224	10.5 ± 2.4	0.024 ± 0.005	0.30 ± 0.05
NGC7135	231	2.2 ± 0.4	0.047 ± 0.010	0.46 ± 0.04
NGC 7192	257	5.7 ± 2.0	0.039 ± 0.015	0.09 ± 0.05
NGC 7332	136	3.7 ± 0.4	0.019 ± 0.002	0.10 ± 0.03
NGC 7377	145	4.8 ± 0.6	0.020 ± 0.002	0.10 ± 0.03

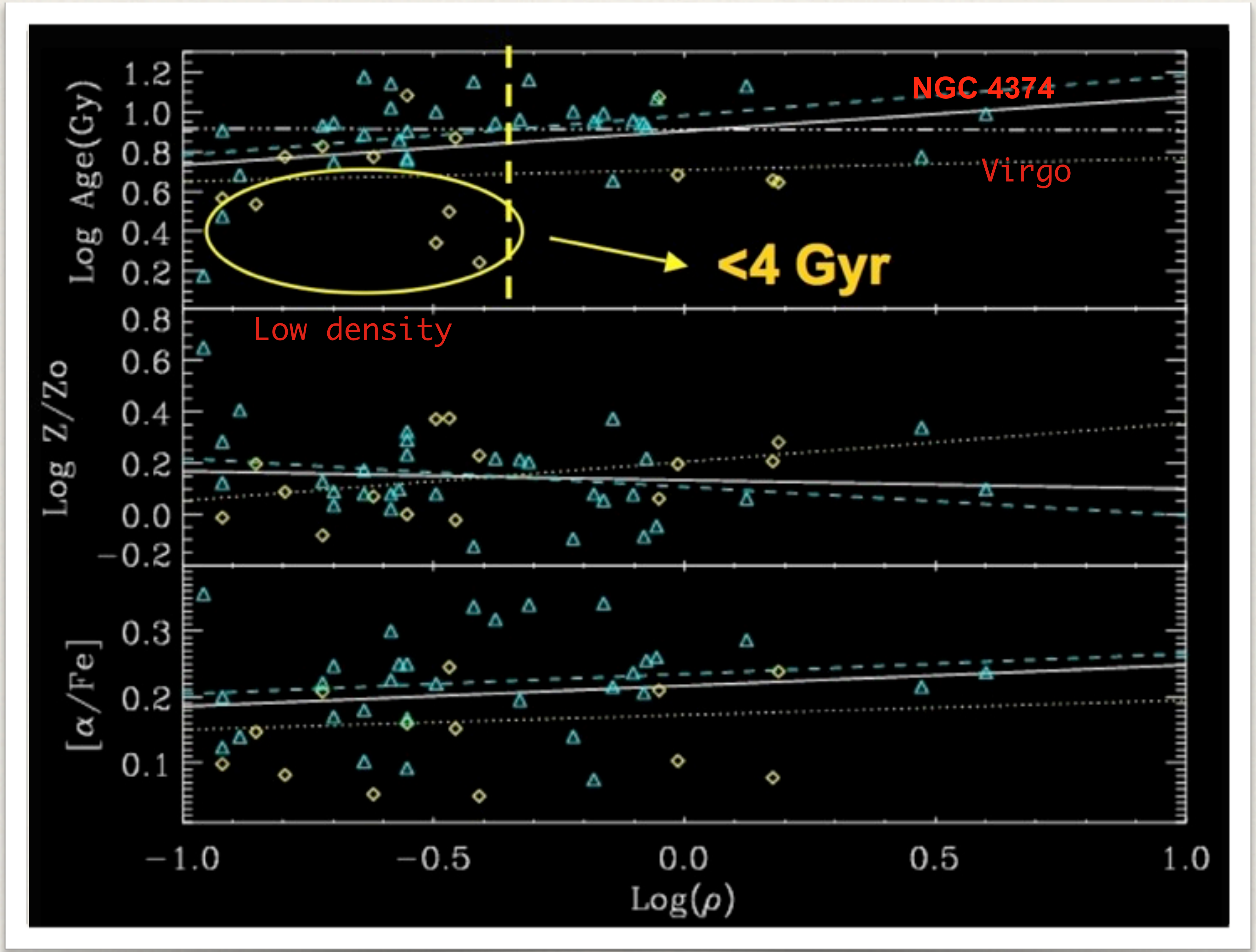

Ages, metallicities and [α/Fe] ratios measured at $r_e/8$ vs. the density of the environment, log ρ [gal Mpc^{-3}] (Tully 1988). Triangles and diamonds indicate E and S0 galaxies respectively. The solid line is the linear fit performed to all the galaxies. Dashed and dotted lines are the best fit to E and S) sub-samples.

Optical: the ionized gas

Subtraction of underlying stellar continuum through new SSPs (Bressan, unpublished) based on MILES spectral library (Sanchez-Blazquez et al. 2006, *3525 - 7500 Å, at 2.3 Å FWHM)*

Emissions are detected in 89% of our ETGs (Phillips et al. (1986) 55-60%; Macchetto et al. (1996) 72-85%; Sarzi et al. 2006 75%; Yan et al. (2006) 52%; Serra et al. (2006) 60%).

The incidence and the strength of the emission is not correlated with the E or S0 class.

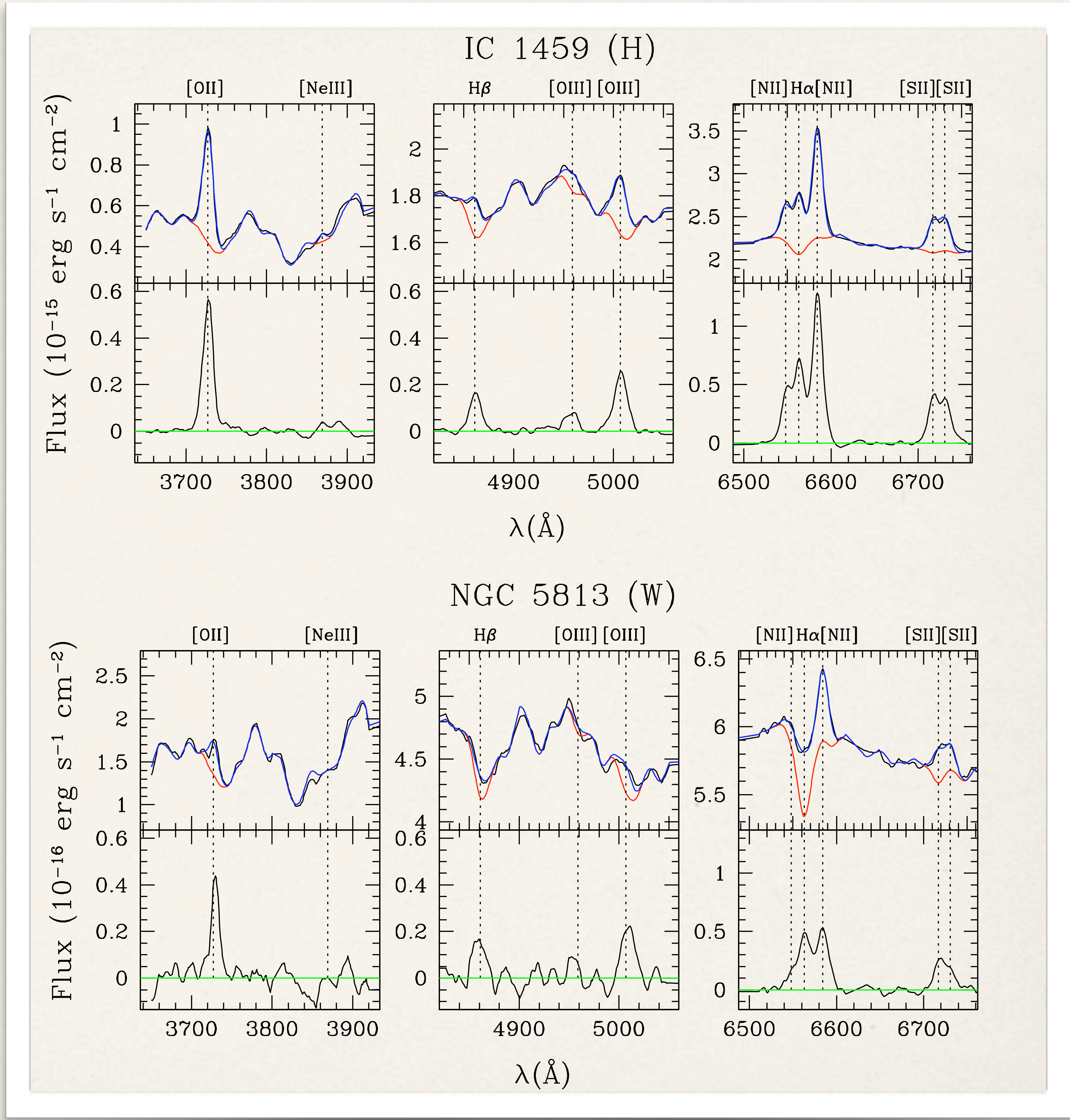

Example of nuclear spectra H (IC 1459) and W (NGC 5813) in the wavelength ranges where most prominent emission lines are measured (observed spectrum=black, spectrum model = red; final spectrum (blu) after addition of the fitted emission line.

Annibali F., Bressan A., Rampazzo R., Zeilinger W.W. 2009, A&A, In Preparation

The bulk of our ETGs are LINERs. A few fall in the Composite area (NGC 3258, NGC 4552, NGC 5193, NGC 5328, NGC 6721, NGC 6876, IC 2006).

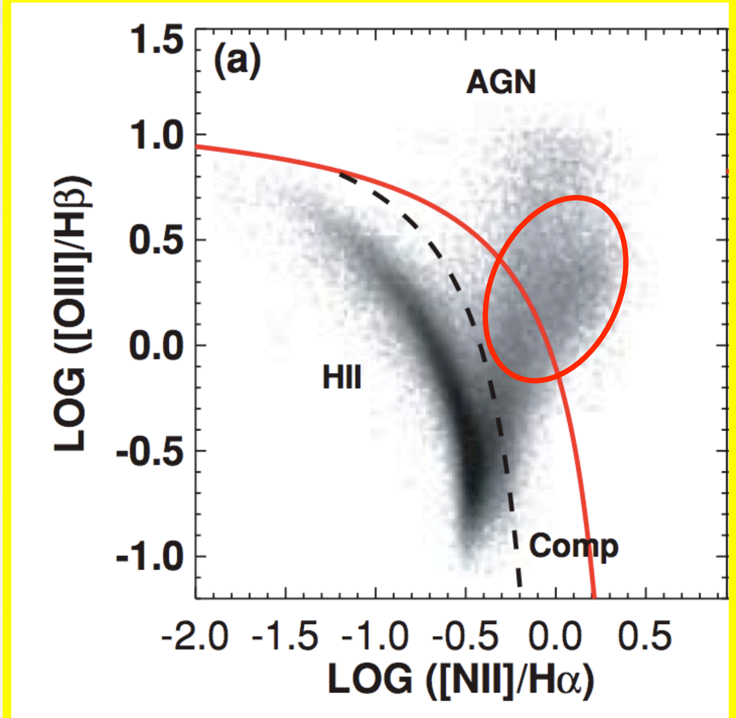

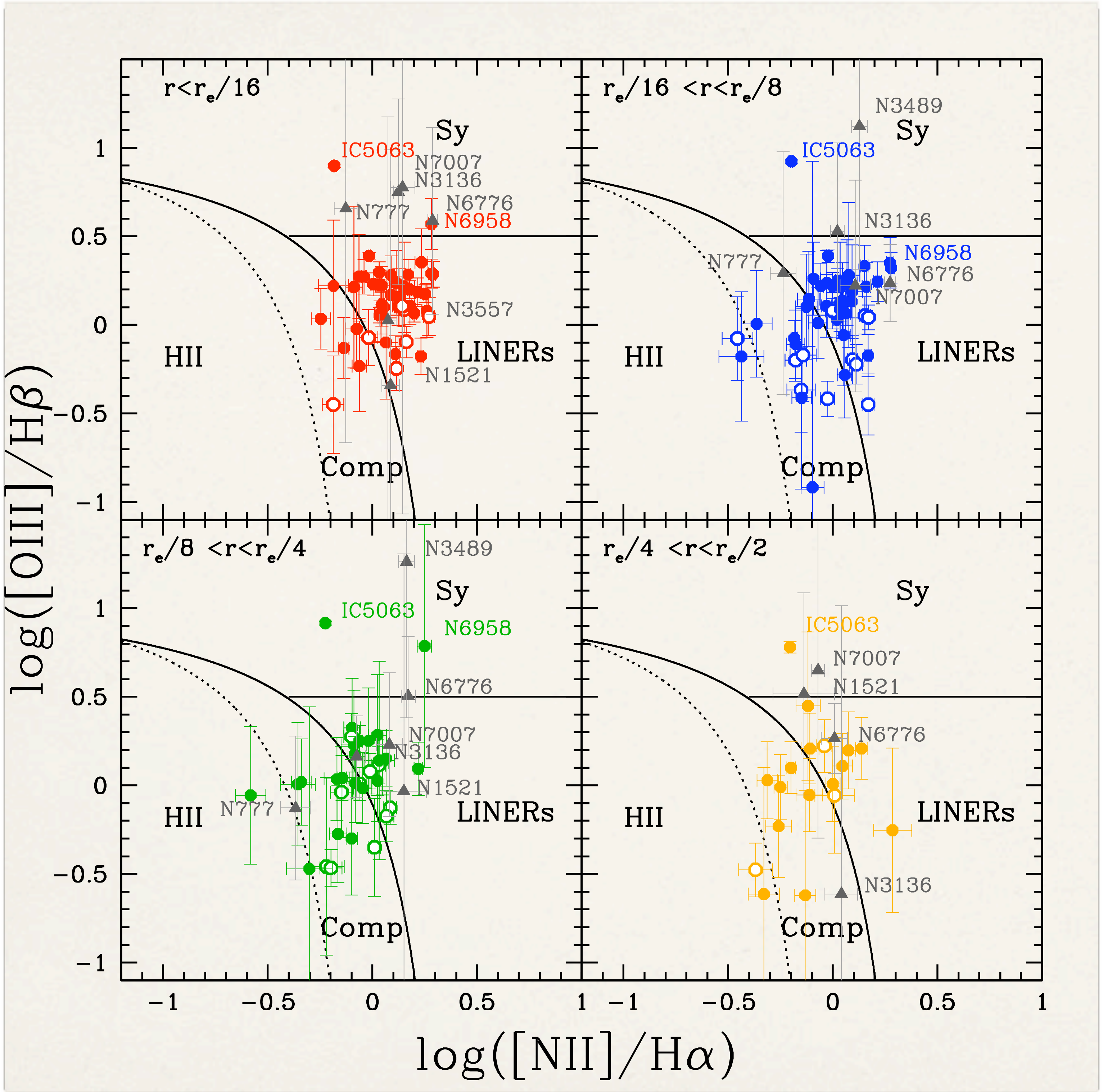

IC 5063, NGC 777, NGC 3489, NGC 3136, NGC 6776, NGC 7007, and NGC 6958 fall in the Seyfert region.

IC 5063 apart, all have large uncertainties in the [OIII]/Hb ratio. due to low Hb and are compatible with LINERs classification within errors.

The component in the ionizing spectrum decreases from the center outwards, and the galaxy classification tend to transit from LINER to Composite class. LINERs with strong lines require far more ionizing photons than AGB stars may provide. LINERs is likely and heterogeneous class of objects.

Extinction corrected BTP diagnostic diagram divided in annuli of increasing galacto-centric distance. The solid curve is the "maximum starburst line" of Kewley et al. (2001), while the dashed line indicates the empirical division between pure star-forming galaxies and AGN-HII composite objects (Kauffmann et al. 2003). The horizontal line at log([OIII]/Hβ)=0.5 separates Seyfert and LINER galaxies (Kewley et al. 2006).

AGN - star formation connection (Terlevich et al 1990; Heckman et al 1997; Kauffmann et al 2003; Cid Fernandes et al 2005; Davies et al 2007; Riffel et al. 2009)

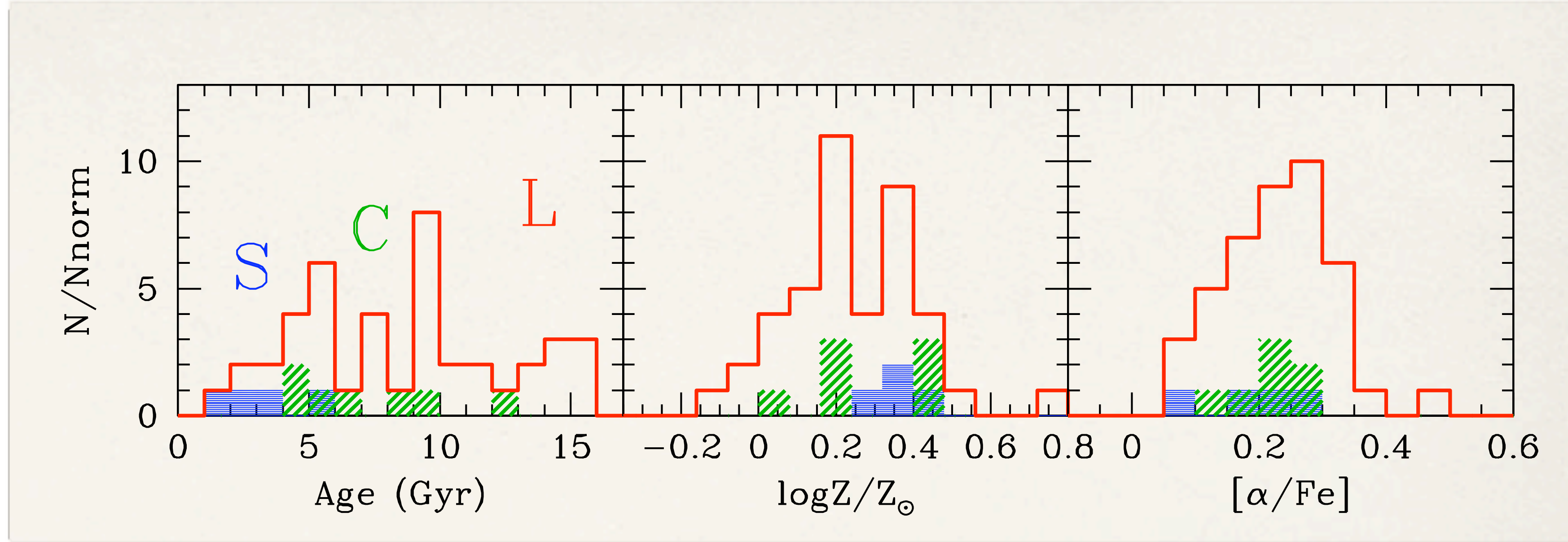

Age, metallicity and [α/Fe] distributions for Seyfert-like (S), LINERS (L) and Composite galaxies. The average Ages for S, C and L are 3.8, 7.5 and 9 Gyr, respectively. For the same classes, the average metallicities are log Z/Z 0.22, 0.29, 0.4 dex. The average [α/Fe] is always 0.2.

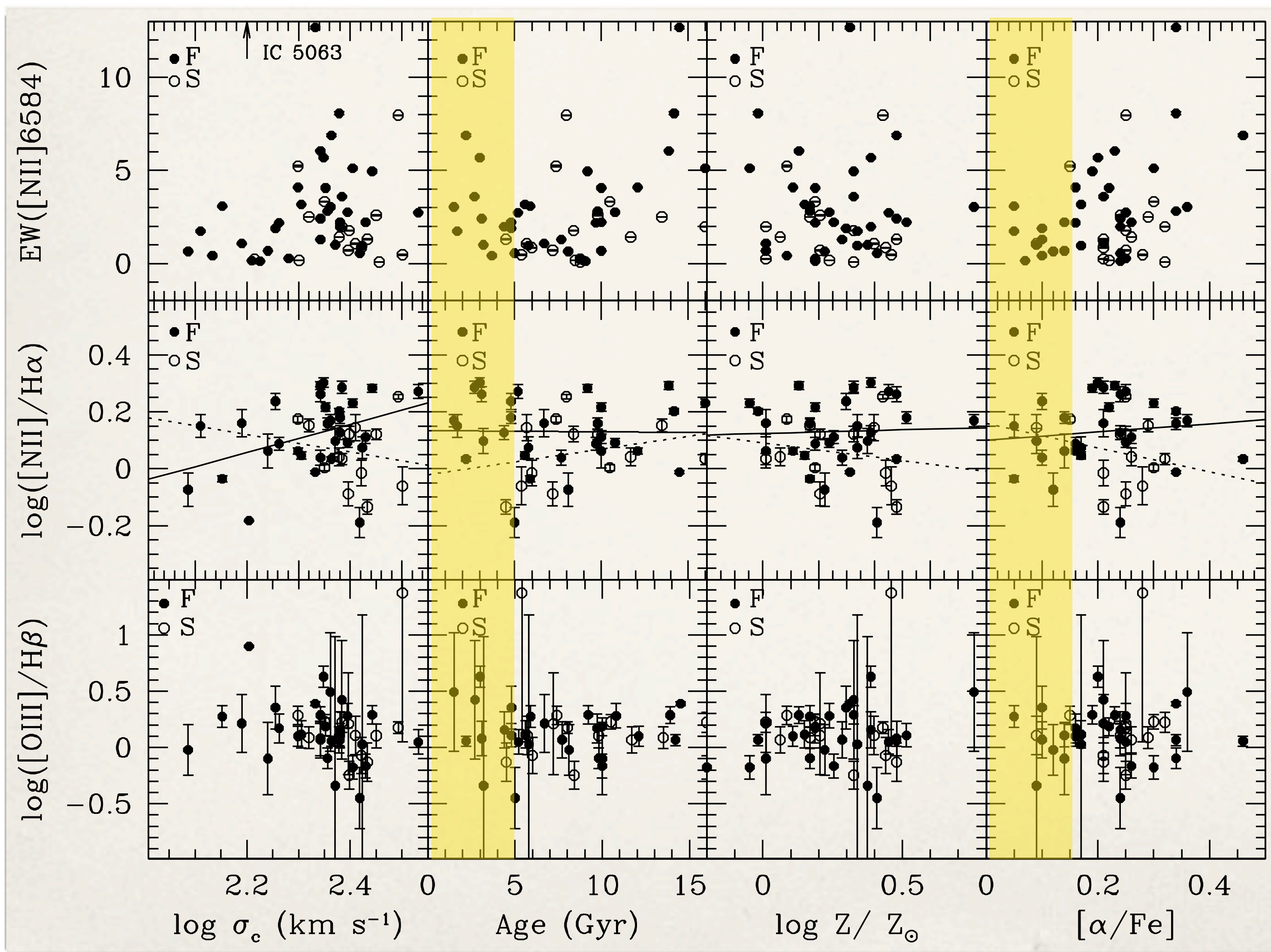

All young (< 5 Gyr) galaxies are Fast-rotators: namely NGC 1209, NGC 1380, NGC 1521, NGC 1553, NGC 3258, NGC 3607, NGC 6721, NGC 6776, NGC 6875, NGC 6958, NGC 7332 and NGC 7377. Seyfert galaxies have luminosity weighted ages ≤ 4 Gyr, and are younger than LINERs/Composite. This support the idea that the star formation and the AGN phenomenon coexist.

Gas vs. stars metallicity

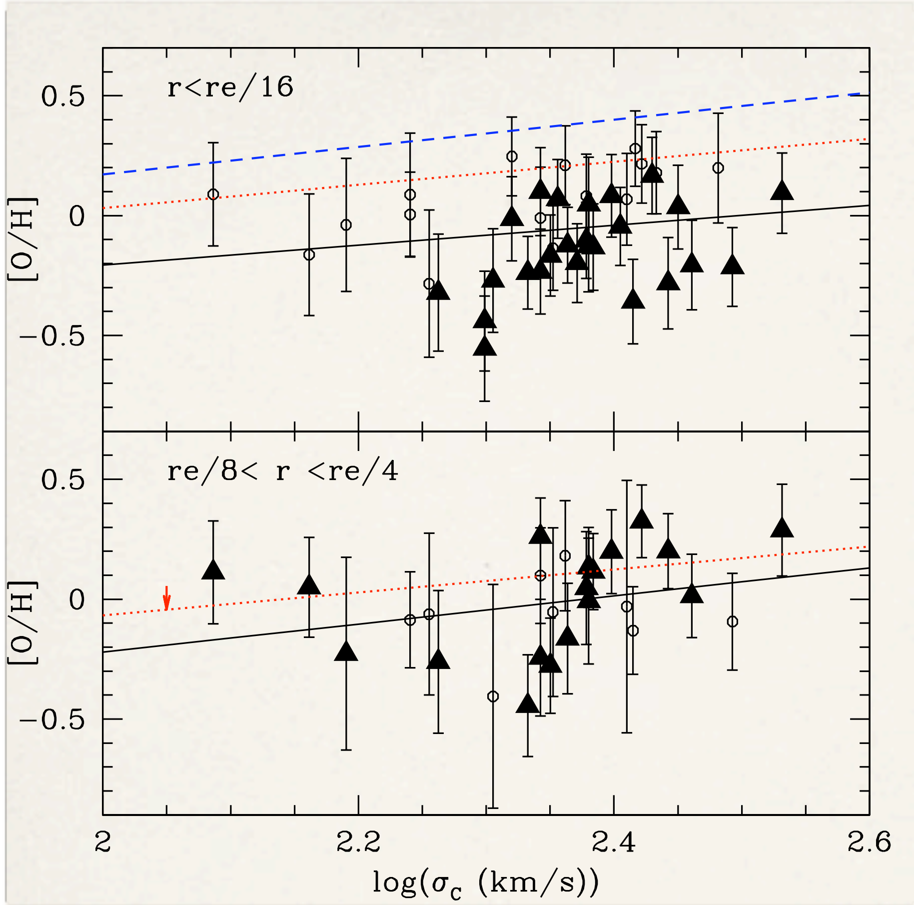

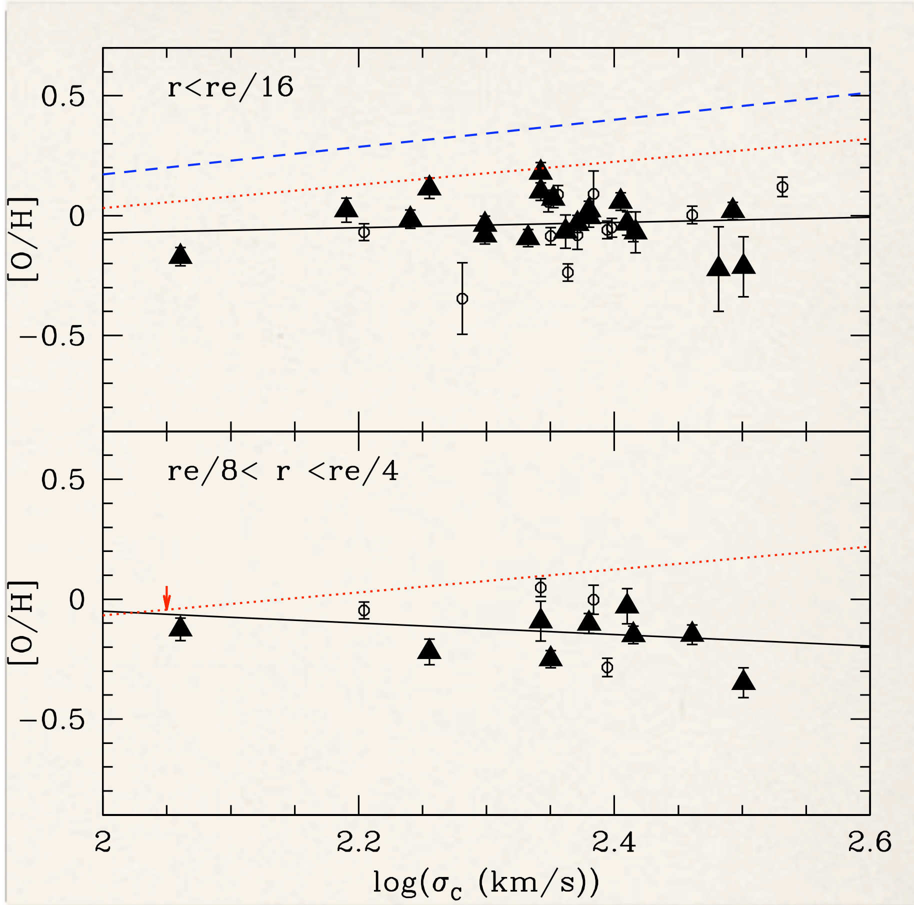

Oxygen abundances derived through HII (top left panels) and the Storchi-Bergmann et al (1998) (bottom) AGN calibration versus σ. Full symbols indicate the high emission galaxies (H).The solid lines are the least-square fits to the data. The dashed and the dotted lines are the metallicity-σ relation derived by Thomas et al. (2005) and Annibali et al. (2007) for the stellar populations of ETGs in low-density environment, respectively.

External gas acquisition ?

Anomalously low O abundance as compared to Fe and Mg also in X -ray emitting gas
(Humprhey & Buote 2006; Ji et al. 2009)

Powering mechanisms....

AGNs accreting at sub-Eddigton rate ? (Kewley et al. 2006; Ho et al. 2006)

Photoionization by old post-AGB stars ?

(Trinchieri & Di Serego Alighieri 1991; Binette 1994; Macchetto et al. 1996; Stasinska et al. 2008)

Fast shocks ? (Heckman 1980; Dopita & Sutherland 1995; Allen et al. 2008)

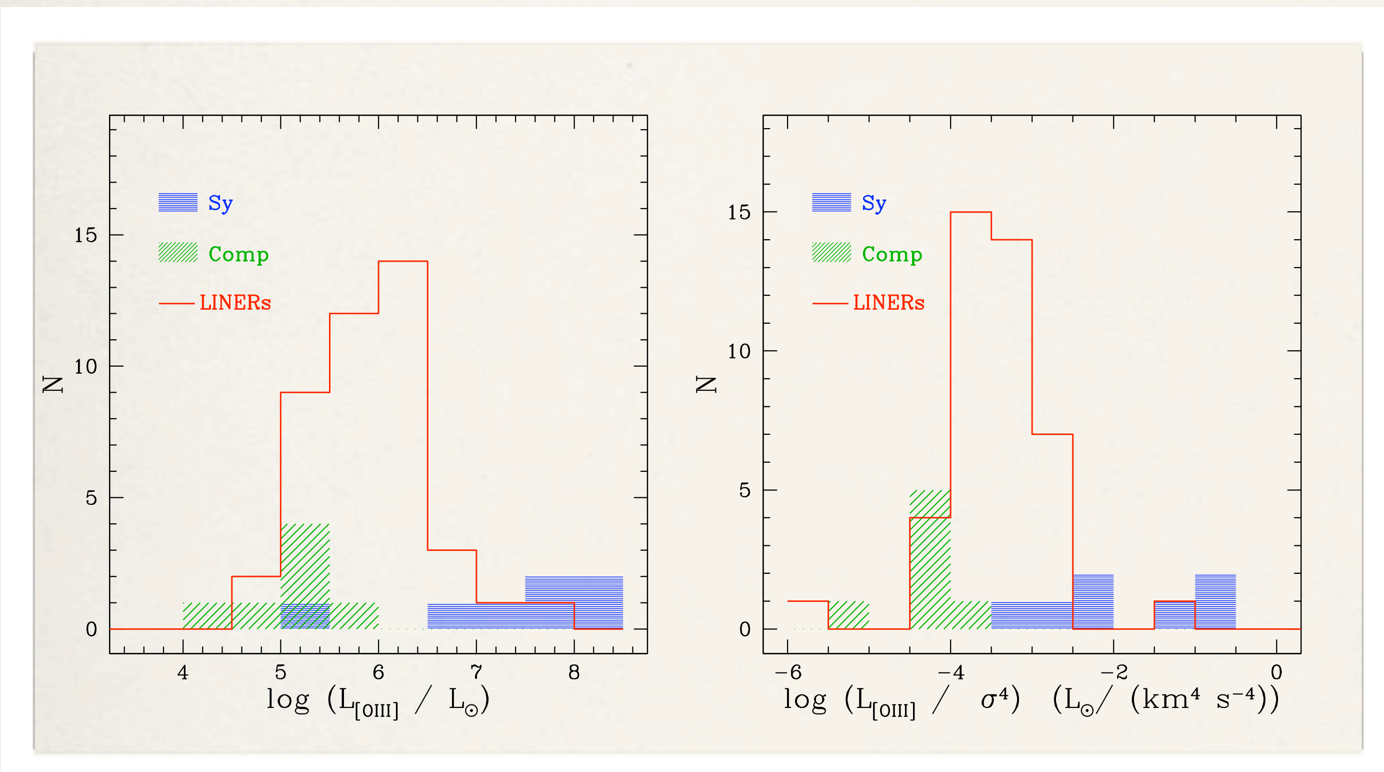

(top left panels) Distribution of the reddening corrected [OIII] luminosity for Seyferts, Composites and Liners. Distribution of L[OIII]/σ^4, where σ is the host galaxy velocity dispersion.

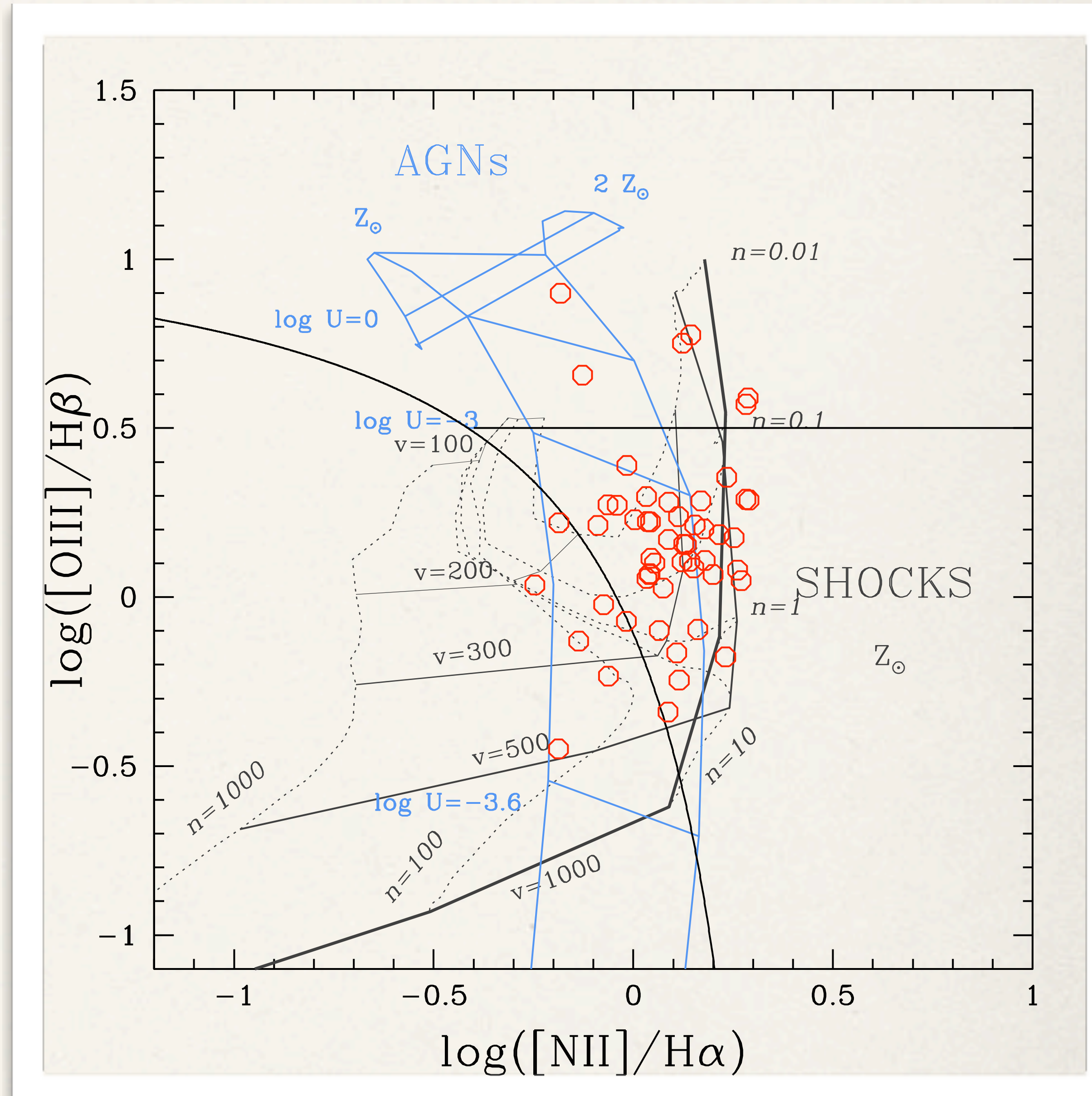

(top right panels) BTP diagram for our galaxies at $r_e < r_e/16$ (red circles) with superimposed the shock models of Allen et al. (2008) and the dusty-AGN models of Groves et al. (2004). The shock models have solar metallicity, densities from n=0.01 cm^{-3} to 1000 cm^{-3}, velocities from n =100 to 1000 km s^{-1} and magnetic parameter B=1. The AGN models have solar and twice solar metallicities, n=1000 cm^{-3} and ionization parameters from $log\ U$ = -4 to 0.

On going works: MIR *SPITZER-IRS* (40/65 ETGs)

“Passive” and “active” ETGs in Virgo: a comparison sample

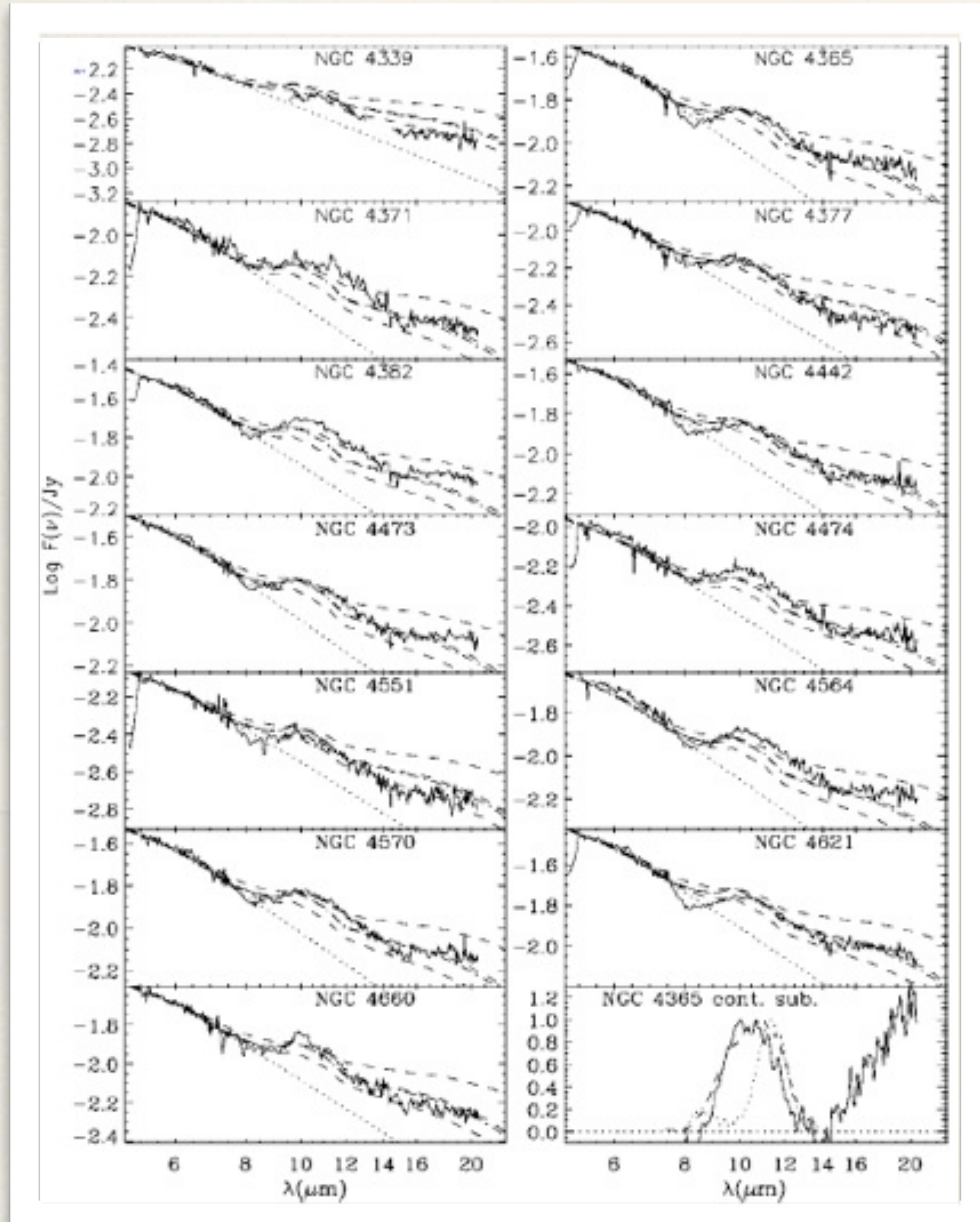

Bressan A., Panuzzo P., Buson L., Clemens M., Granato G.L. Et Al. 2006, ApJ, 639, L55

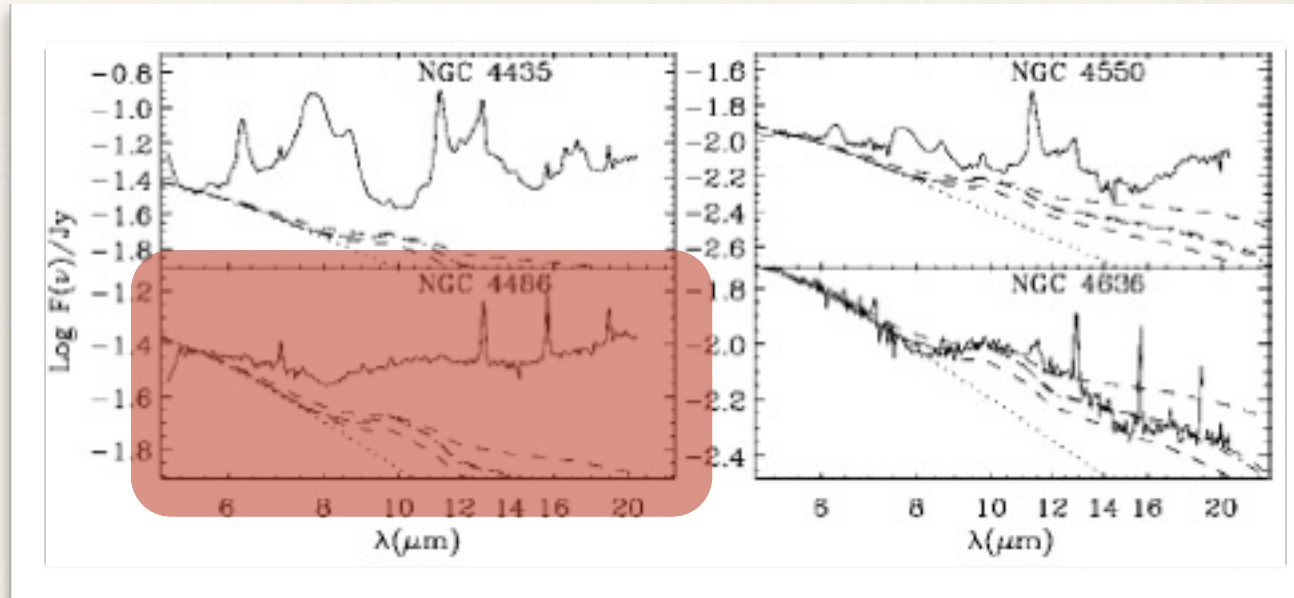

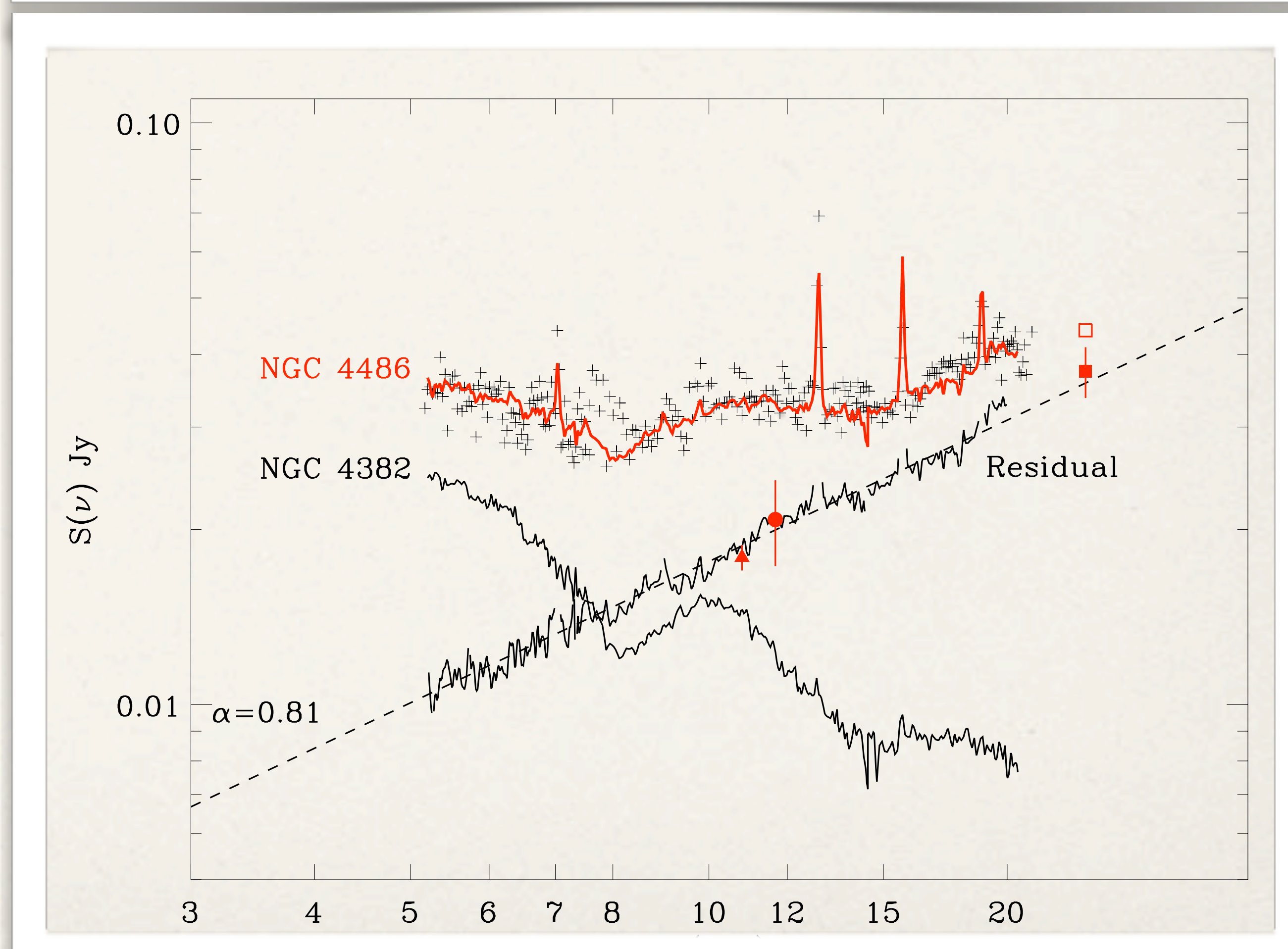

Buson L., Bressan A., Panuzzo P., Rampazzo, R., Valdes J.R. Et Al. 2009, Ap,J In Press

“Passive” and “active” ETGs in the low density sample (LDE)

Table 2. The *Spitzer*–IRS observations

ident	PI	ID	SL1 [s×Cycle]	SL2 [s×Cycle]	LL2 [s×Cycle]	LL1 [s×Cycle]
NGC 1052	Kaneda	30483	60×2	60×2	30×2	30×2
NGC 1209	Rampazzo	30256	60×6	60×6	120×16	120×8
NGC 1297	Rampazzo	30256	60×19	60×19	120×14	120×8
NGC 1366	Rampazzo	30256	60×11	60×11	120×14	120×8
NGC 1389	Rampazzo	30256	60×9	60×9	120×14	120×8
NGC 1407	Kaneda	3619/30483	60×2	60×2	30×2	30×2
NGC 1426	Rampazzo	30256	60×12	60×12	120×14	120×8
NGC 1453	Bregman	3535	14×8	14×8	30×6	
NGC 1533	Rampazzo	30256	60×3	60×3	120×5	120×3
NGC 1553	Rampazzo	30256	60×3	60×3	120×3	120×3
NGC 2974	Kaneda	3619/30483	60×2	60×2	30×3	30×3
NGC 3258	Rampazzo	30256	60×8	60×8	120×14	120×8
NGC 3268	Rampazzo	30256	60×9	60×9	120×14	120×8
NGC 3557	Kaneda	30483	60×3	60×3	30×3	30×3
NGC 3818	Rampazzo	30256	60×19	60×19	120×14	120×8
NGC 3962	Kaneda	3619/30483	60×2	60×2	30×3	30×3
NGC 4374	Rieke	82	60×4	60×4	120×4	120×4
NGC 4552	Bregman	3535	14×8	14×8	30×6	
NGC 4636	Bressan	3419	60×3	60×3	120×5	
NGC 4696	Kaneda	3619/30483	60×2	60×2	30×3	30×3
NGC 4697	Bregman	3535	14×8	14×8	30×6	
NGC 5011	Rampazzo	30256	60×6	60×6	120×12	120×8
NGC 5044	Rampazzo	30256	19	19	14	8
NGC 5077	Rampazzo	30256	60×12	60×12	120×14	120×8
NGC 5090	Kaneda	30483	60×4	60×4	30×3	30×3
NGC 5638	Bregman	3535	14×8	14×8	30×6	
NGC 5812	Bregman	3535	60×6	60×6	120×12	120×8
NGC 5813	Bregman	3535	14×8	14×8	30×6	
NGC 5831	Bregman	3535	14×8	14×8	30×6	
NGC 5846	Bregman	3535	14×8	14×8	30×6	
NGC 5898	Rampazzo	30256	60×11	60×11	120×14	120×8
NGC 6868	Rampazzo	30256	60×6	60×6	120×13	120×8
NGC 7079	Rampazzo	30256	60×19	60×19	120×14	120×8
NGC 7192	Rampazzo	30256	60×12	60×12	120×14	120×8
NGC 7332	Rampazzo	30256	60×7	60×7	120×14	120×8
IC 1459	Kaneda	30483	60×3	60×3	30×2	30×2
IC 2006	Bregman	3535	14×8	14×8	30×6	
IC 3370	Kaneda	3619/30483	60×2	60×2	30×3	30×3
IC 4296	Antonucci	20525	240×2	240×2	120×3	120×3
IC 5063	Gorjan	30572	14×2	14×2	30×1	30×1

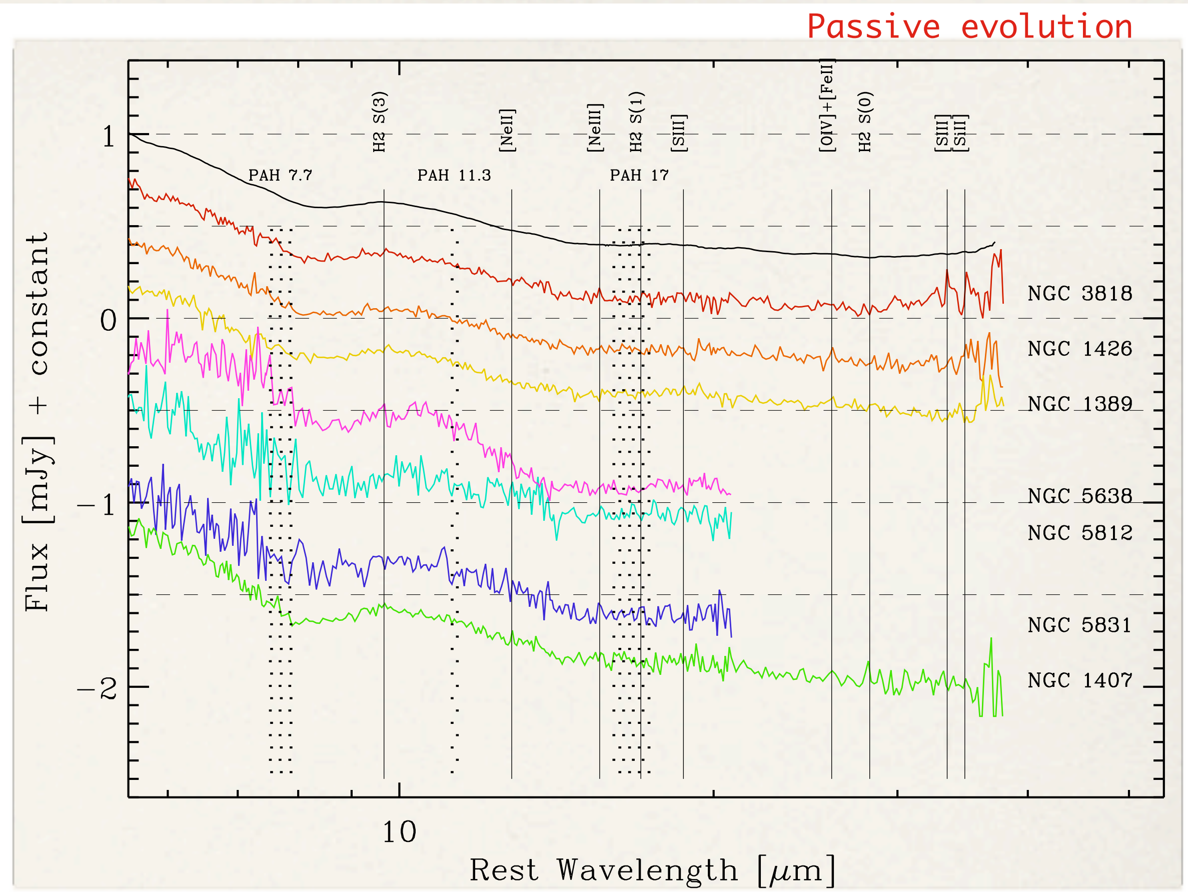

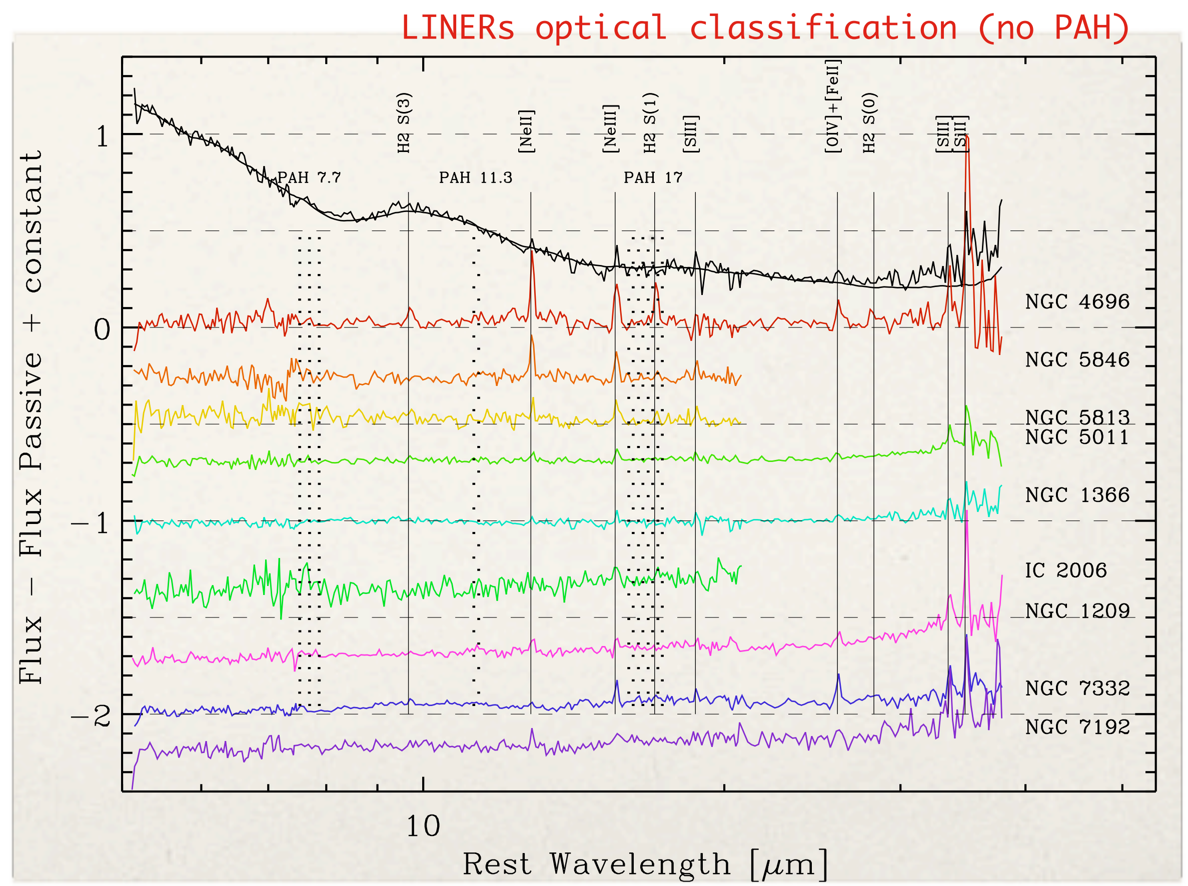

Panuzzo P., Rampazzo R., Bressan A., Vega O. Et Al. 2009, In Preparation

LINERs optical classification (lines + PAH in MIR)

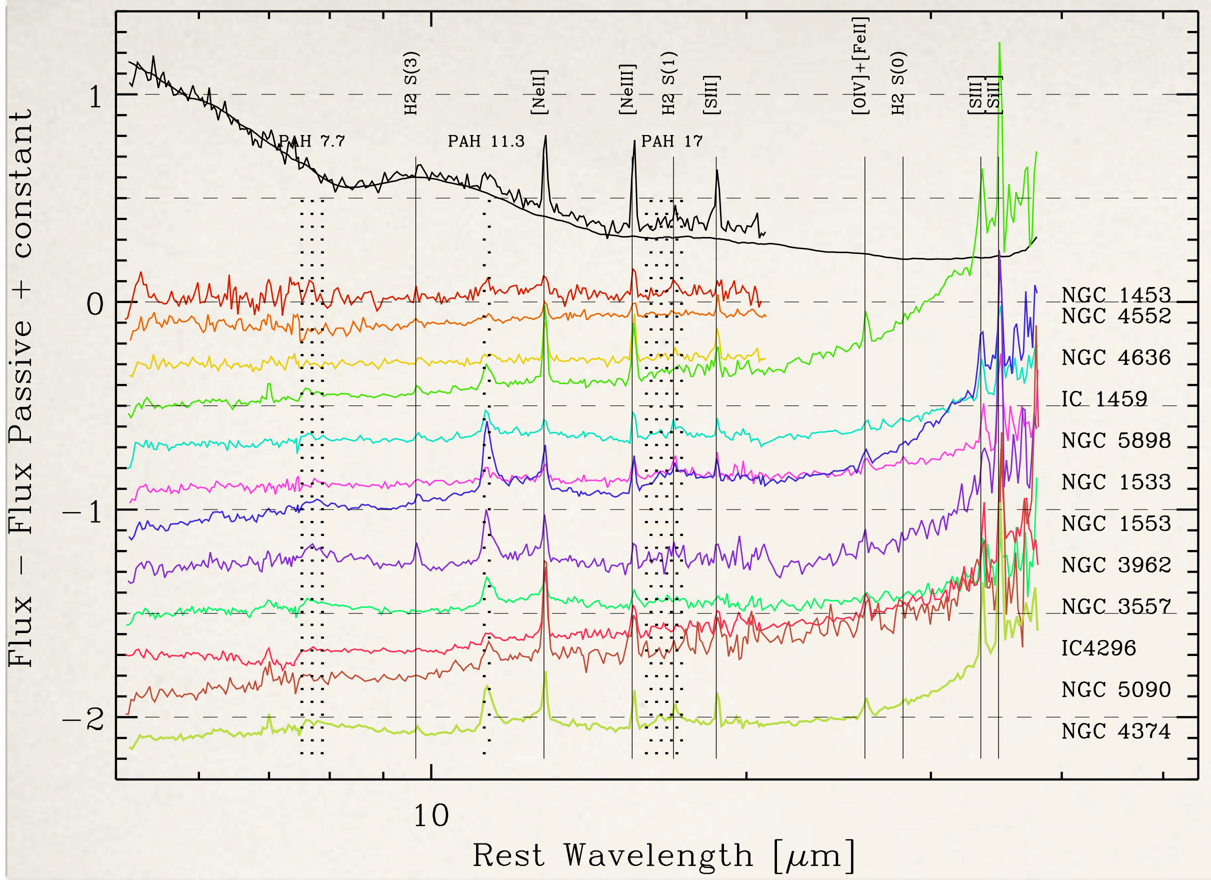

LINERs optical classification (H2 lines + PAH in MIR)

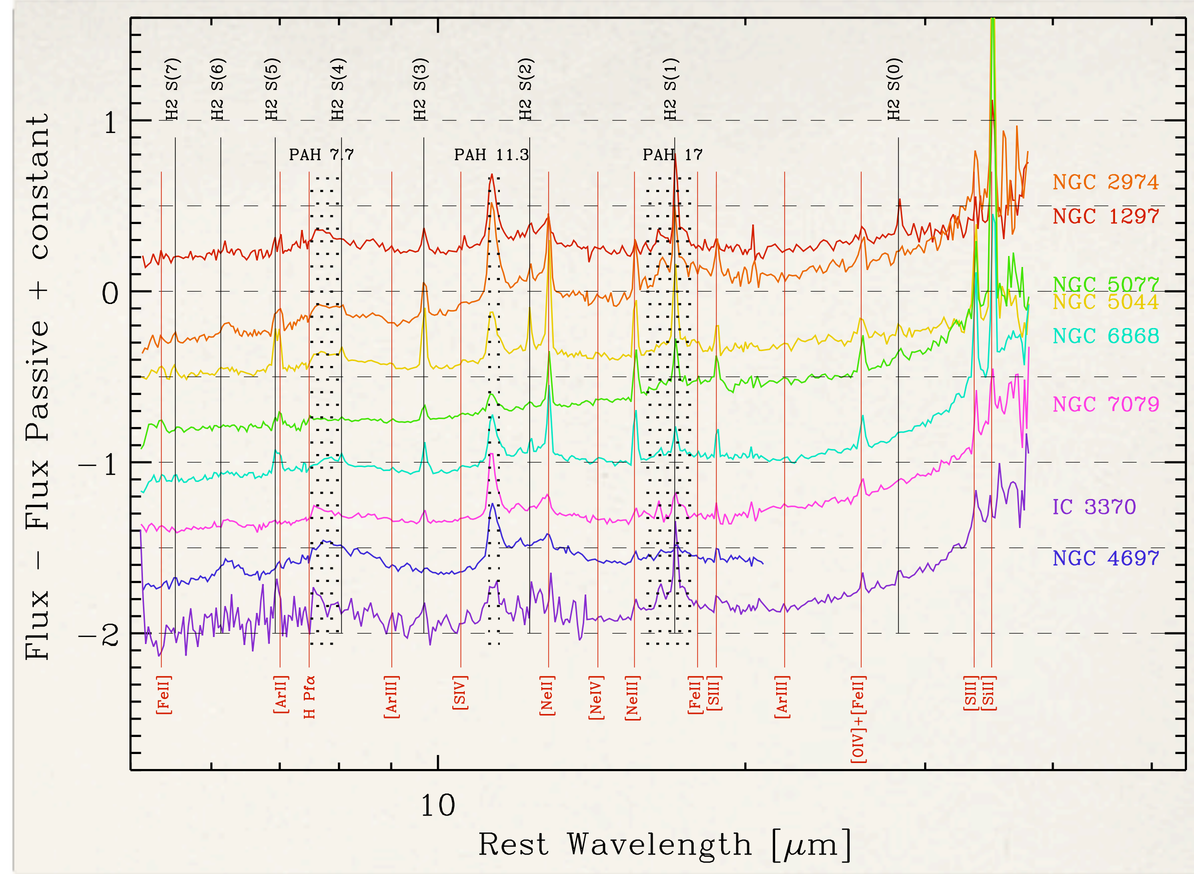

NGC 3258 Composite NGC 3268 LINER (starbursts PAH dominated in MIR)

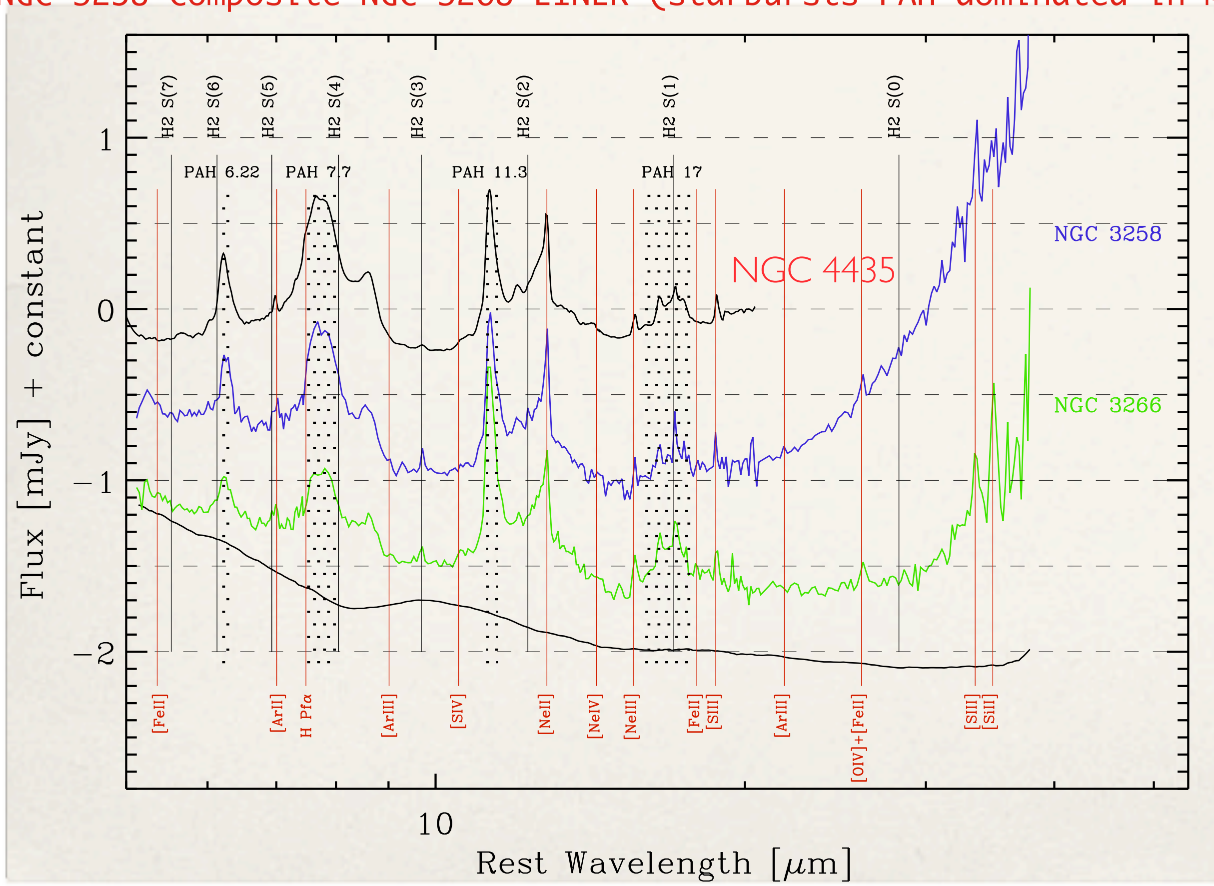

NGC 1052 LINER IC 5063 AGN (AGN in MIR)

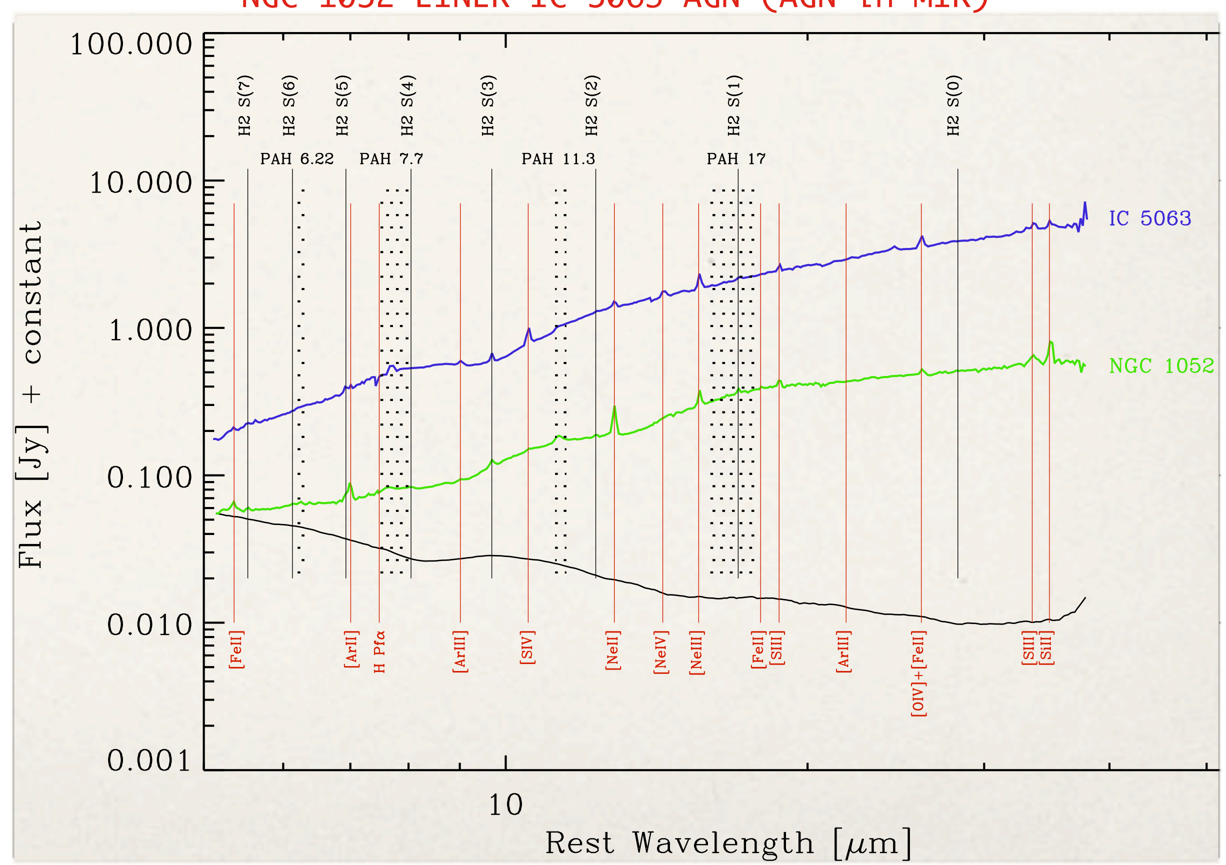

OPTICAL

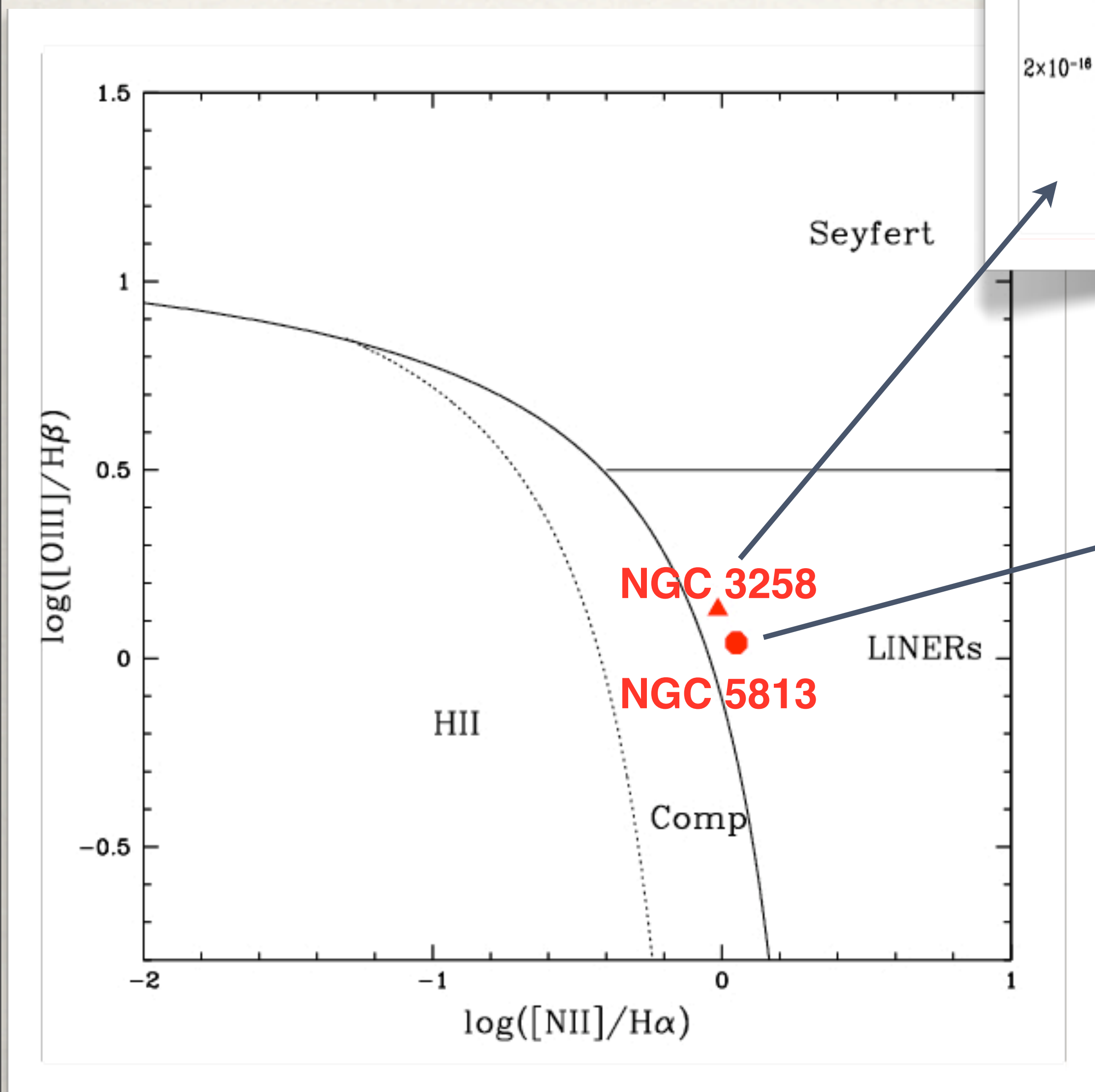

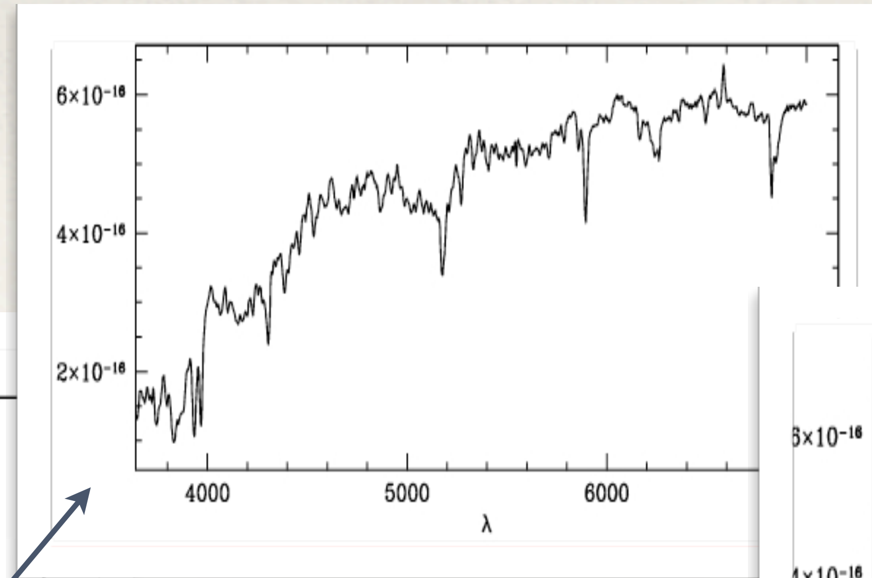

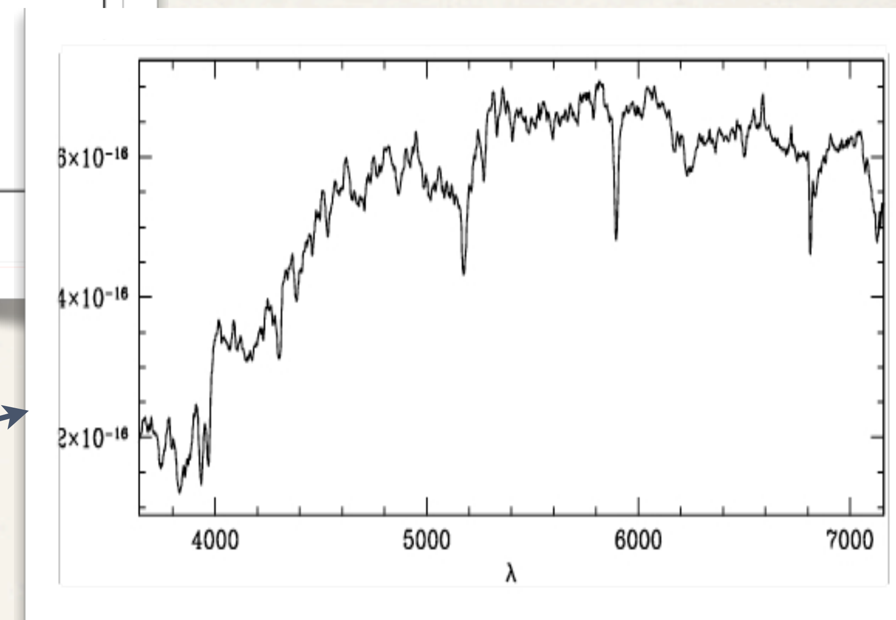

Mid Infrared

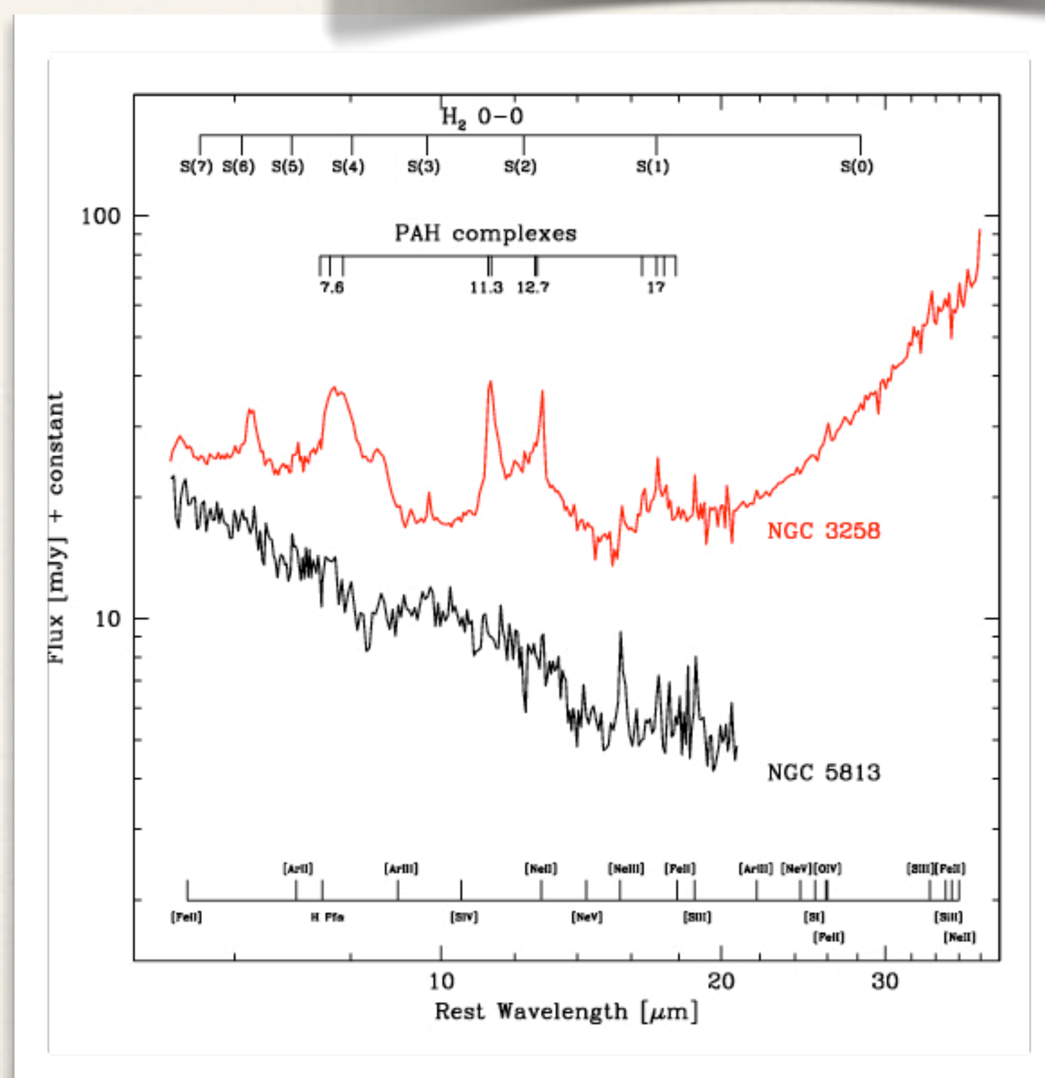

About 60% of our ETGs show clear PAH emission (in the Kaneda sample 14/18 i.e. 78%)
About 42% of our ETGs show clear H2 emission (in the Kaneda sample 15/18 i.e. 83%)
some of ETGs show the full H2 0-0 series (S(0) to S(7))

More frequently detected are the following lines:

[NeII] 12.81 [SIII] 18.73 & 33.40
[NeIII] 15.55 [SiII] 34.81
[OIV+FeII] blend 25.91+25.98

We expect to better classify ETGs "activity" in the nuclear part through mixed optical-MIR diagnostic diagrams.

In particular optical-lines vs. PAH emission ...

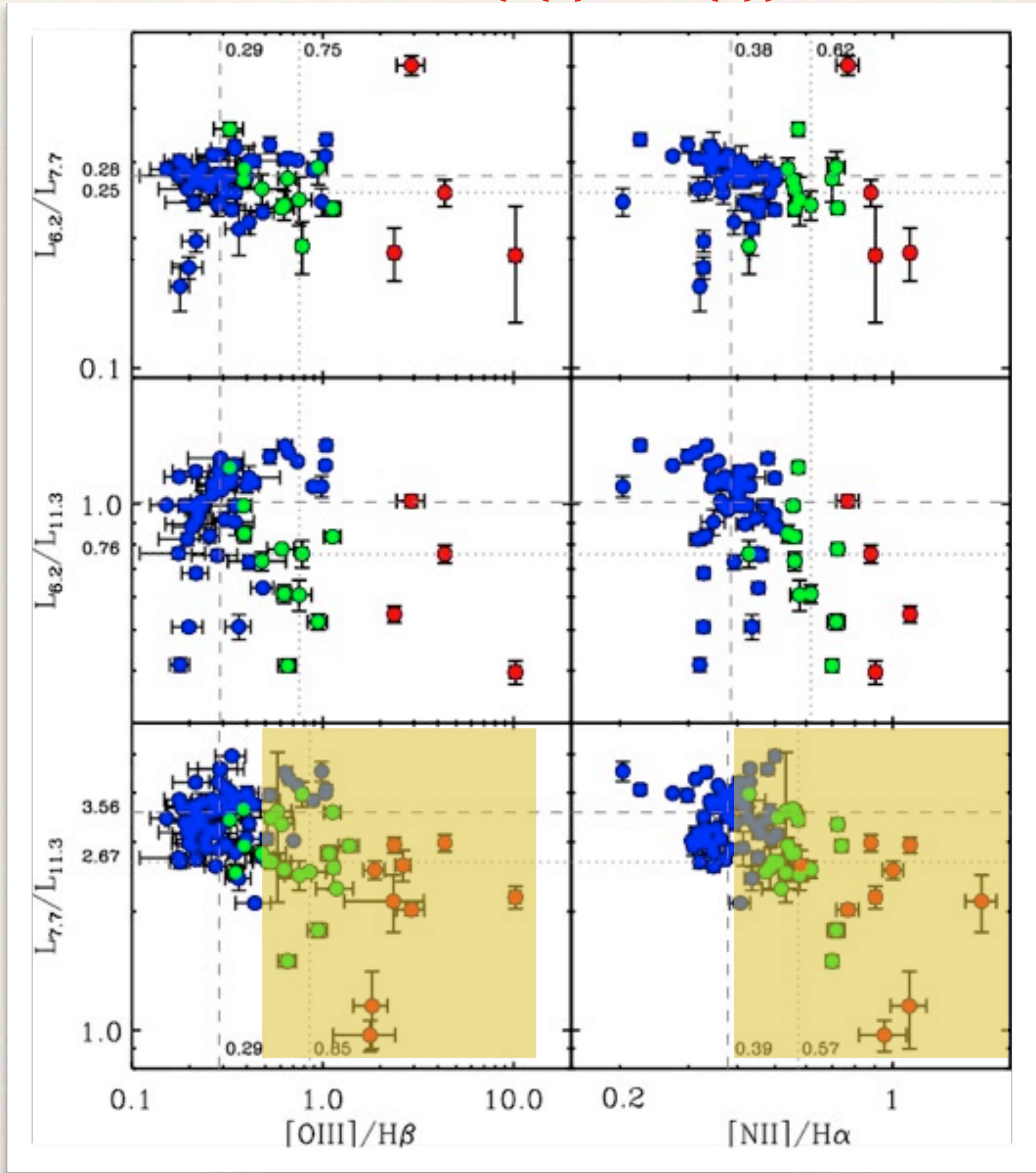

PAH ratio vs. [NII]/Hα and [OIII]/Hβ. Red dots are Seyferts, green dots Composite and blue dots Star Forming (from O'Dowd et al. 2009 ApJ 705, 885). Data are from Spitzer SDSS GALEX Spectroscopic Survey (SSGSS).

.... and either optical vs. MIR emission lines or MIR emission line diagnostic diagrams.

E.g. some results about H_2 ETGs: NGC 1297, NGC 3258, NGC 4374, NGC 4435, NGC 5044

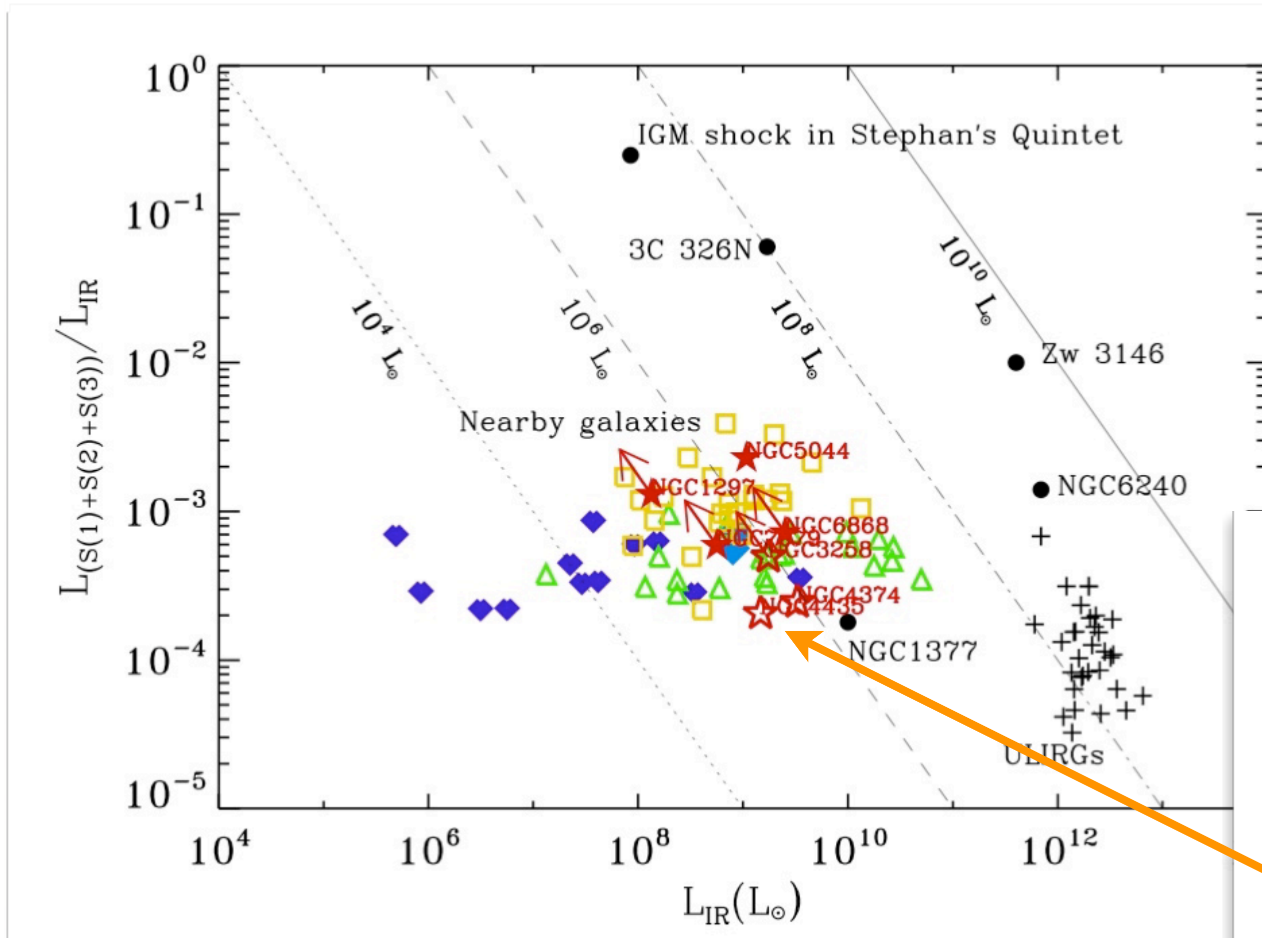

The ratio of the luminosity in the sum of the S(1), S(2), S(3) lines (of the ground vibrational state) of H_2 to the IR luminosity of the system is plotted vs. the IR luminosity for some of our ETGs (stars). For comparison, dwarfs + tidal dwarfs (diamonds), star-forming galaxies (triangles), LINERs+Seyferts nuclei (squares), ULIRGs and the shock heated IGM in the Stefan's Quintet are also shown (see Soifer et al. 2008, ARA&A, 46, 201). Arrows indicate lower limits.

NGC 4435 is an Elliptical located in the Virgo cluster interacting with the spiral NGC 4438. Here we show the comparison in the range 0.1 mm to 30 cm between the observed SED of NGC 4435 central region and our model. The thick white line represents the model for the total SED, i.e. a starburst component plus an old stellar component. The best fist of the NGC 4435 SED can be obtained with a old stellar population of 8 Gyr (98.5%) and 200 Mys (1.5%). We did not measured an appreciable AGN activity in the galaxy (< 2%, if any).(Panuzzo et al. 2007, ApJ, 656, 206). See Vollmer et al. (2005, A&A, 441, 473) for simulation and CO observations.

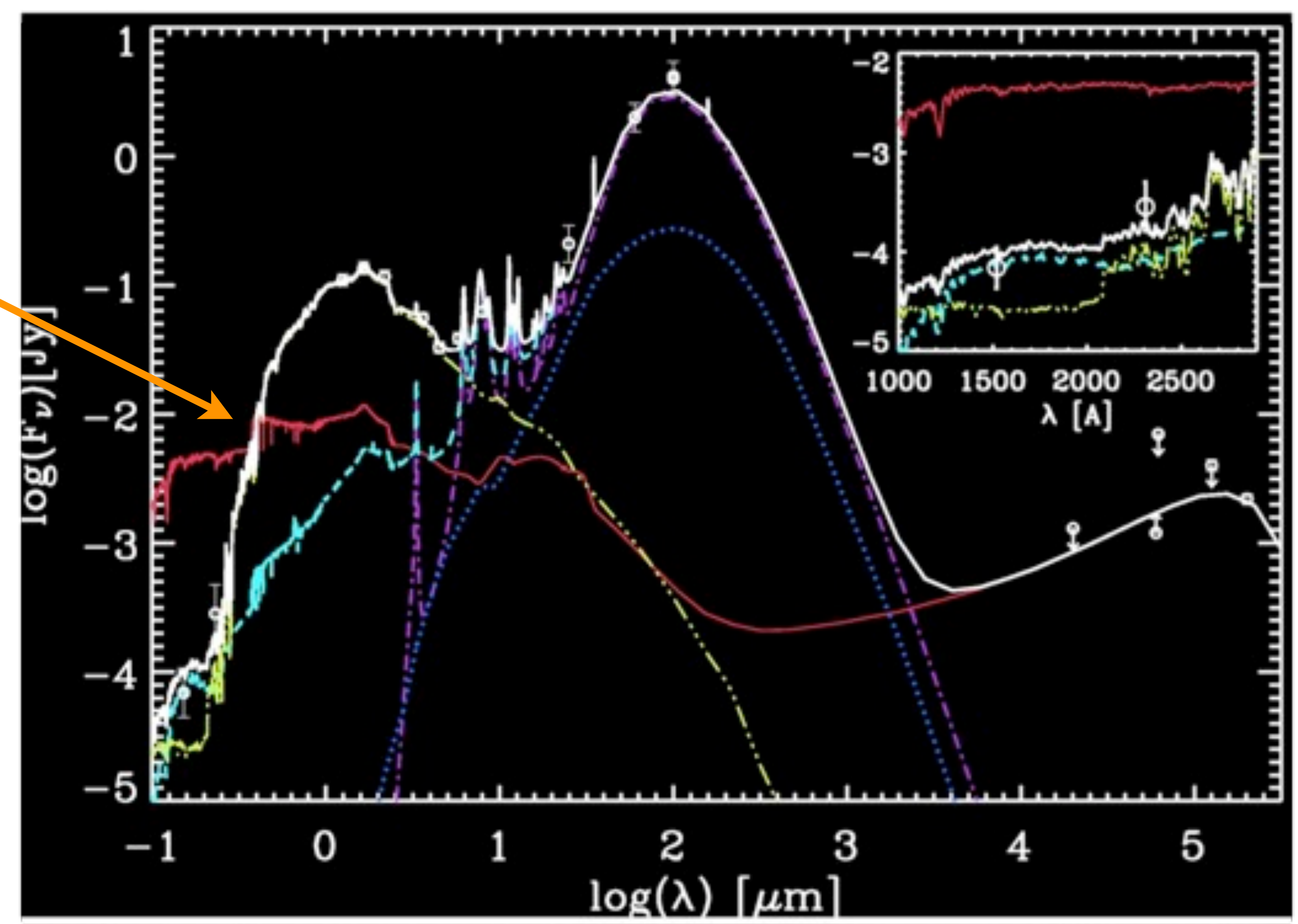

Far UV *GALEX* imaging (40/65 ETGs)

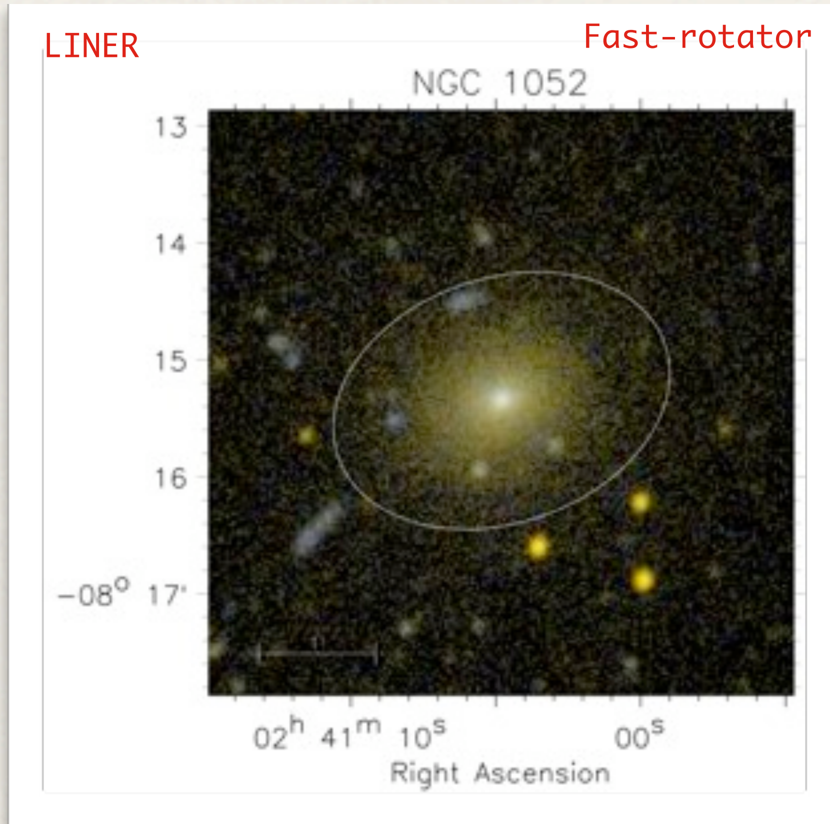

FUV and NUV combined + SLOAN (bottom) 5'x5' images of the elliptical galaxy (E4) NGC 1052. Right panels display FUV and NUV surface brightness luminosity profiles and (FUV-NUV) color profiles.

From a nuclear to a galactic view of "rejuvenation" phenomena

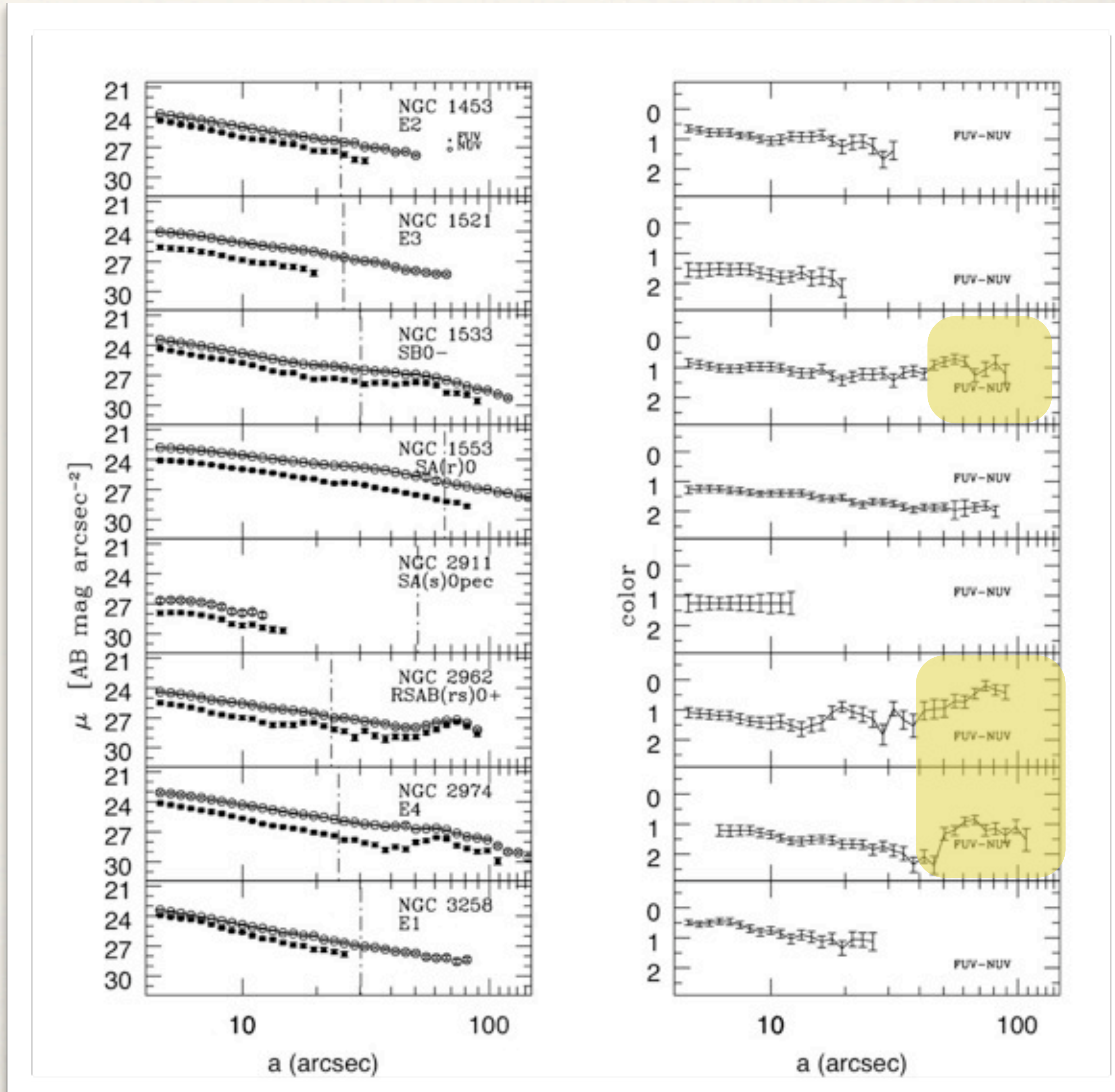

Marino A., Rampazzo R., Bianchi L., Annibali F., Bressan A. Et Al. 2009, In Preparation

LINER

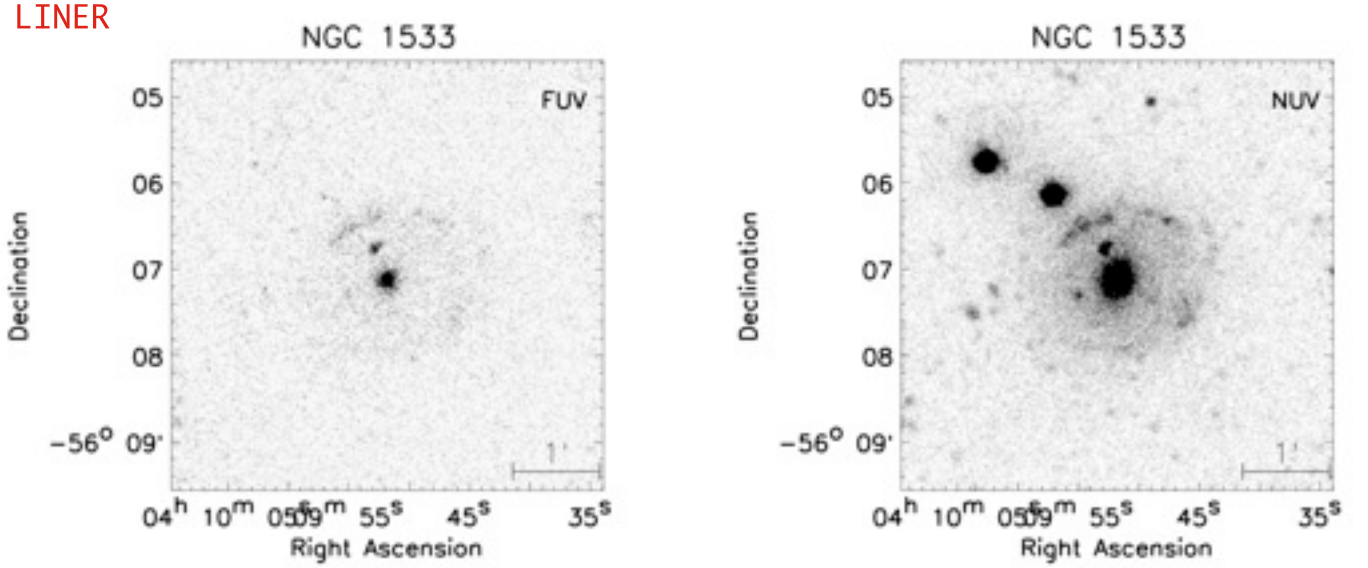

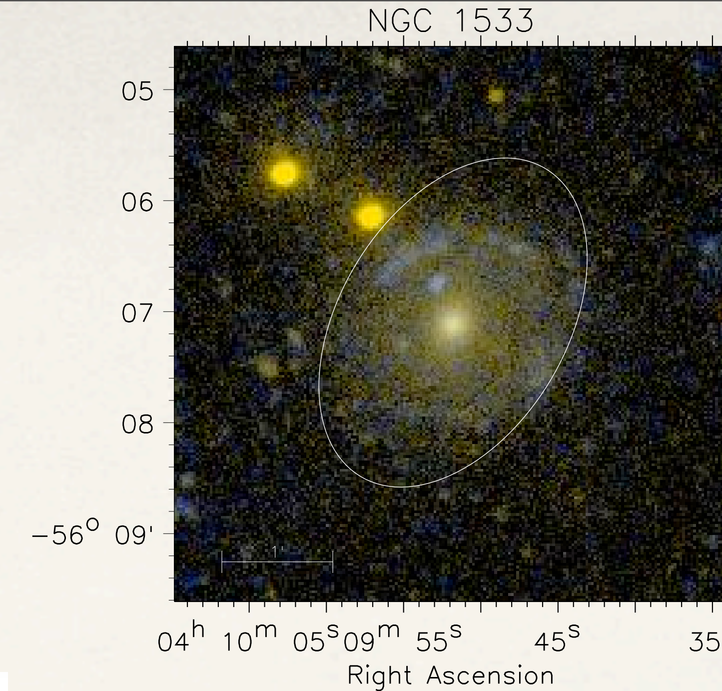

FUV and NUV combined. The ellipse is the D_{25} isophote.

Age=4.8 ± 0.7

LINER

Fast-rotator

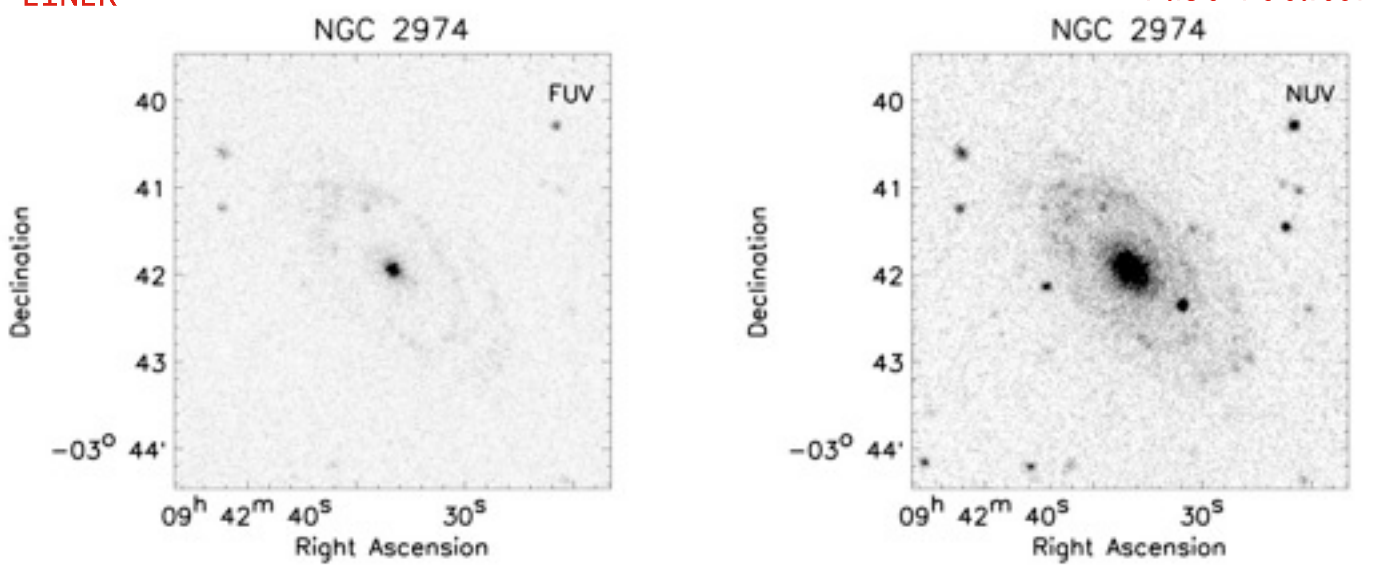

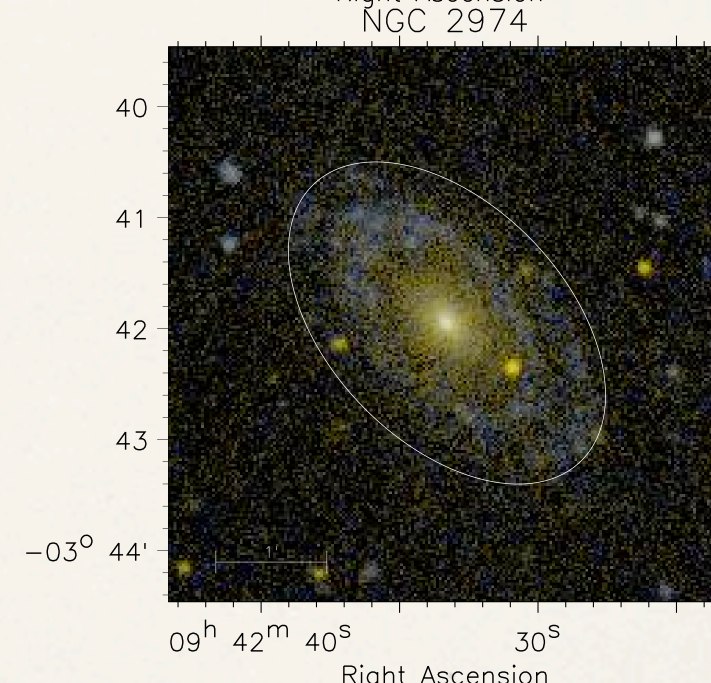

Age=13.9 ± 3.6

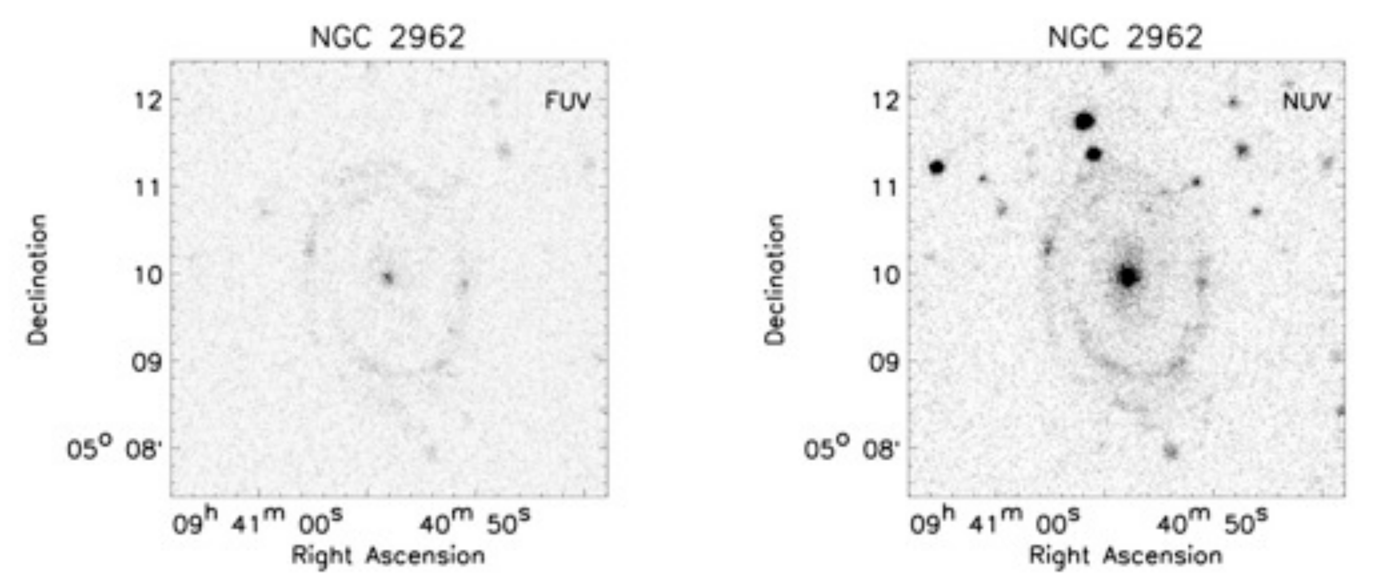

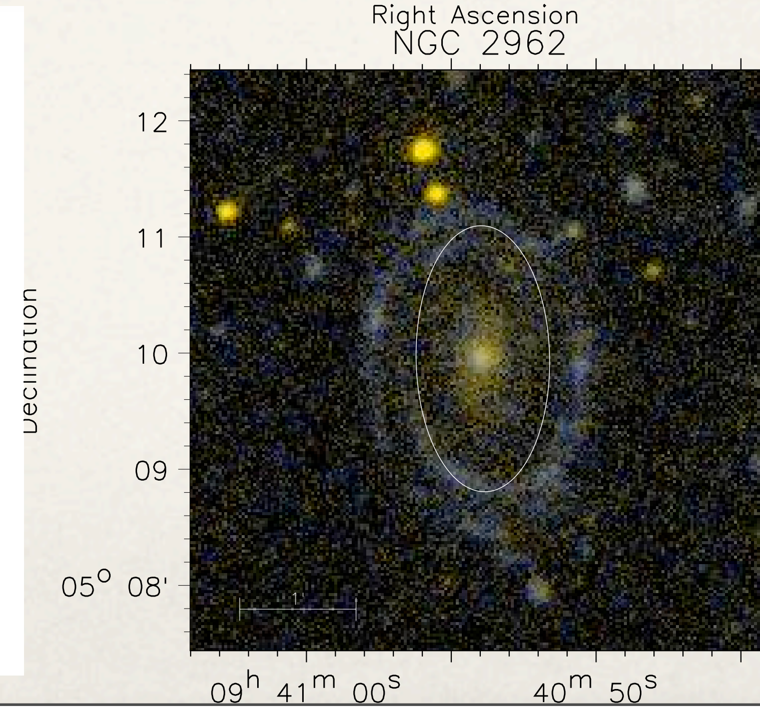

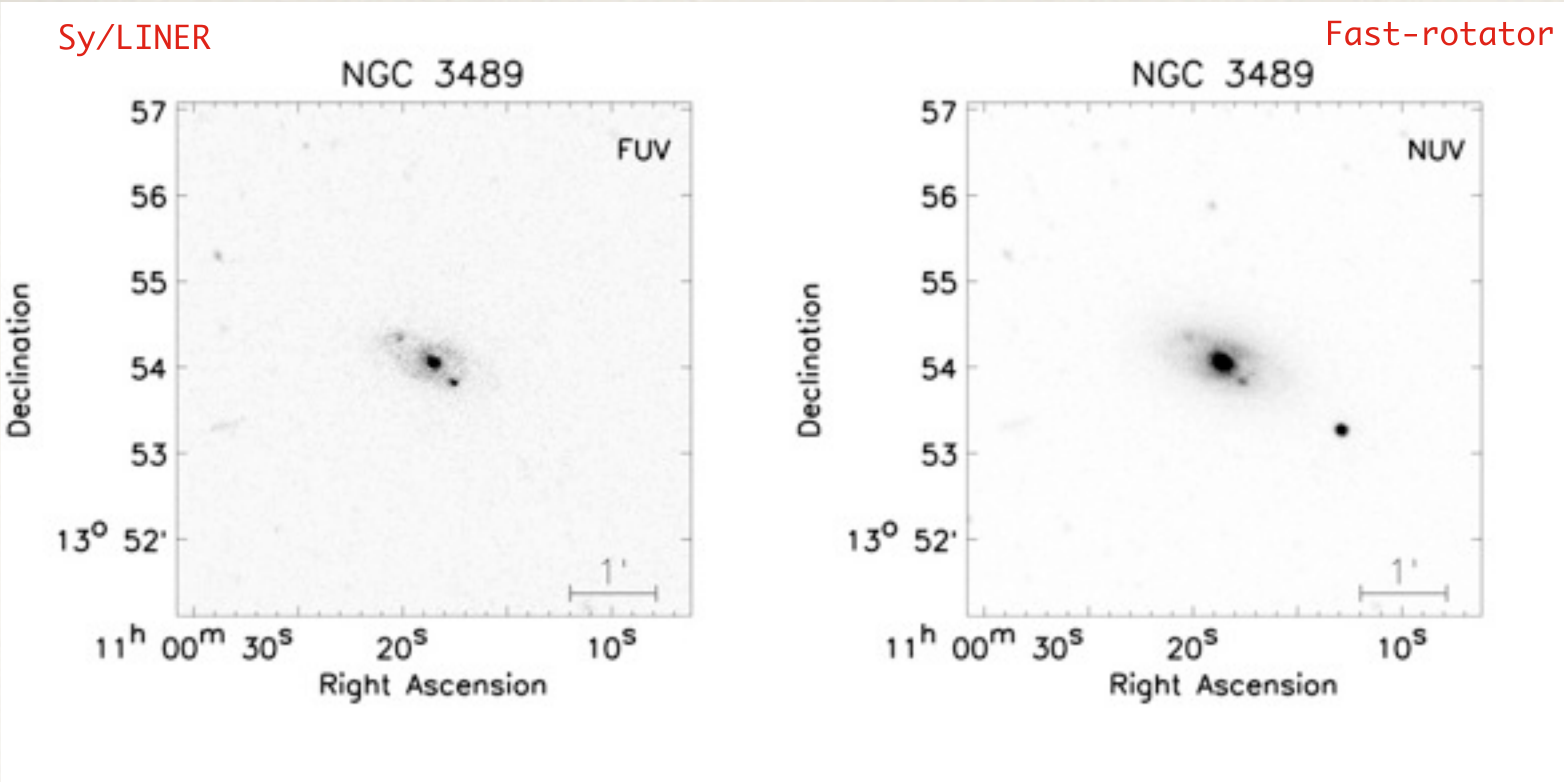

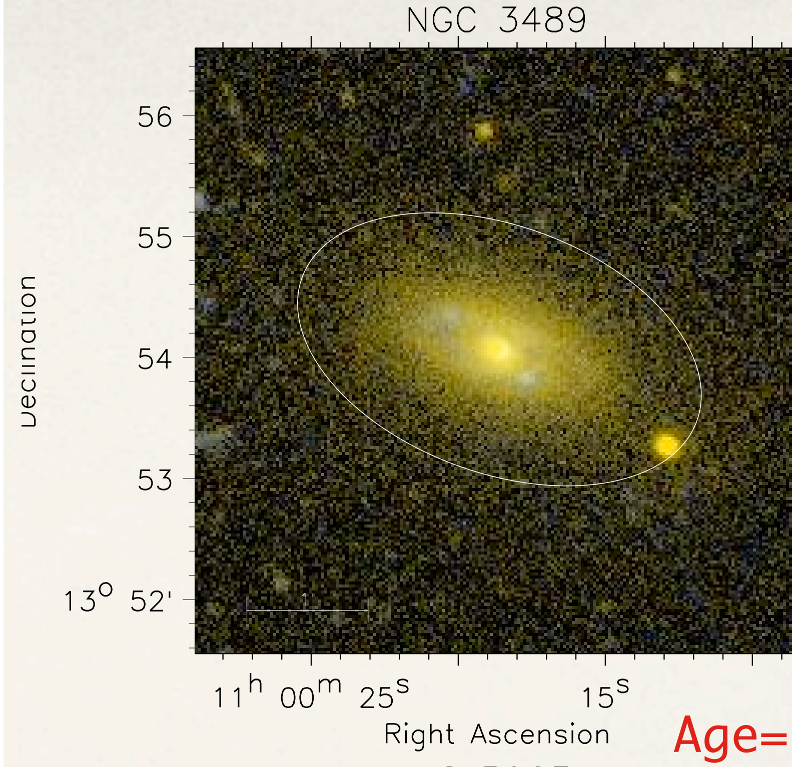

Age=1.7 ± 0.1

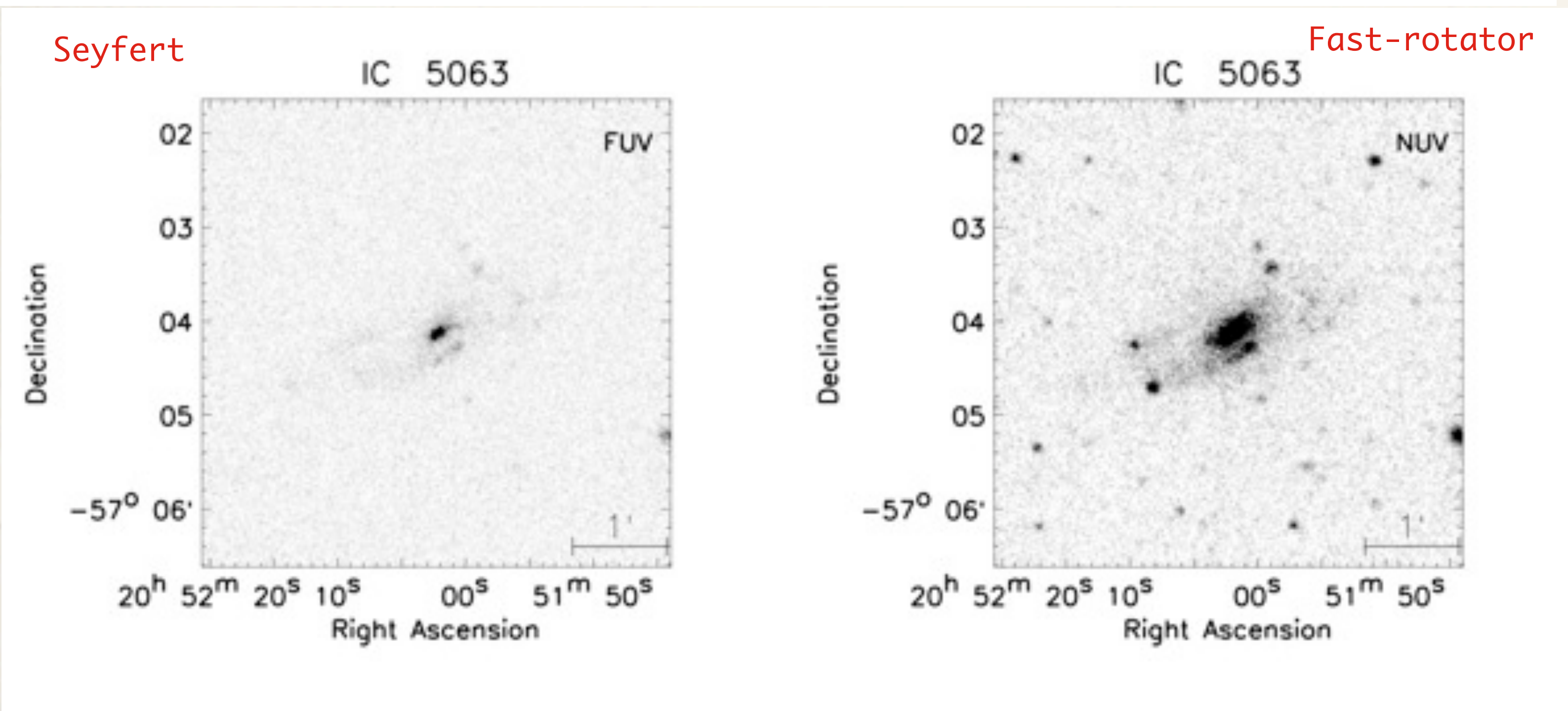

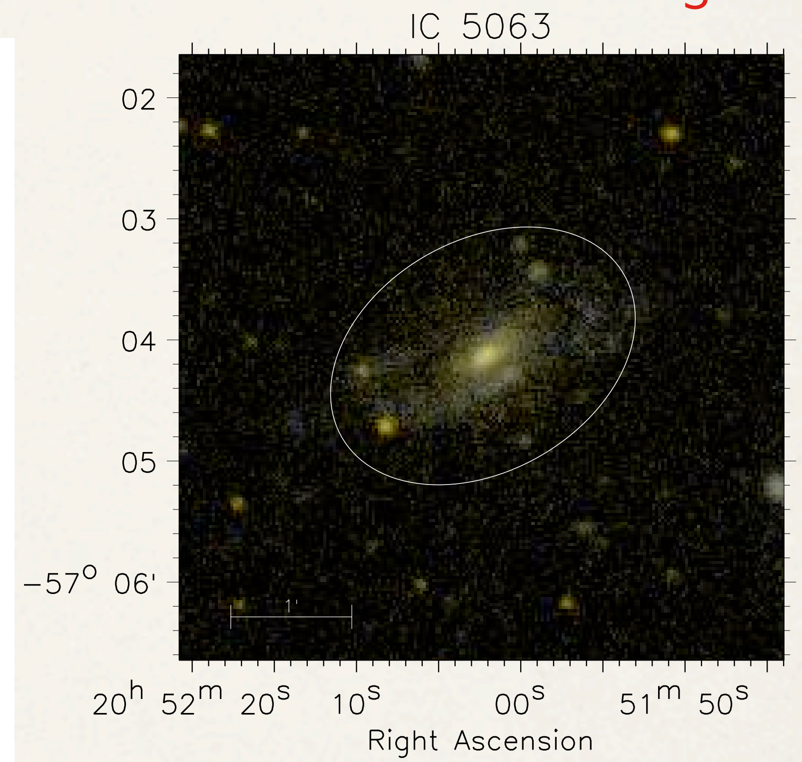

FUV and NUV full resolution + combined images. Blue areas are dominated by the FUV emission. Some barred S0s, fast rotators, show peculiar ring/arm-like features.

Likely these rings have an internally driven origin (e.g. orbits crowding and gas accumulation at the Lindblad's resonances; see Buta & Combes 1996) ....

... and differ both from rings generated by galaxy-galaxy interaction (e.g. head-on collisional rings, and from merging events, e.g. polar rings).

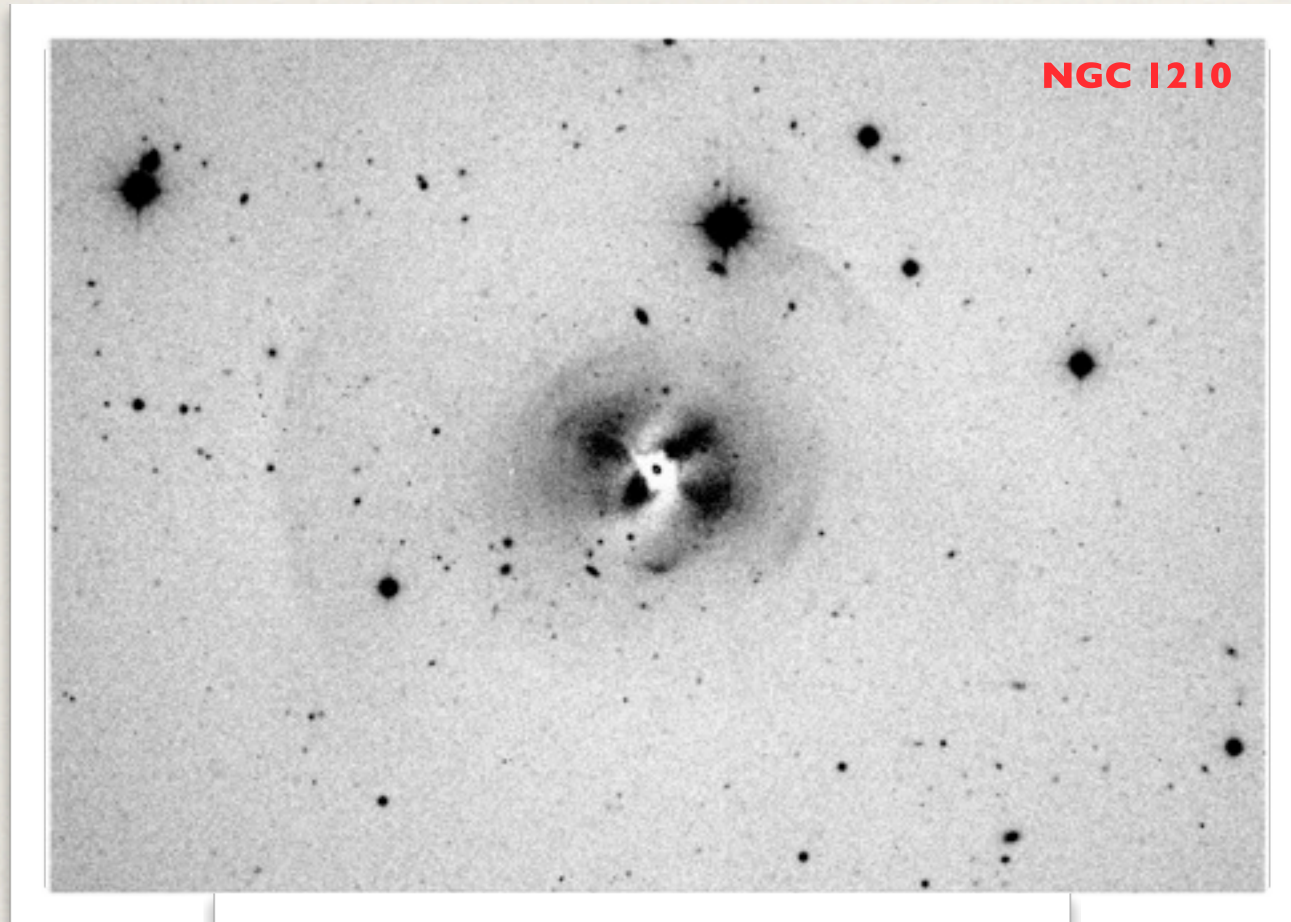

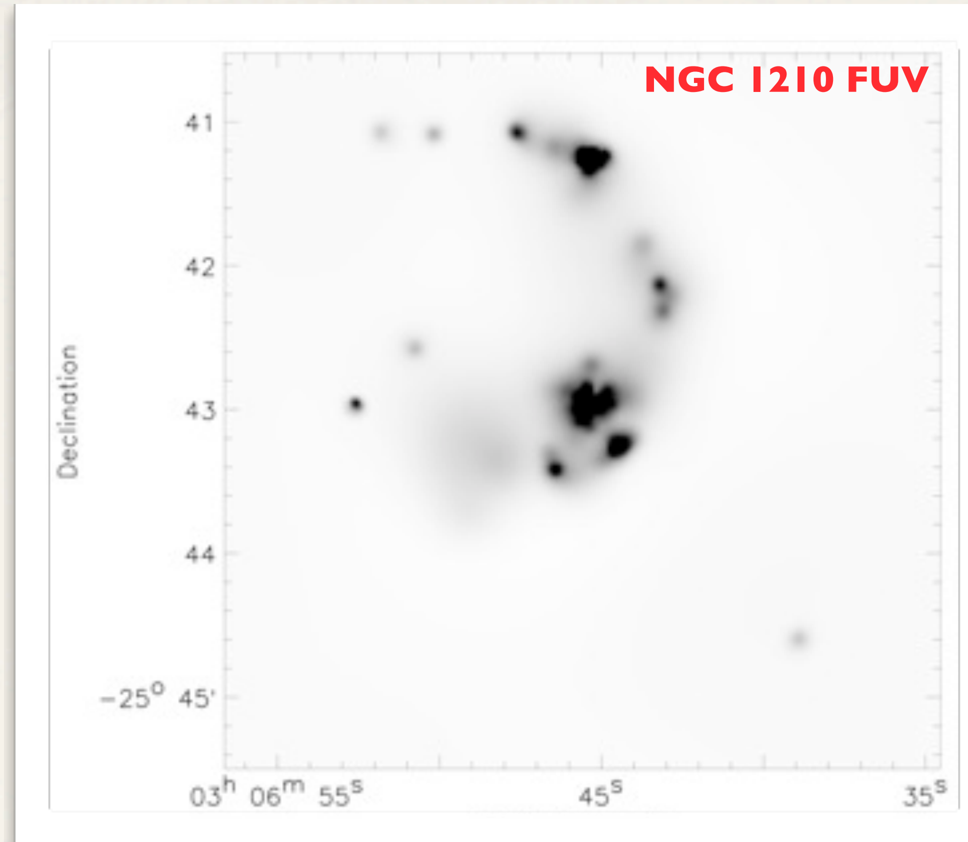

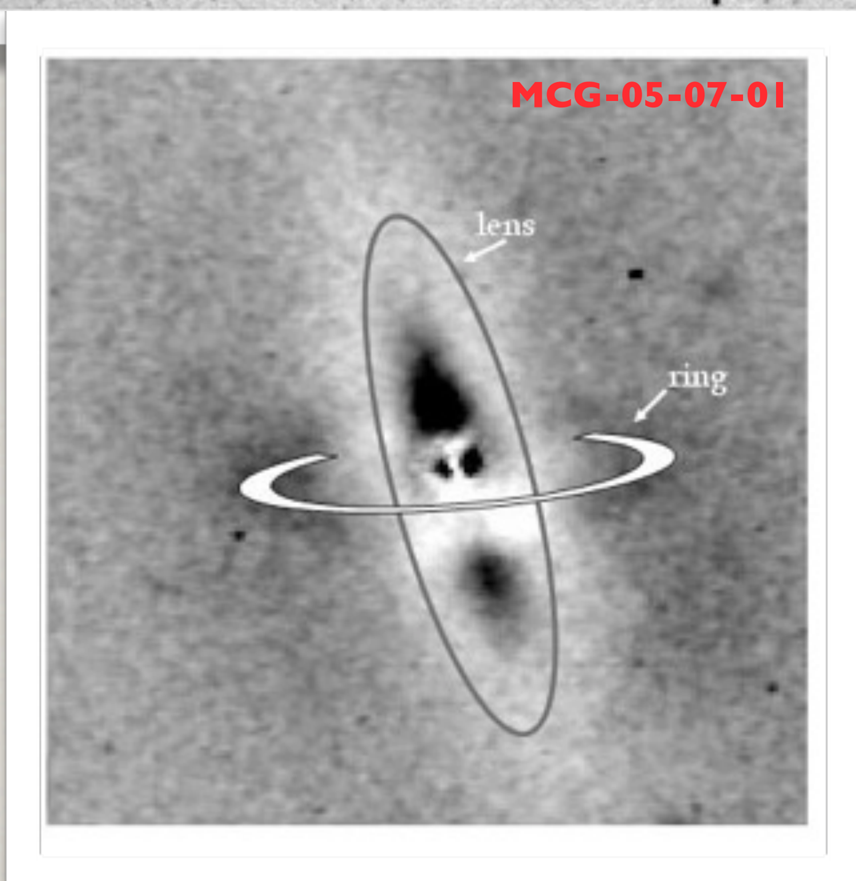

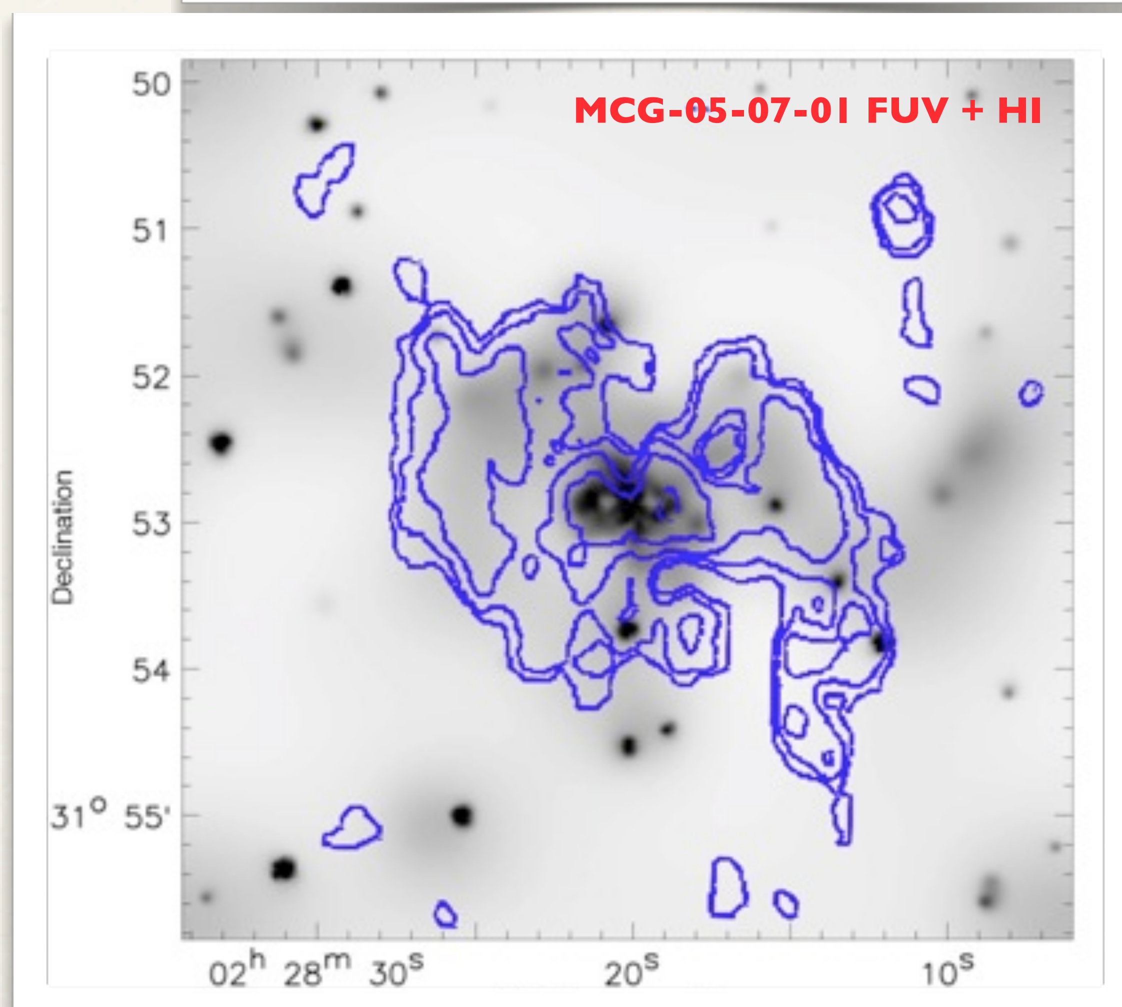

Marino A., Iodice E., Tantalo R., Piovan L. Et Al. 2009, A&A, In Press

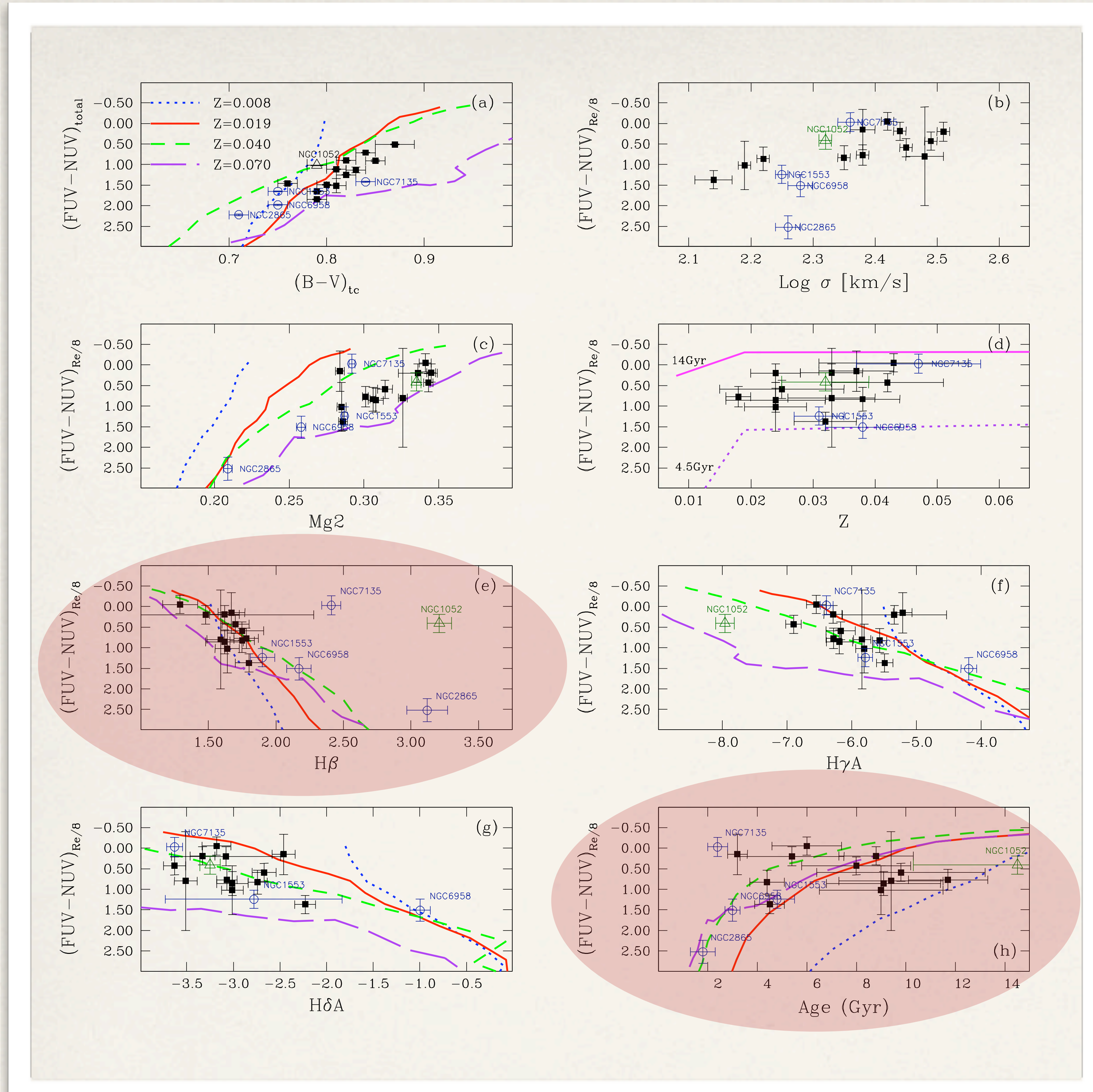

GALEX total (FUV - NUV) color vs. corrected total (B-V) color. (FUV - NUV) color within an aperture of $r_e/8$ radius vs. central velocity dispersion (b panel), Mg2-line strength index (c panel), Z (average galaxy metallicity) (d panel), Hβ (e panel), HγA (f panel), HδA (g panel)} line-strength indices and the the average Age (h panel) estimated in the [Age, Z, [α-Fe] space (Annibali et al. 2007).

Rampazzo R., Marino A., Tantalo R., Bettoni D., Buson L., Chiosi C. Et Al. 2007, MNRAS, 381, 245

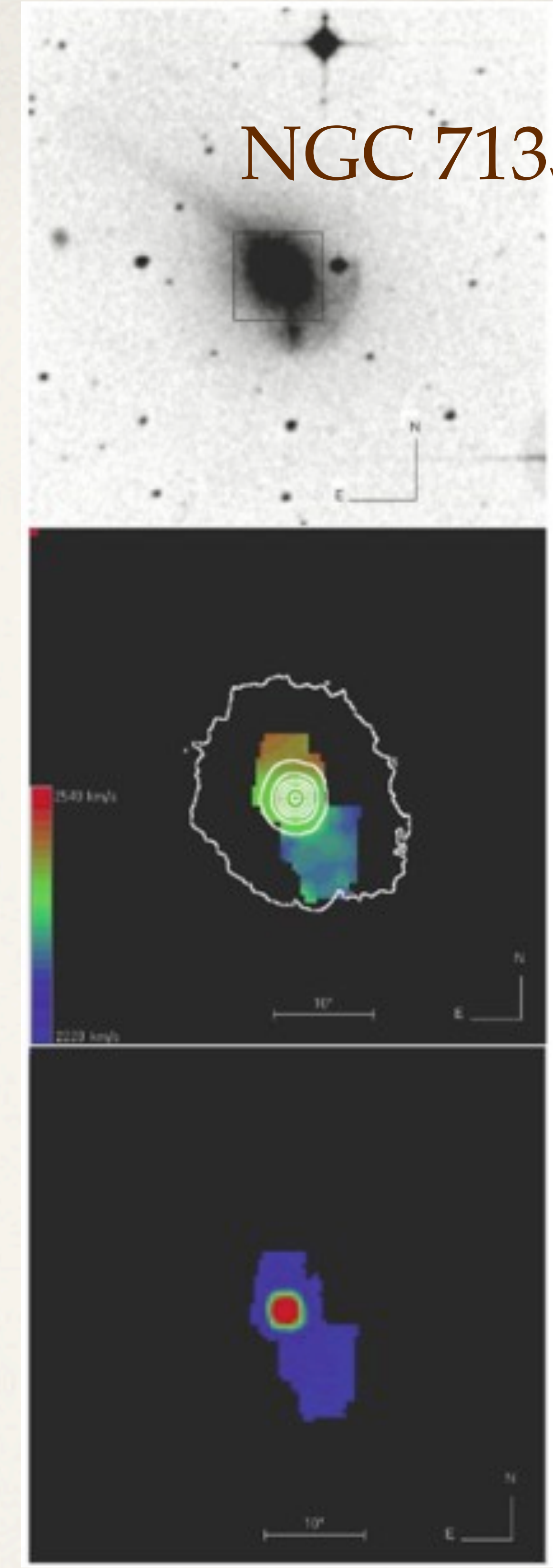

Velocity field (mid panel) and monochromatic Hα image. The DSS image has a FOV of 5'x5'; the box indicate the FOV of the FP observations.

Rampazzo R., Plana H., Longhetti M., Amram P., Boulesteix J., Gach J.-L., Hernadez O. 2003, MNRAS, 343, 819

The hot gas and the environment

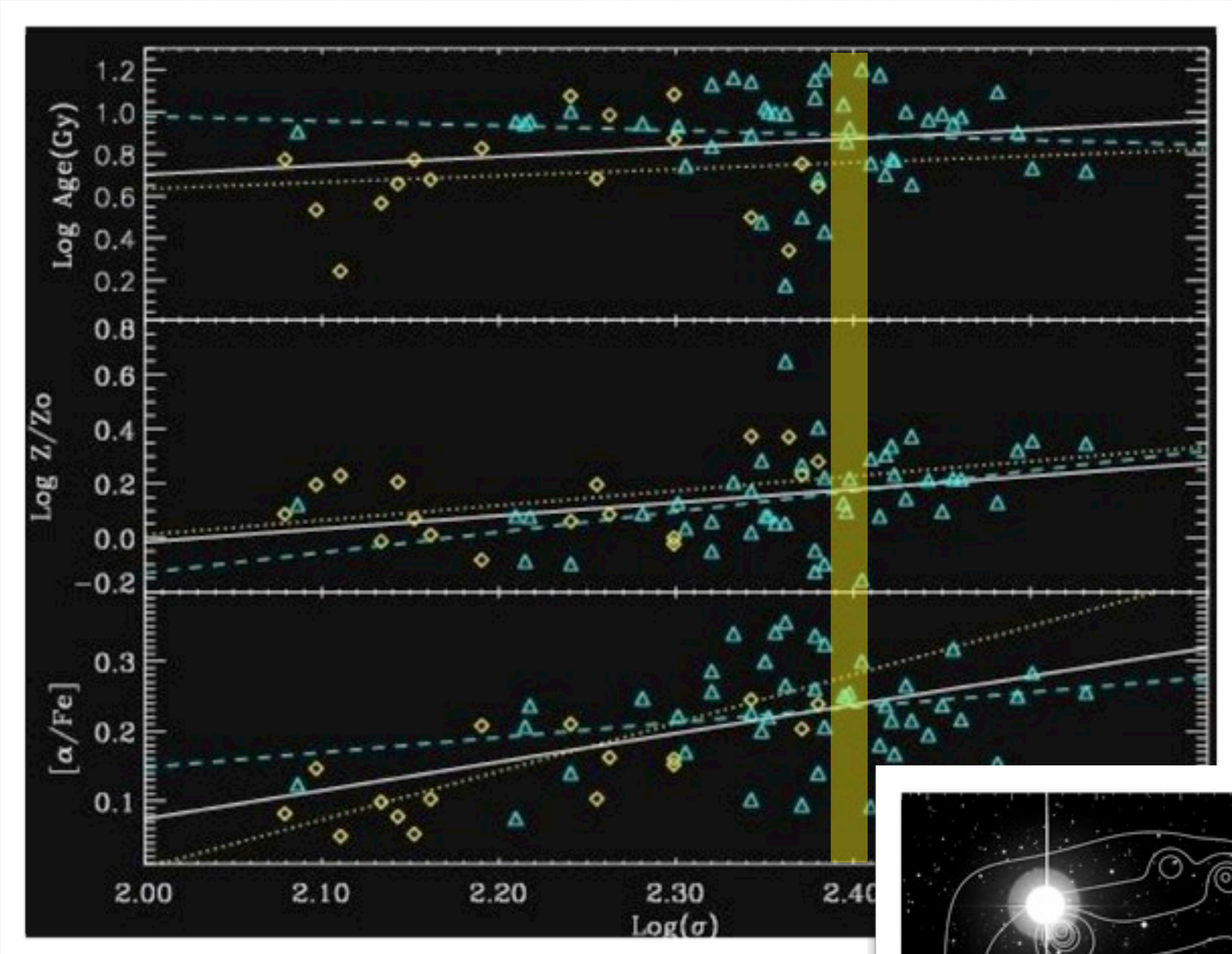

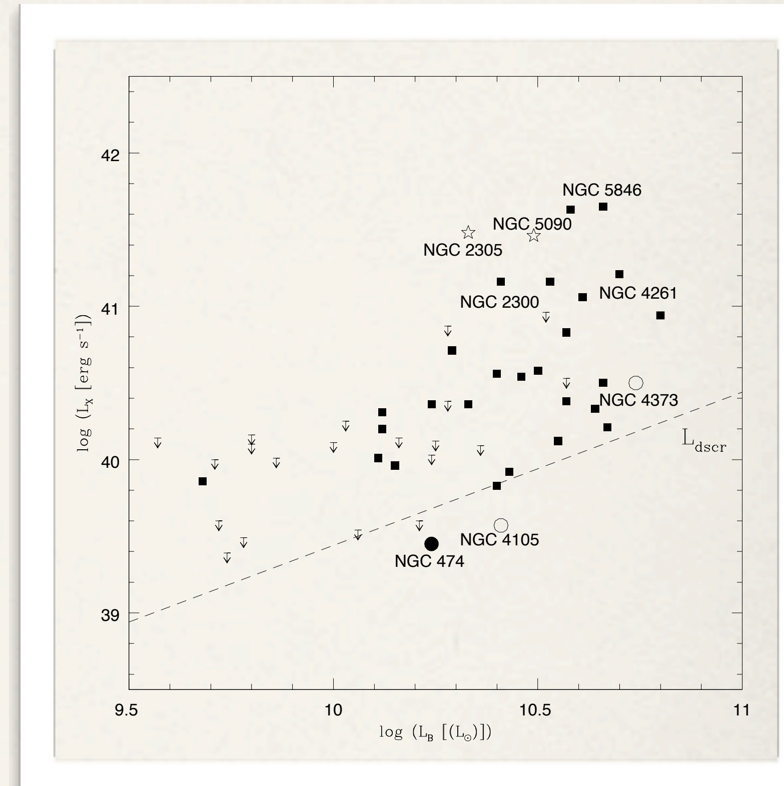

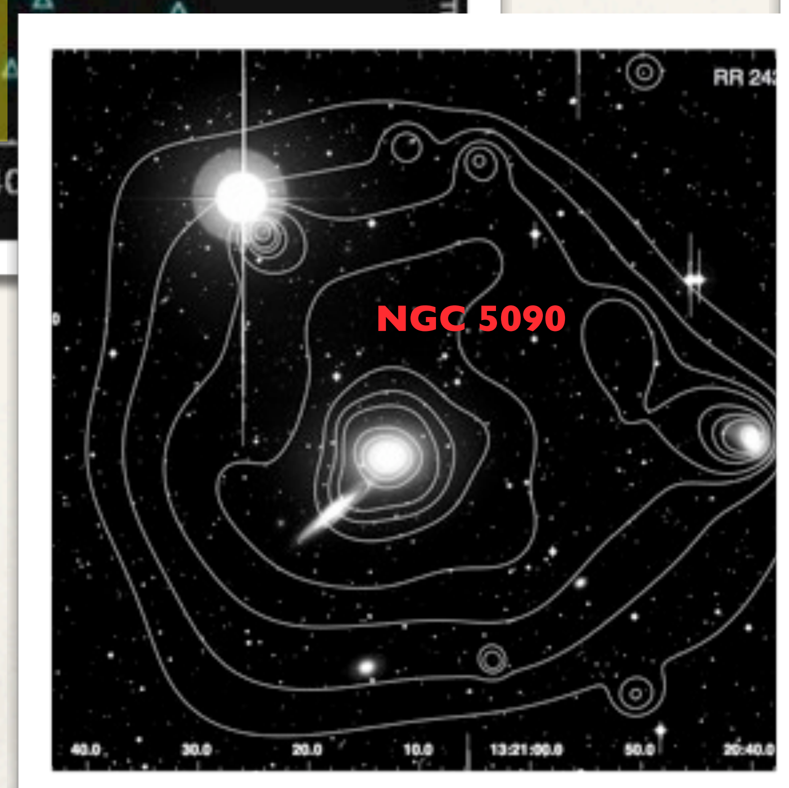

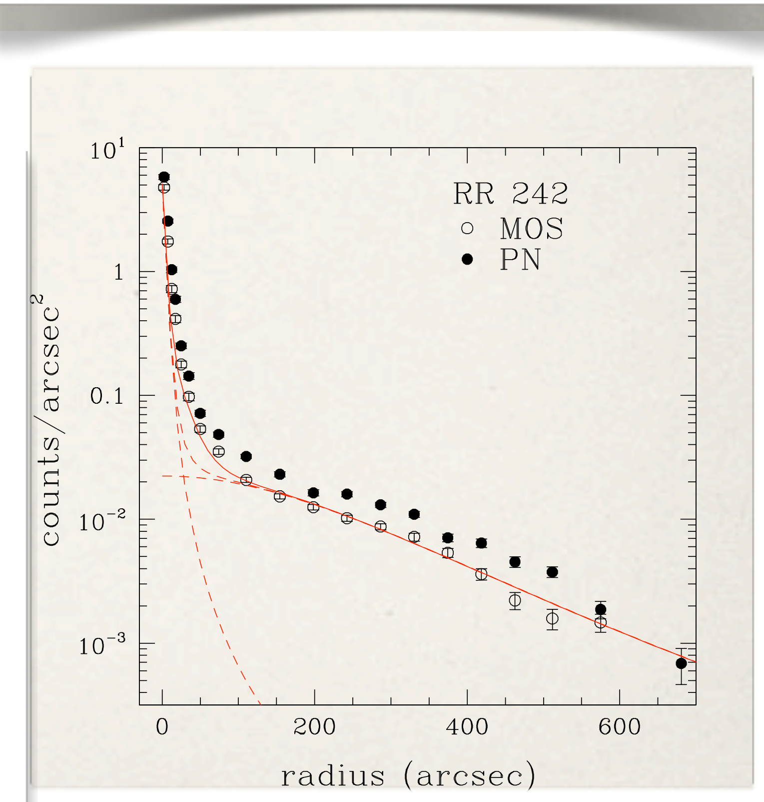

(top) Log s - Age, metallicity, a-enhancement relations for our ETGs. (top right) Position in the L_X vs L_B plane of some of our ETGs. (bottom left) X-ray emission of NGC 5090 and (bottom right) luminosity profile of the X-ray emission centred on NGC 5090.

ETGs in LDE

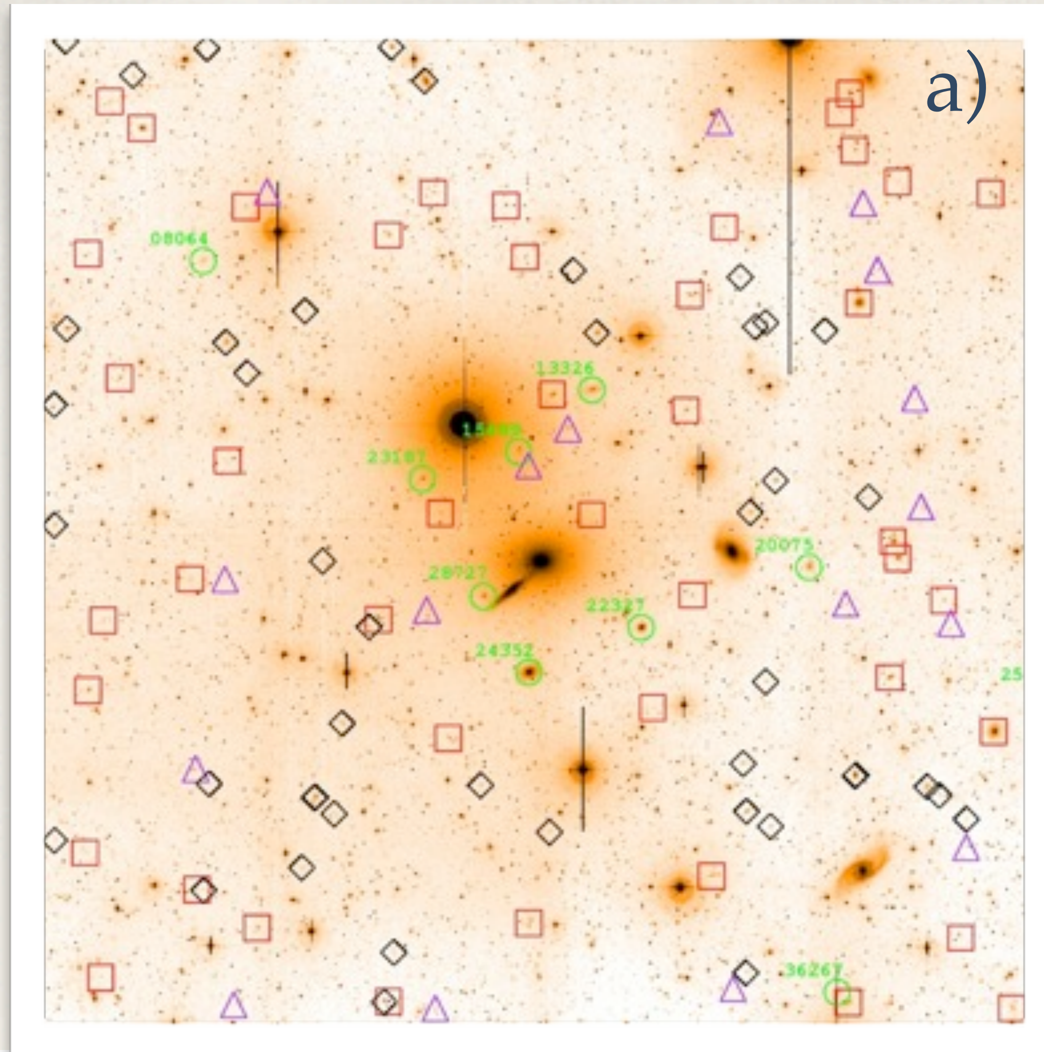

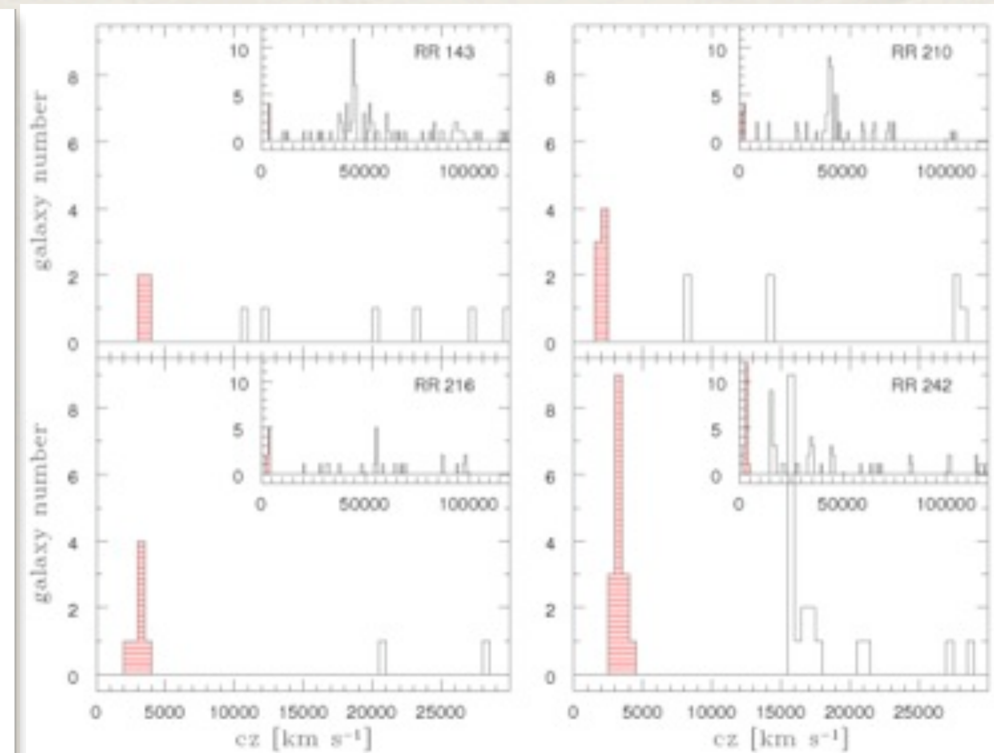

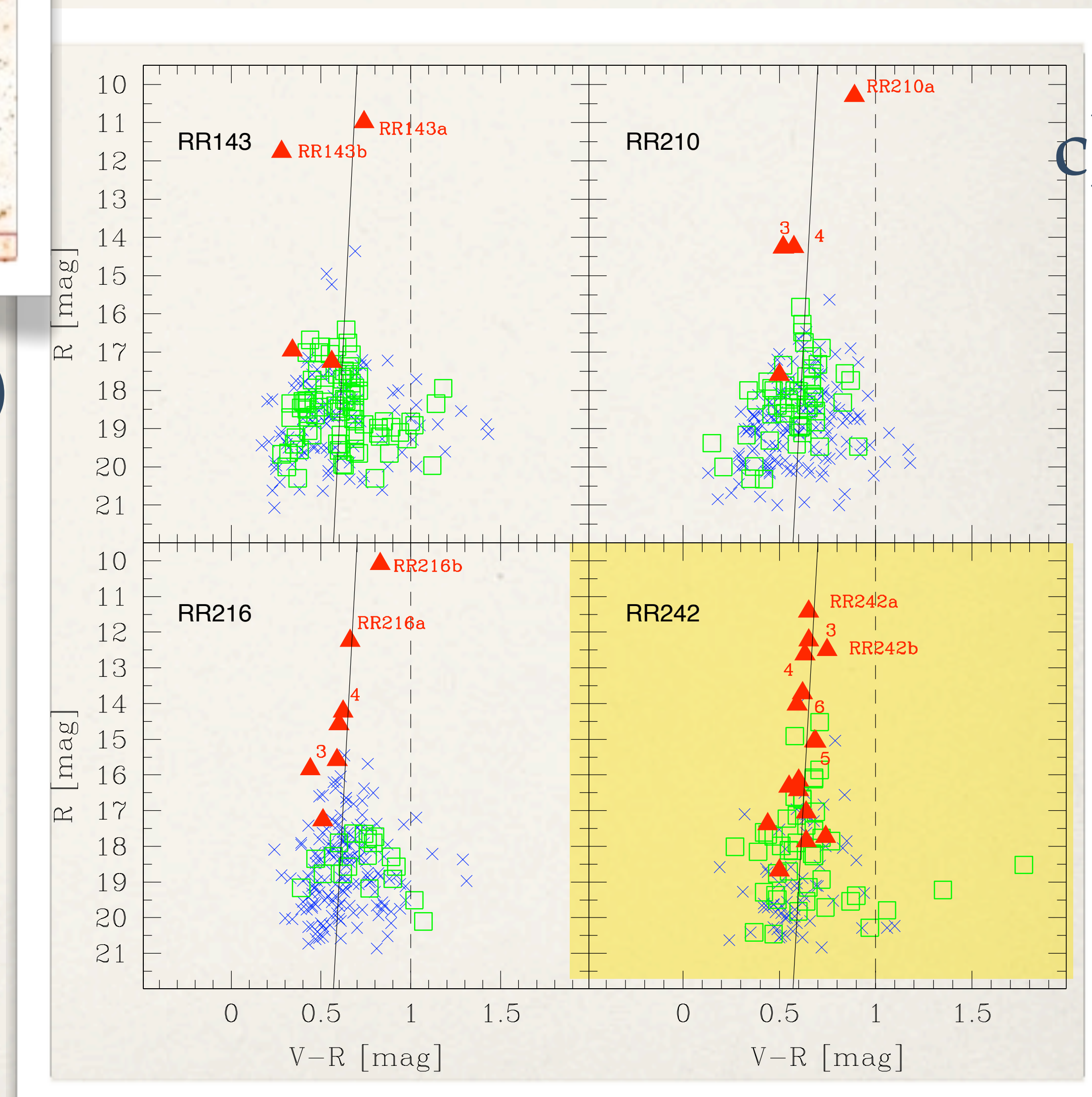

The faint galaxy population

(panel a) WFI image of the NGC 5090 group. Object in labeled in green are members of the group.

(panel b) The group in the redshift space (yellow box).

(panel c) Red triangles are the grup members plotted in a color magnitude plot (yellow box). The solid line is the Virgo red sequence shifted to the group distance.

(panel d) The Hamabe-Kormendy relation for bright and "ordinary members" of the group NGC 5090.

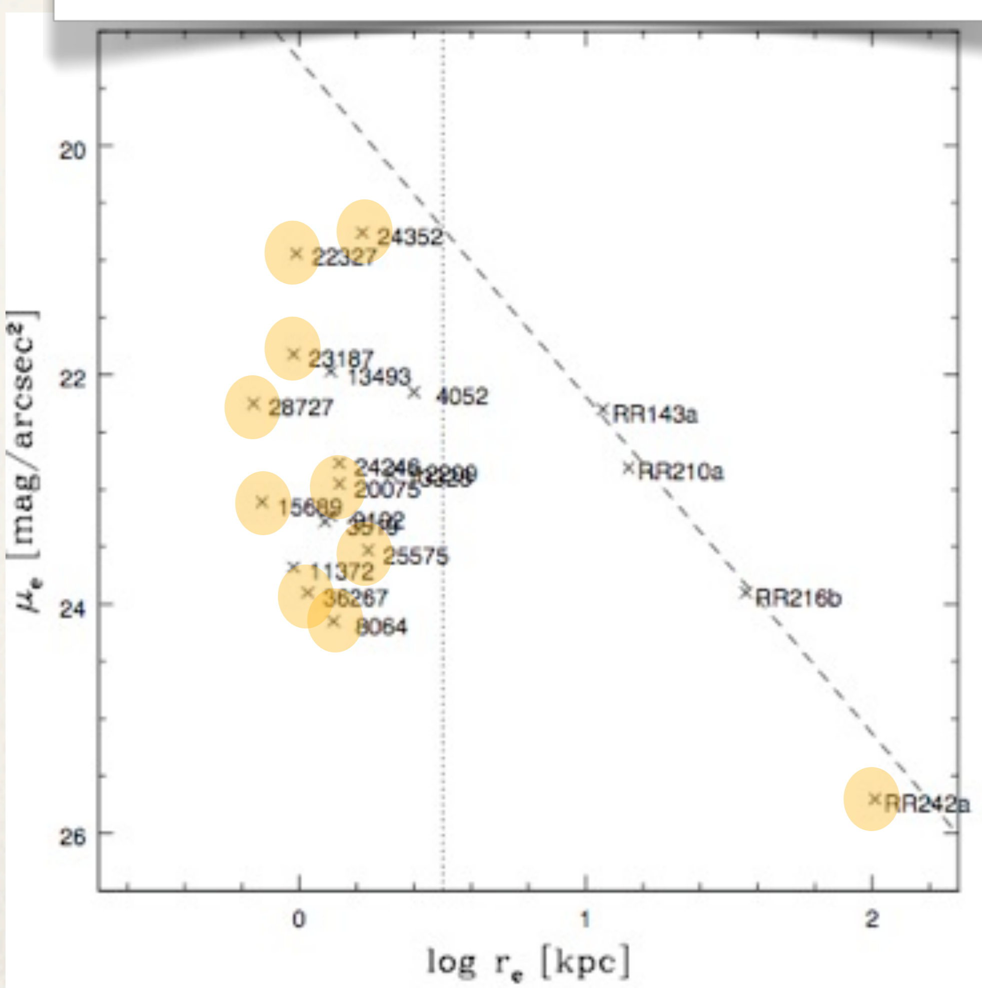

(Grützbauch R., Zeilinger W.., Rampazzo R. Et Al. 2009, A&A, 502, 473)

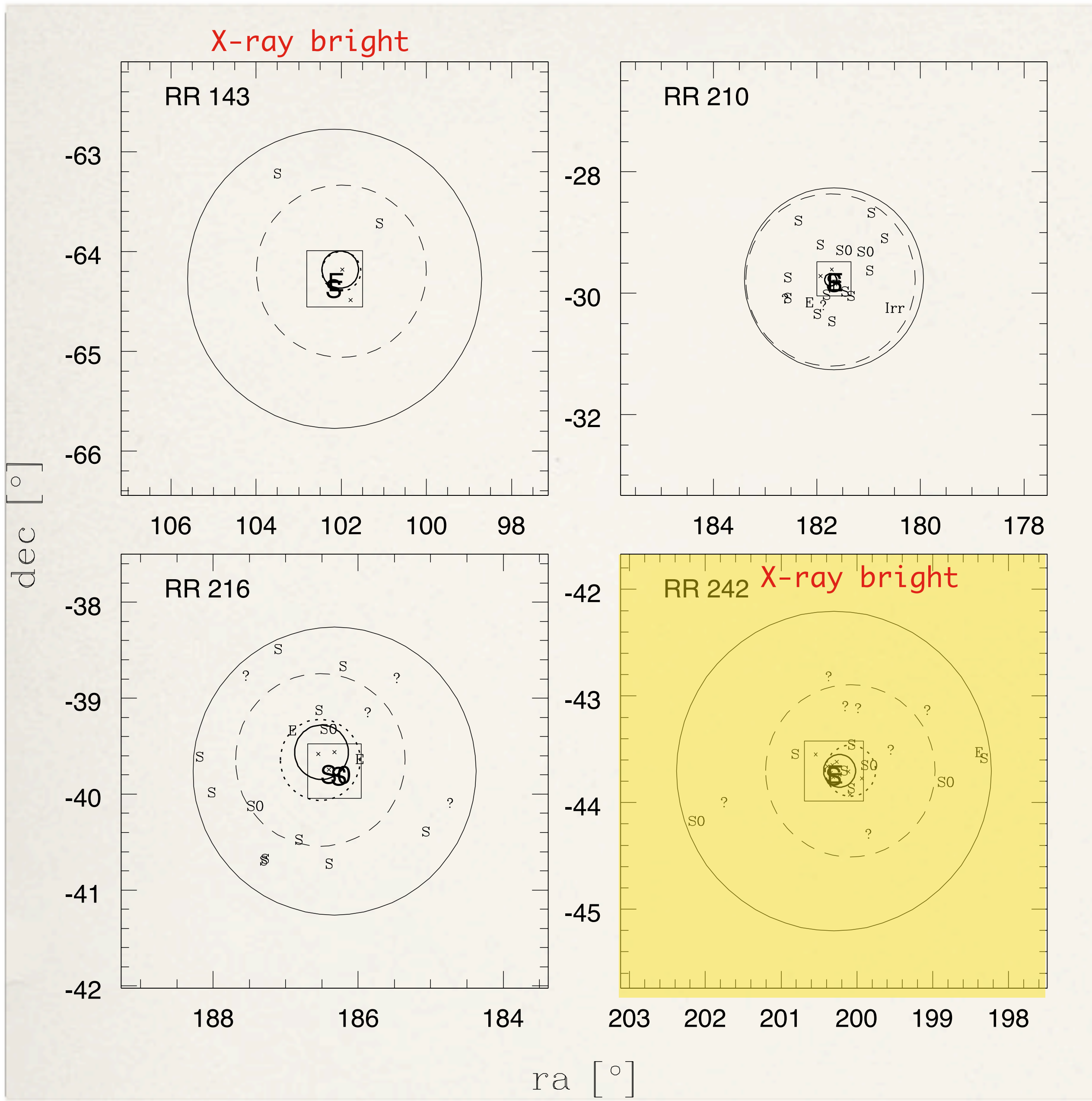

Position of the group members galaxies moved to a common distance (in the yellow box is indicated the NGC 5090 group). The large circle is 90’ search radius around the E member; the central circle is the luminosity weighted harmonic radius of the group centered on the optical group centre. The square is the WFI field.

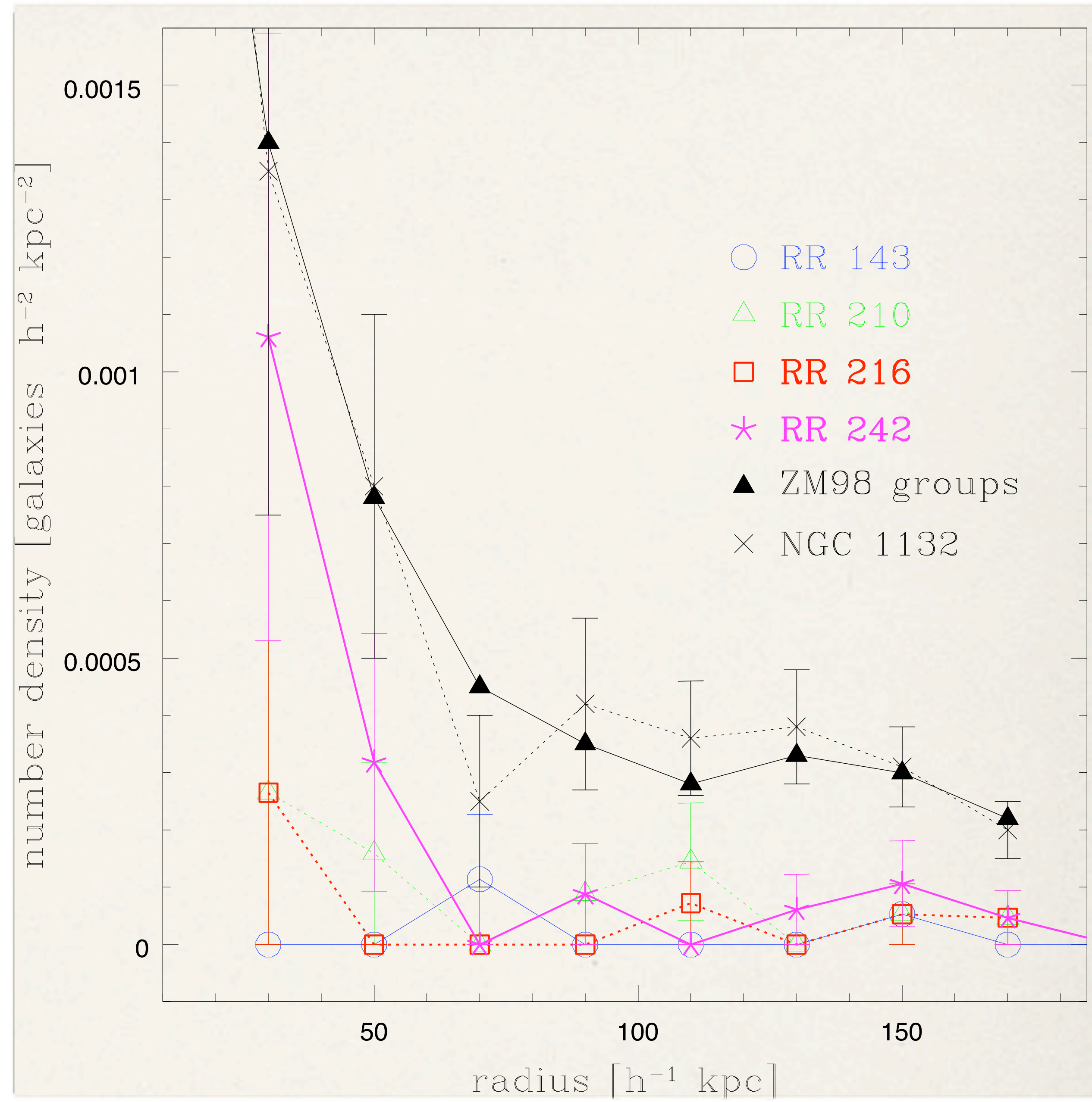

Radial density profile of faint group members galaxies. Notice the concentration of faint galaxies towards the center (the E member) in the case of NGC 5090. For comparison are shown the the radial distribution of galaxies in the group studied by Zabludoff & Mulchay (1998) and the galaxie in the fossil group around NGC 1132 (Muchaey & Zabludoff 1999).

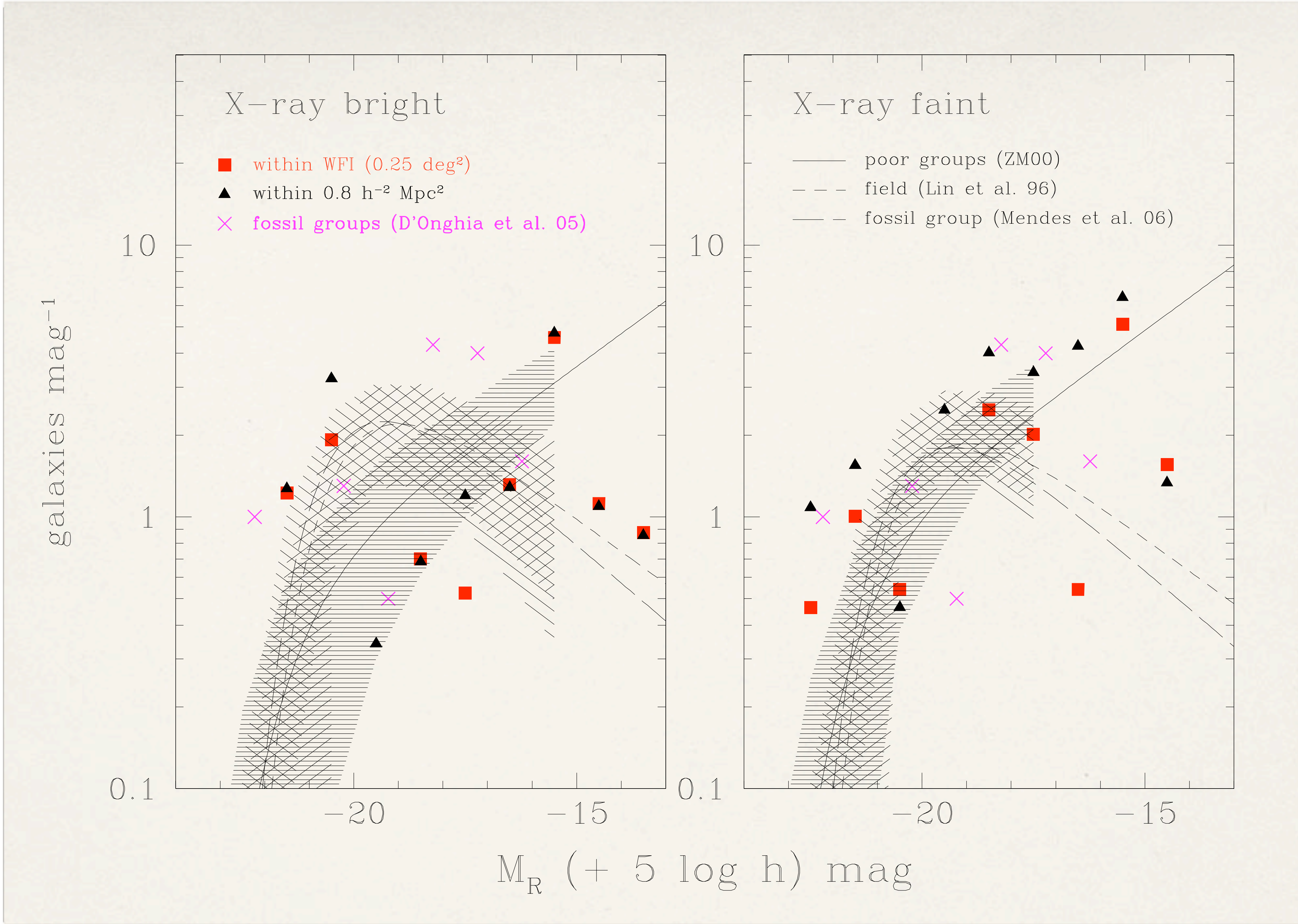

Optical Luminosity Functions (OLF) of 4 groups. The OLF of the 2 X-ray bright and the 2 X-ray faint groups are combined respectively. The OLFs are computed for the large scale sample (black triangles) and the WFI field sub-sample (red squares). Note that outside the WFI the radial velocity information comes from NED and i highly incomplete at fainter magnitudes. The magenta crosses show the OLF of a sample of simulated fossil groups from D'Onghia et al. (2005). The solid line is the OLF found for a sample of Xray-bright poor groups by Mulchaey & Zabludoff (2000). The short dashed line show the OLF of the local field (Lin et al. 1996), whereas the long dashed line is the OLF of a fossil group observed by Mendes de Oliveira et al. (2006). All OLF use spectroscopically confirmed members only and are completeness corrected in a similar way as our counts. The shaded regions around each OLF shows the 1 s deviations expected due to our low number statistics. obtained from a set of Monte Carlo simulations.

Some conclusions:

- ETGs life in LDE is quite eventful ! Optical, Far UV and MIR observations concur to suggest a large spread in Age likely due to recent star formation episodes.

- According to our small Virgo and LDE samples (especially in view of MIR observations) we suggest that the Age spread in LDE is larger than in dense environments.

- The younger and less α-enhanced ETGs in our sample are Fast-rotators: this seems consistent with galaxies which have experienced minor merges and accreted a significant amount of gas (see Cappellari et al. 2008; see also GALEX + HI observations).

- Both Fast & Slow-rotators show morphological and kinematics peculiarities, Slow-rotators in a higher fraction with respect to Fast rotators (59% vs. 36%), i.e. they have also suffered by interaction/accretion episode. We calculated that ETGs have acquired up to 25% of their mass through accretion episodes.

- Most of our ETGs are LINERS. No correlation between the galaxy "activity" and fast/slow-rotators class. Still unclear the powering mechanisms: Optical+MIR (PAH + lines) diagnostic diagrams seem promising in this respect.

- The warm gas [O/H] abundance seems lower than that of stars (under a lot of assumptions): likely another indication, together with many kinematical gas-stars decoupling, of an external acquisition of the gas

- Environments of ETGs, with similar optical & kinematic properties, appear very different: the OLFs of ETGs dominated groups is not universal (at odds with Mulchaey 2000).

- The recent ongoing interaction in which the ETG member of X-ray faint systems is involved could have decreased the luminosity of any surrounding X-ray emitting gas. X-ray emission likely maps different evolutionary phases of the group.

- The faint galaxy population surrounding ETGs are earlier in type (no Irregulars), old, gas and metal poor and with very low α-enhancements. Very few show interaction signatures; some of them show emission lines but they are not gas rich systems.

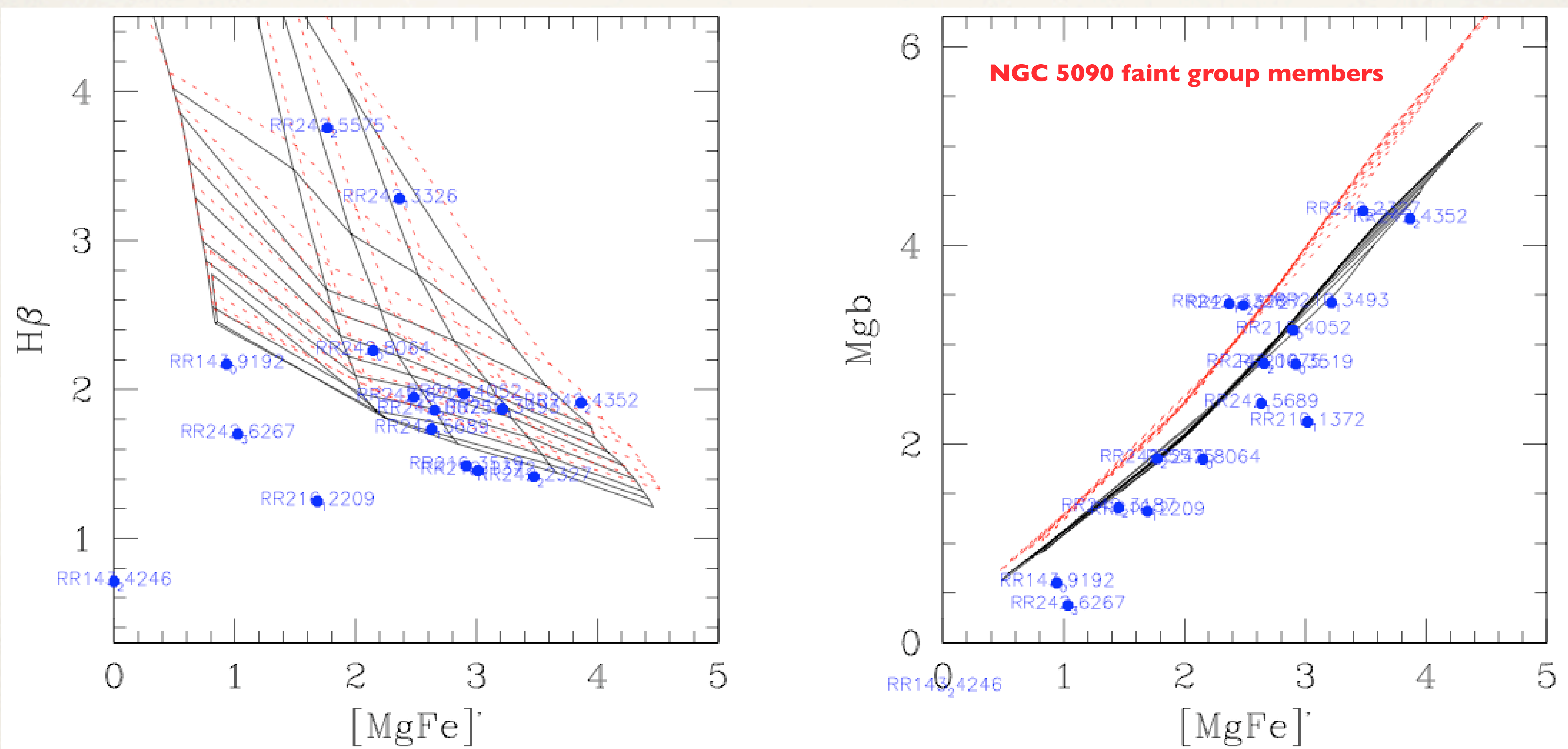

Future investigations

- Modeling of the entire SED of our ETGs combining far UV, optical, NIR and MIR information.

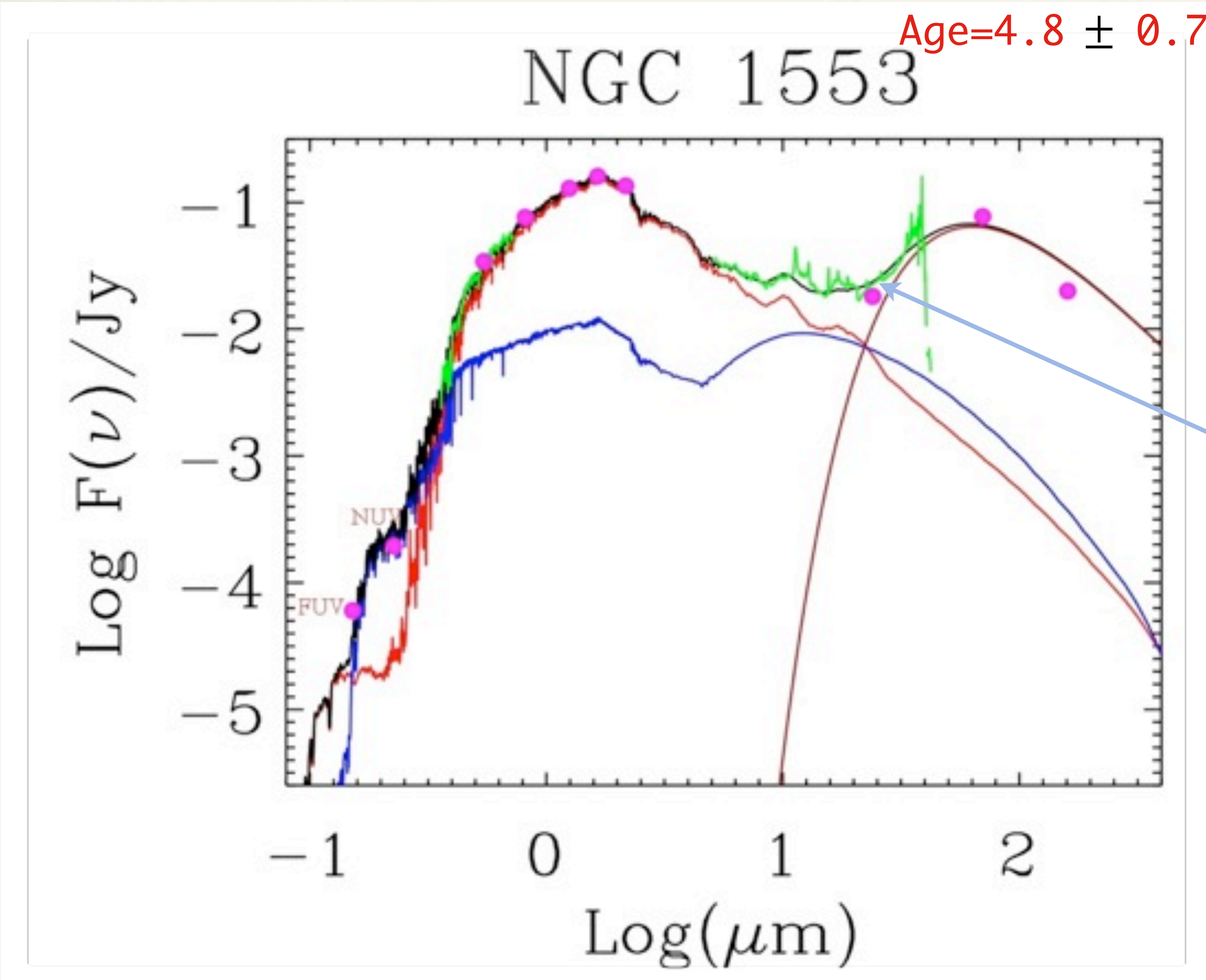

Rough model of the SED in NGC 1553, a shell galaxy gravitationally paired up with NGC 1549 (5 ″ nuclear aperture). Together with a 10 Gyr old SSP of solar metallicity a small fraction, 1.5% in mass, of a young 0.35 Gyr SSP (two times solar) is needed to fit the *GALEX* data.

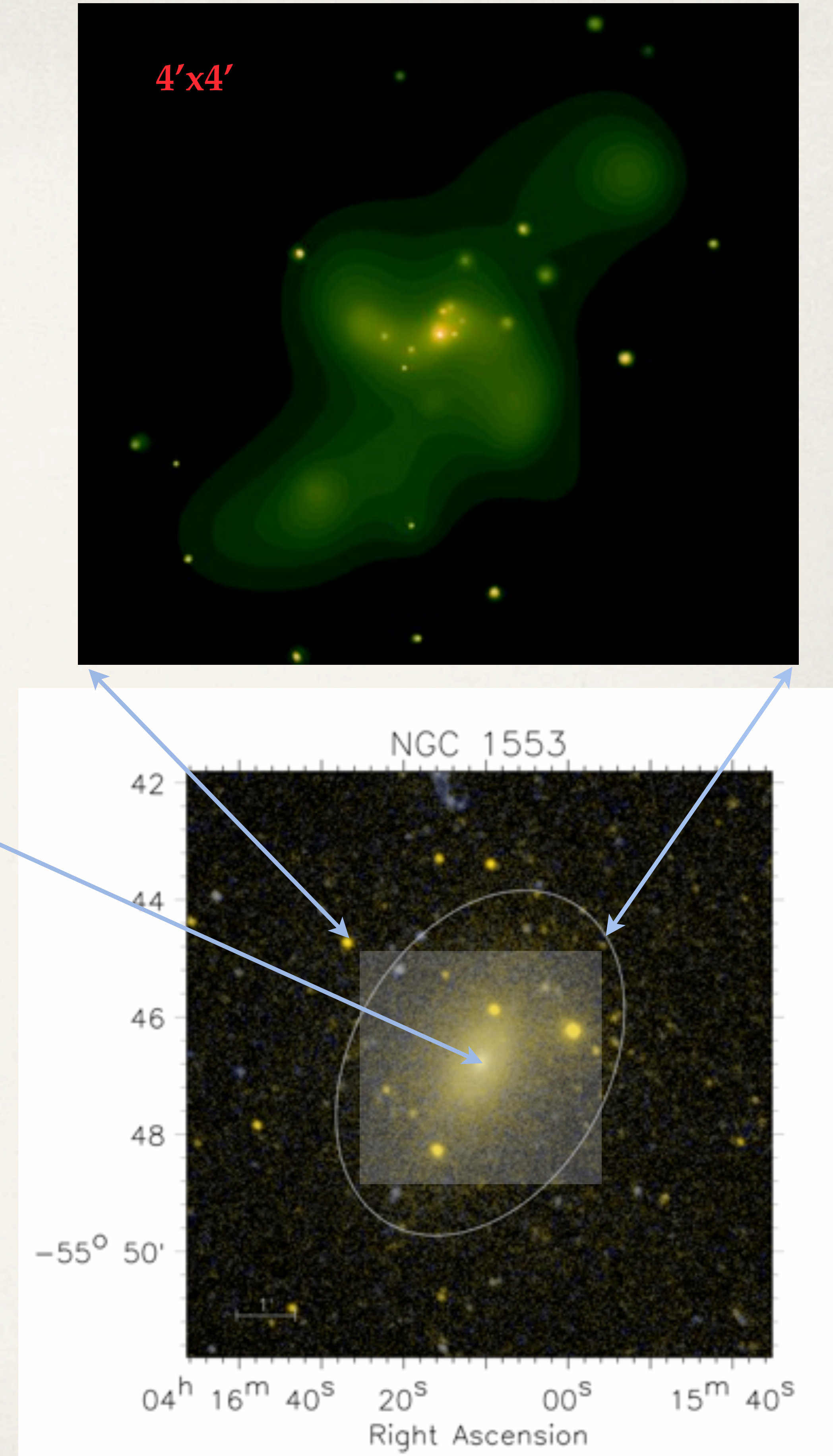

Chandra X-ray emission (Blanton et al. 2003) and GALEX image of NGC 1553 (Marino et al. 2009).

- Nuclear, galactic & group scale ionized gas distribution and kinematics

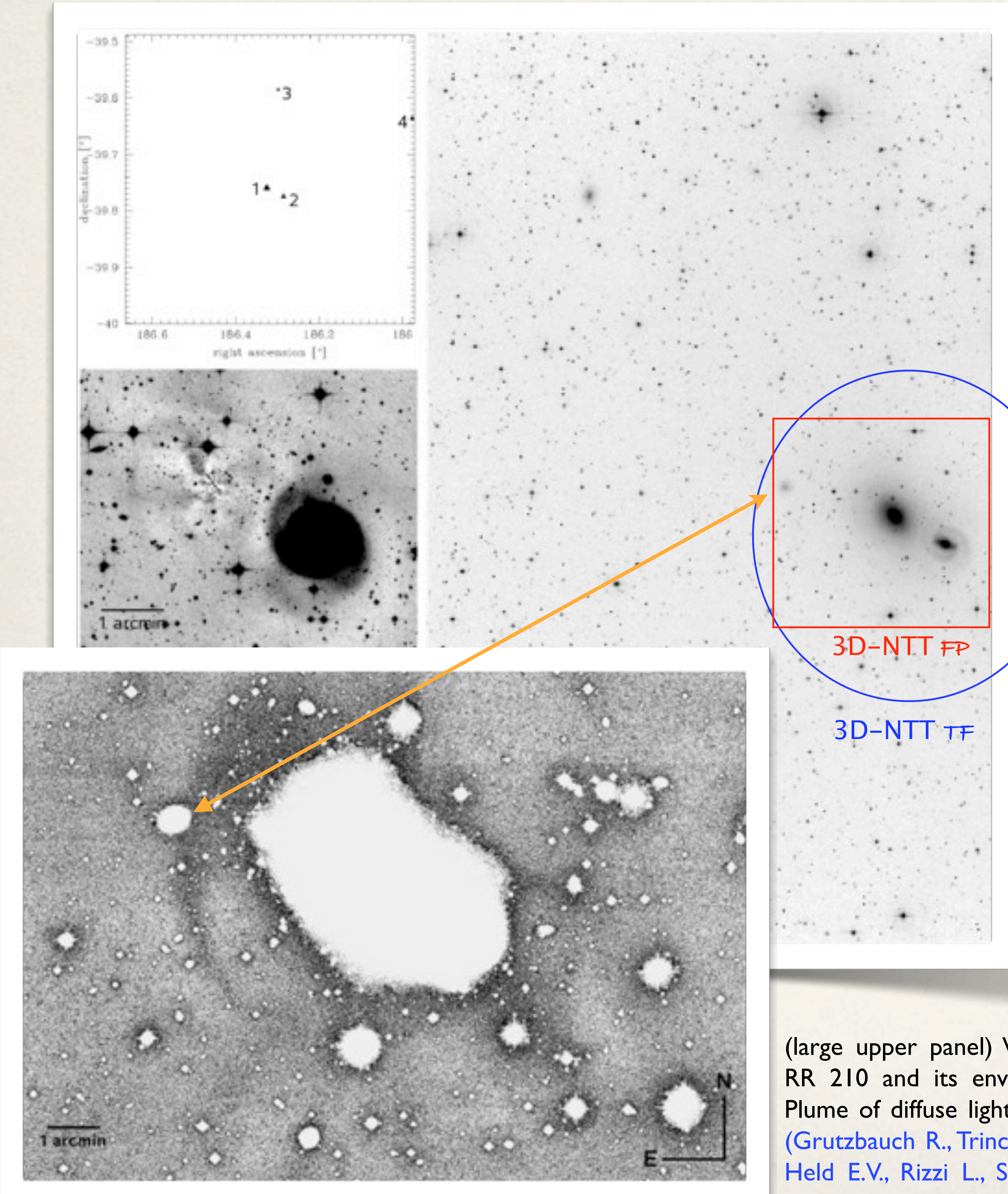

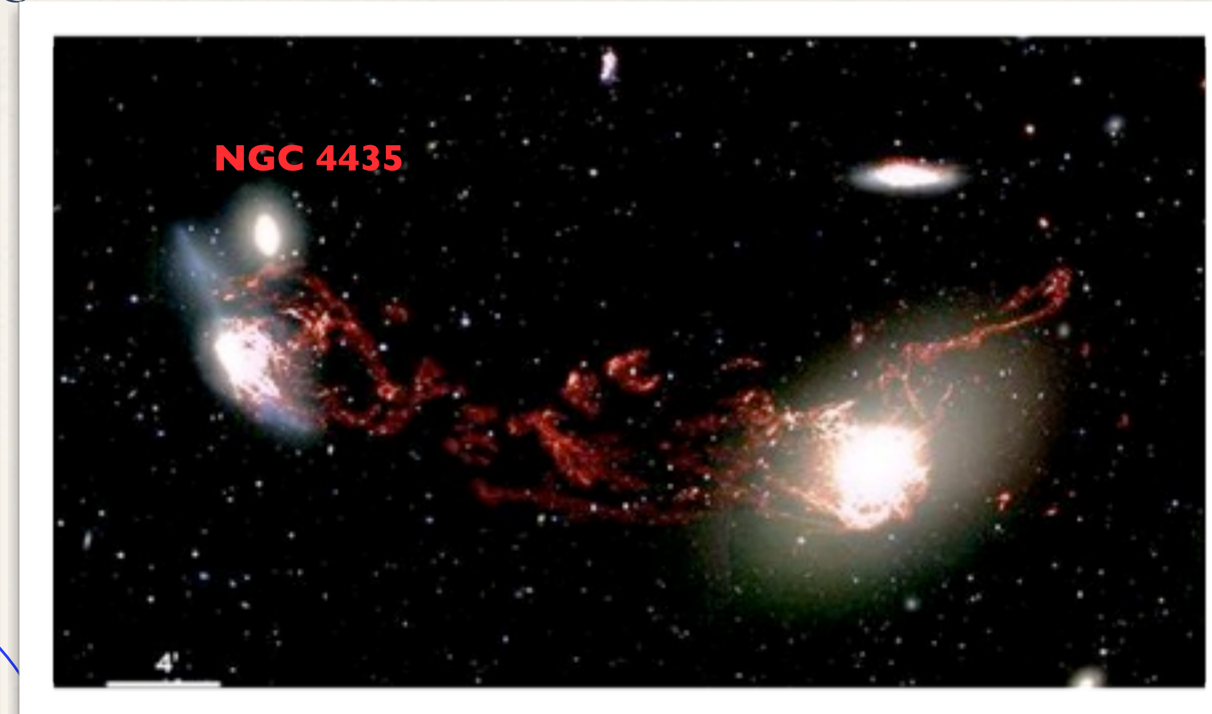

This continuum subtracted Hα+[NII] image of M86 and NGC 4438 may provide an observational evidence of gas heating through gravitational interactions. The spiral is missing 95% of its cold gas (Tal et al. 2009).

(large upper panel) WFI R-band image of RR 210 and its environment. (left panel) Plume of diffuse light detected in RR 210. (Grutzbauch R., Trinchieri G. Rampazzo R., Held E.V., Rizzi L., Sulentic J.W., Zeilinger W.W. 2007, ApJ, 133, 220)

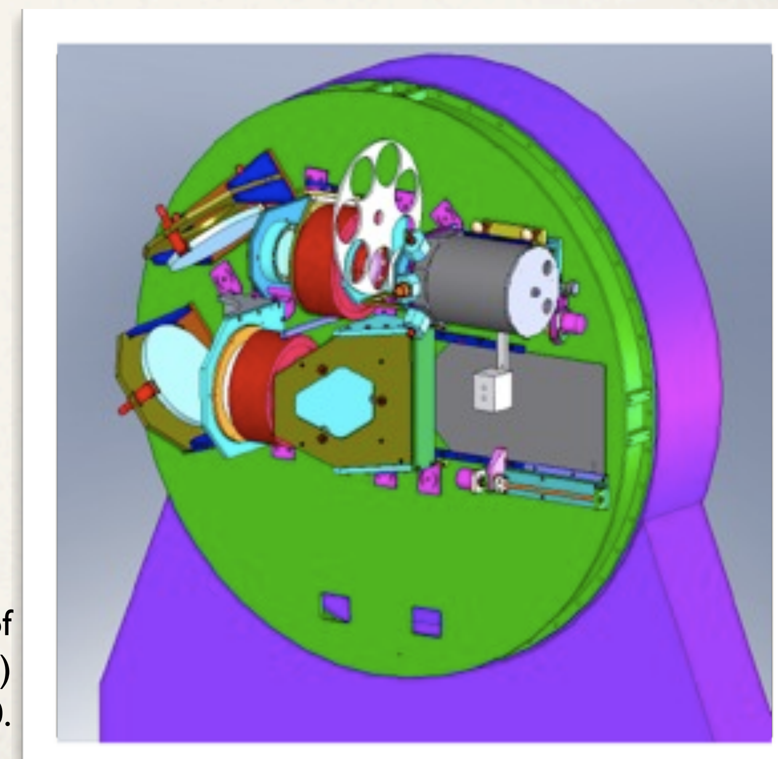

3D-NTT TUNABLE FILTER + FABRY-PEROT.